GEOFORSCHUNGSZENTRUM POTSDAM
STIFTUNG DES ÖFFENTLICHEN RECHTS

Scientific Technical Report

Structural Observations at the Southern Dead Sea Transform from Seismic Reflection Data and ASTER Satellite Images

Dissertation

zur Erlangung des akademischen Grades
Doktor der Naturwissenschaften (Dr. rer. nat.)
in der Wissenschaftsdisziplin Geologie

eingereicht an der
Mathematisch–Naturwissenschaftlichen Fakultät
der Universität Potsdam

Dagmar Kesten

Potsdam, April 2004

Gutachter:

Prof. Dr. Michael Weber (GeoForschungsZentrum & Universität Potsdam)

Prof. Dr. Hans-Jürgen Götze (Universität Kiel)

Prof. Dr. Jonas Kley (Universität Jena)

Tag der Disputation: 28. Oktober 2004

Abstract

Following work is embedded in the multidisciplinary study DESERT (DEad SEa Rift Transect) that has been carried out in the Middle East since the beginning of the year 2000. It focuses on the structure of the southern Dead Sea Transform (DST), the transform plate boundary between Africa (Sinai) and the Arabian microplate. The left-lateral displacement along this major active strike-slip fault amounts to more than 100 km since Miocene times. The DESERT near-vertical seismic reflection (NVR) experiment crossed the DST in the Arava Valley between Red Sea and Dead Sea, where its main fault is called Arava Fault. The 100 km long profile extends in a NW–SE direction from Sede Boqer/Israel to Ma'an/Jordan and coincides with the central part of a wide-angle seismic refraction/reflection line.

Near-vertical seismic reflection studies are powerful tools to study the crustal architecture down to the crust/mantle boundary. Although they cannot directly image steeply dipping fault zones, they can give indirect evidence for transform motion by offset reflectors or an abrupt change in reflectivity pattern. Since no seismic reflection profile had crossed the DST before DESERT, important aspects of this transform plate boundary and related crustal structures were not known. Thus this study aimed to resolve the DST's manifestation in both the upper and the lower crust. It was to show, whether the DST penetrates into the mantle and whether it is associated with an offset of the crust/mantle boundary, which is observed at other large strike-slip zones.

In this work a short description of the seismic reflection method and the various processing steps is followed by a geological interpretation of the seismic data, taking into account relevant information from other studies.
Geological investigations in the area of the NVR profile showed, that the Arava Fault can partly be recognized in the field by small scarps in the Neogene sediments, small pressure ridges or rhomb-shaped grabens. A typical fault zone architecture with a fault gauge, fault-related damage zone, and undeformed host rock, that has been reported from other large fault zones, could not be found. Therefore, as a complementary part to the NVR experiment, which was designed to resolve deeper crustal structures, ASTER (Advanced Spacebourne Thermal Emission and Reflection Radiometer) satellite images were used to analyze surface deformation and determine neotectonic activity.

The NVR experiment showed, that the Dead Sea Transform cuts through the whole crust into the upper mantle, forming a ∼15 km wide deformation zone in the lower crust. Some minor shear deformation might also occur at a mid-crustal boundary. An offset of the crust/mantle boundary was not observed. Strong lower crustal reflectors below the Jordanian highlands are attributed to sill-like mafic intrusions that are not necessarily related to transform motion.

In the upper crust brittle deformation is associated with various subparallel faults. Although the Arava Fault is clearly the main active fault segment of the southern DST,

it is proposed, that it has accomodated only a small part of the overall 105 km of sinistral plate motion. There is evidence for sinistral displacement along other faults, based on geological studies and satellite images. Furthermore a subsurface fault is revealed ∼5 km west of the Arava Fault on a Jordanian shallow seismic reflection profile close to the NVR line. Whereas the seismic data show a flower structure typical for strike-slip faults, on the satellite image this fault is not expressed in the Pliocene sediments, implying that it has been inactive for the last few million years.

Taking together various lines of evidence it is suggested here, that at the beginning of transform motion deformation occurred in a rather wide belt, with the reactivation of older ∼N–S striking structures. Later, deformation became concentrated in the region of today's Arava Valley. Till ∼5 Ma ago there might have been another, now inactive fault trace approximately 5 km west of the AF that took up lateral motion. Together with a rearrangement of plates 5 Ma ago (Joffe and Garfunkel, 1987), the main fault trace shifted to the position of today's Arava Fault.

Kurzfassung

Die folgende Arbeit ist Teil des multidisziplinären Projektes DESERT (DEad SEa Rift Transect), welches seit dem Jahr 2000 im Nahen Osten durchgeführt wird. Dabei geht es primär um die Struktur der südlichen Dead Sea Transform (DST; Tote–Meer–Transformstörung), Plattengrenze zwischen Afrika (Sinai) und der Arabischen Mikroplatte. Seit dem Miozän beträgt der sinistrale Versatz an dieser bedeutenden aktiven Blattverschiebung mehr als 100 km. Das steilwinkelseismische (NVR) Experiment von DESERT querte die DST im Arava Tal zwischen Rotem Meer und Totem Meer, wo die Hauptstörung auch Arava Fault genannt wird. Das 100 km lange Profil erstreckte sich von Sede Boqer/Israel im Nordwesten nach Ma'an/Jordanien im Südosten und fällt mit dem zentralen Teil einer weitwinkelseismischen Profillinie zusammen.

Steilwinkelseismische Messungen stellen bei der Bestimmung der Krustenstruktur bis zur Krusten/Mantel-Grenze ein wichtiges Instrument dar. Obwohl es kaum möglich ist, steilstehende Störungszonen direkt abzubilden, geben abrupte Veränderungen des Reflektivitätsmuster oder plötzlich endende Reflektoren indirekte Hinweise auf Transformbewegung. Da bis zum DESERT Experiment keine anderen reflexionsseismischen Messungen über die DST ausgeführt worden waren, waren wichtige Aspekte dieser Transform–Plattengrenze und der damit verbundenen Krustenstruktur nicht bekannt. Mit dem Projekt sollte deshalb untersucht werden, wie sich die DST sowohl in der oberen als auch in der unteren Kruste manifestiert. Zu den Fragestellungen gehörte unter anderem, ob sich die DST bis in den Mantel fortsetzt und ob ein Versatz der Krusten/Mantel-Grenze beobachtet werden kann. So ein Versatz ist von anderen grossen Transformstörungen bekannt.

In der vorliegenden Arbeit werden zunächst die Methode der Steilwinkelseismik und die Datenverarbeitung kurz erläutert, bevor die Daten geologisch interpretiert werden. Bei der Interpetation werden die Ergebnisse anderer relevanter Studien berücksichtigt. Geologische Geländearbeiten im Gebiet des NVR Profiles ergaben, dass die Arava Fault zum Teil charakterisiert ist durch niedrige Steilstufen in den neogenen Sedimenten, durch kleine Druckrücken oder Rhomb-Gräben. Ein typischer Aufbau der Störungszone mit einem Störungskern, einer störungsbezogenen Deformationszone und einem undeformierten Ausgangsgestein, wie er von anderen großen Störungszonen beschrieben worden ist, konnte nicht gefunden werden. Deshalb wurden zur Ergänzung der Reflexionsseismik, welche vor allem die tieferen Krustenstrukturen abbildet, ASTER (Advanced Spacebourne Thermal Emission and Reflection Radiometer) Satellitendaten herangezogen, um oberflächennahe Deformation und neotektonische Aktivität zu bestimmen.

Mit dem NVR Experiment konnte gezeigt werden, dass die DST durch die gesamte Kruste bis in den oberen Erdmantel reicht und in der unteren Kruste durch eine ∼15 km breite Deformationszone gekennzeichnet ist. Zusätzlich könnte auch an der Grenze zwischen oberer und unterer Kruste Scherdeformation auftreten. Ein Versatz der

Krusten/Mantel-Grenze konnte nicht beobachtet werden. Starke Unterkrustenreflektoren in Jordanien werden auf magmatische 'sills', flächenhafte Intrusionen in die Unterkruste, zurückgeführt und stehen genetisch nicht unbedingt mit der DST im Zusammenhang.

Spröde Deformation drückt sich in der Oberkruste durch die Existenz verschiedener paralleler Störungen aus. Die Arava Fault ist zwar momentan eindeutig die aktive Hauptstörung, doch wird hier vorgeschlagen, dass sie nur einen relativ geringen Teil des Gesamtversatzes von 105 km erfahren hat. Sinistraler Versatz an anderen Störungen ist durch geologische Studien und Satellitenbilder belegt. Ausserdem wurde auf einem oberflächennahen Reflexionsprofil in der Nähe der NVR Linie eine Störung ∼5 km westlich der Arava Fault entdeckt. In der Seismik kann eindeutig eine Blumenstruktur, charakteristisch für Blattverschiebungen, erkannt werden. Da auf dem Satellitenbild keine Störung in den pliozänen Sedimenten identifizierbar ist, war diese Störung in den letzten paar Millionen Jahren vermutlich nicht aktiv.

Unter Berücksichtigung verschiedener Beobachtungen liegt es nahe, dass zu Beginn der Transformbewegung die oberflächennahe Deformation auf eine breitere Zone ausgedehnt war, in der ältere ∼N–S streichende Störungen reaktiviert wurden. Erst später konzentrierte sich die Deformation auf den Bereich des heutigen Arava Tals. Bis vor ungefähr 5 Ma fand ein Teil des sinistralen Versatzes wahrscheinlich an einer heute nicht mehr aktiven Störung ca. 5 km westlich der Arava Fault statt. Mit einer Neuordnung der Platten vor 5 Ma (Joffe and Garfunkel, 1987) verlagerte sich die Hauptstörung an die Position der heutigen Arava Fault.

Contents

1 Introduction

With the implementation of plate tectonics in the nineteensixties and seventies, the nature of plate boundaries have attracted the attention of all geoscientists. Next to oceanic spreading centres and subduction zones, transform faults represent a main type of plate boundary, characterized by complex geology and variable crustal structures that are still not fully understood. Whereas oceanic transform faults usually link various segments of mid-oceanic ridges and are tens to hundreds of kilometers long, continental transform faults occur in quite different tectonic settings and might extend over distances of more than thousand kilometers. Apart from the San Andreas Fault in California, the Dead Sea Transform in the Middle East, which this study focuses on, ranks certainly among the most famous continental transforms. Mainly being a sinistral strike-slip fault system, the Dead Sea Transform (DST) is the plate boundary between the Sinai microplate to the W and the Arabian plate to the E (Fig. 1.1). It connects the zone of oceanic spreading in the Red Sea with the Zagros–Taurus collision zone.

Especially the southern part of the transform is characterized by a relatively narrow, 10–20 km wide, valley that is bordered by marginal normal faults and elevated flanks (Fig. 1.2). Due to its surface expression there had been an extensive and persistent debate about the character of this plate boundary, whether presenting a continental rift zone with negligible lateral offset (Blanckenhorn, 1893, 1896; Picard, 1943, 1987; Dubertret, 1970; Bender, 1968; Mart, 1991) or primarily a transform fault (Quennell, 1958, 1959; Freund, 1961, 1965; Freund *et al.*, 1968, 1970; Bartov, 1974; Steinitz *et al.*, 1978; Bartov *et al.*, 1980; Garfunkel, 1981; Joffe and Garfunkel, 1987). The geophysical and geological indications for the latter have been substantiated during the last few decades and voices favouring the rift model have been outvoted. Now there seems to be substantial evidence for a cumulative left-lateral displacement along the DST of ∼105 km during the last 18 Ma, with only some minor transverse (∼W-E) extension having occurred along normal faults.
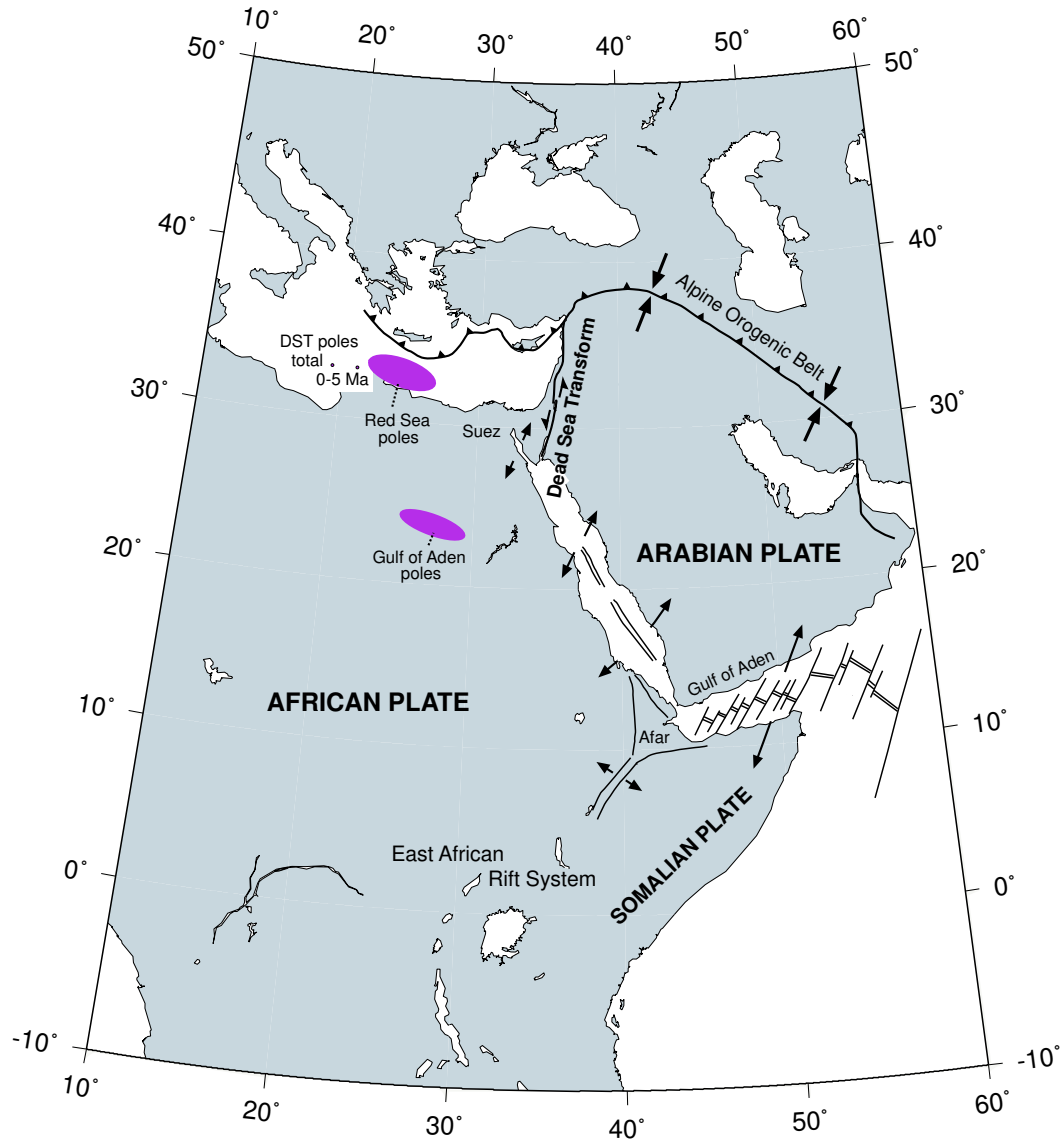
Figure 1.1: Plate tectonic setting of the Middle East; modified after Joffe and Garfunkel (1987).

Till the beginning of the year 2000, however, there had not been any seismic reflection/refraction study crossing the DST, mainly because of its rather critical location at national borders. But especially when determining deeper crustal structures and the topography of the crust/mantle boundary, seismic methods provide valuable tools to better constrain the results of other geophysical methods (e.g. gravity and magnetics). Thus eventually, with the common wish to better understand large continental strike-slip zones, the multinational and strongly interdisciplinary project DESERT (DEad SEa Rift Transect; see e.g. DESERT Group, 2000) was

brought into being, as a cooperation of German, Israeli, Jordanian and Palestinian scientists. In March 2000 a near-vertical seismic reflection (NVR) transect of 100 km length was carried out between Sede Boqer/Israel and Ma'an/Jordan, coinciding with the central part of a ∼300 km long seismic refraction/reflection profile (WRR) from the Gaza strip in the NW to the Jordanian highlands in the SE (Fig. 1.2). The Dead Sea Transform was crossed in the Arava Valley, where its major segment is called Arava Fault (AF). In combination with the other subprojects of DESERT, including a teleseismic study and various high-resolution magnetotelluric and seismic experiments, following questions were addressed:

- What is the geometry of the main transform fault(s)?

- Are there (hidden) parallel faults? Are they connected with each other at a certain depth?

- Can detachment horizons be recognized in the crust?

- What is the crustal structure down to the crust/mantle boundary?

- Does the DST influence the shape of the crust/mantle boundary?

- Does rifting play a role in the dynamics of the DST?

The near-vertical seismic reflection experiment, which is focus of this work, addresses most of the afforementioned questions, especially those related to the deeper crustal structure. Concerning the shallow crustal structure of the DST, the results from the NVR experiment are combined with other relevant geophysical data and geologic observations at the surface.

The Arava Fault as main active branch of the southern DST is, at least partly, recognized on aerial photographs and satellite images because of its morphological expression. It can be traced across the alluvium, forming small, steeply dipping scarps, except where the fault is covered by sand dunes or recent alluvial fans. Pressure ridges and rhomb-shaped grabens, both related to strike-slip deformation, occur at various scales. In the young fluviatile sediments it is, however, hardly possible to make statements of the internal structure of the fault zone using geological methods. Even the scarce outcrops located at the fault do not exhibit the typical fault zone architecture – a main gouge zone, a fault related damage zone, and an undeformed host rock – that is well known from other fault studies (Chester and Logan, 1986; Chester *et al.*, 1993; Schulz and Evans, 1998; Faulkner *et al.*, 2003). Thus,
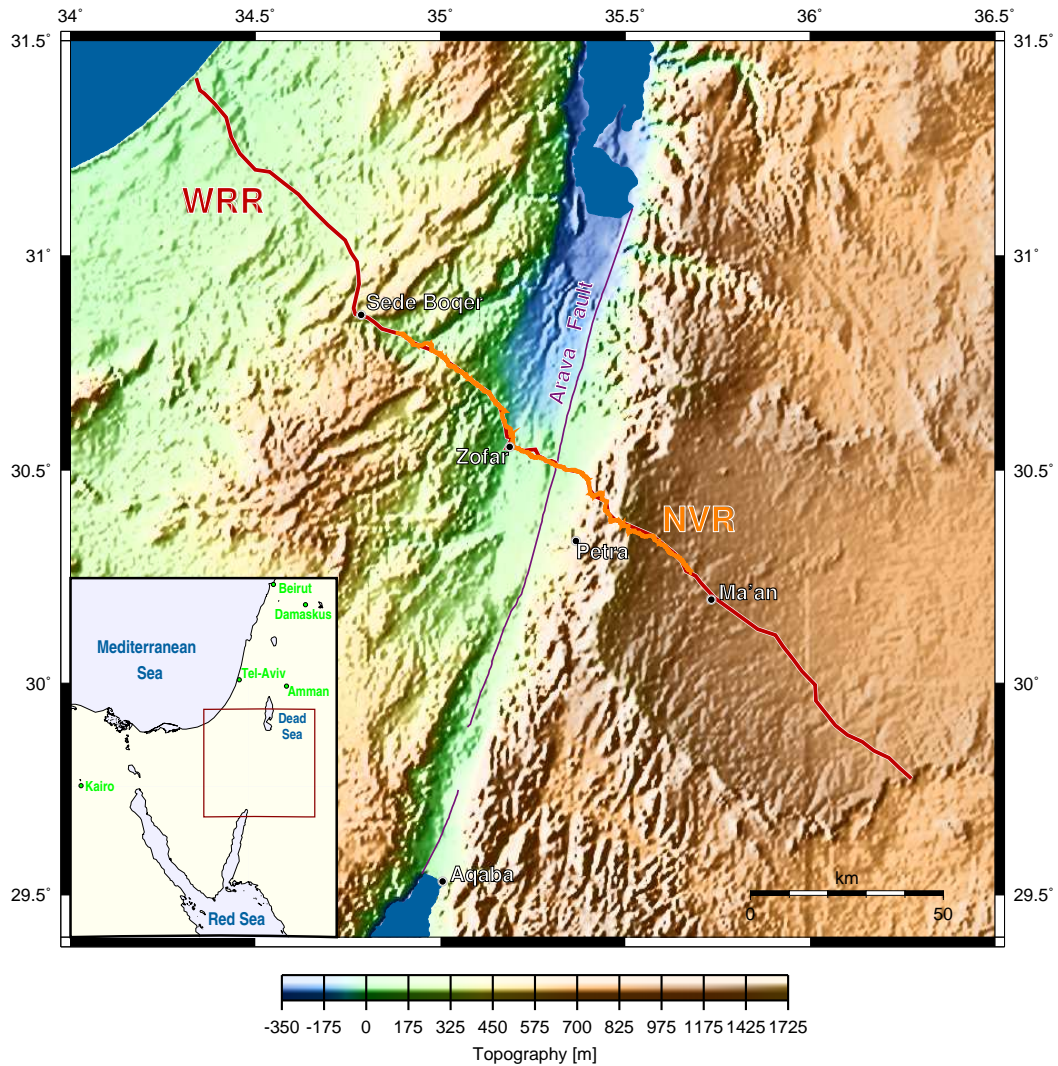
Figure 1.2: Location of seismic experiments within the DESERT project. Given in red is the wide-angle reflection/refraction (WRR) experiment, orange indicates the near-vertical seismic reflection (NVR) profile. The Arava Fault is schematically depicted in magenta.

high-resolution ASTER (Advanced Spaceborne Thermal Emission and Reflection Radiometer) images were used as a complementary tool to obtain some information on neotectonics and (near)surface geology. Related to the shallow subsurface structure as seen in the seismic data, the kinematic implications of the observations are discussed.

2 Geological Overview

2.1 Regional Geology

2.1.1 Geologic Evolution and Paleogeography

The study area is located at the northwestern edge of the Arabo-Nubian Shield (ANS), a block of continental crust that consists mainly of juvenile (i.e. mantle derived) Late Proterozoic rocks (Stoeser and Camp, 1985; Stern, 1994). Regarding both isotopic and chemical data of xenoliths, the involvement of older crustal material in the lower crust of the ANS seems highly improbable (Henjes-Kunst *et al.*, 1990; Ibrahim and McCourt, 1995; McCourt *et al.*, 1990; Stern, 1994). The ANS is part of the East African Orogen, which developed during the so called Pan-African Orogenic Cycle ∼950–600 Ma ago, and is one of the most voluminous events of juvenile crust formation on Earth. Its various structures constitute fossil fragments of a Neoproterozoic Wilson Cycle, representing the opening and closing of an ocean basin that lay between the older crustal blocks of East and West Gondwanaland (Stern, 1994; Kröner, 1984). During the late compressional stage of the Pan-African orogeny (∼715–630 Ma), terranes or microplates were accreted at the northeastern edge of the African Craton, associated with widespread calk-alkaline ('I-type') plutonism and metamorphism (Stoeser and Camp, 1985). Between ∼620–580 Ma the collisional tectonic regime was gradually replaced by extensional tectonics (Husseini, 1989). Fast erosion started 610 Ma ago and removed the upper 8–12 km of the crust within 20 Ma (Garfunkel, 2000). Molasse-like sediments formed while igneous activity continued, now having a mostly alkaline ('A-type'), intraplate character (alkali-rich granites and rhyolites). Linked to the A-type granites are extensive bimodal mafic to felsic dike swarms, that were emplaced 600–540 Ma ago (Kessel *et al.*, 1998) and that mark the extensional tectonic regime. On the base of NE–SW trending dikes and magmatic bodies being elongated in a NNE–SSW direction, a Late Pro-

terozoic rift axis being parallel to the recent DST was suggested by various workers ('geosuture concept', see e.g. Bender, 1968; Husseini, 1989). Stern *et al.* (1984) and Clark (1985) proposed a major rift boundary along today's Gulf of Aqaba in Late Proterozoic to Early Paleozoic times. Garfunkel (2000) assumed a regional dilation of ~20 km in NW–SE direction, as in many areas dikes comprise 5% of the country rocks, but did not see any evidence for a related Late Proterozoic continental rifting phase. NNE–SSW trending magnetic anomalies in the Neoproterozoic basement of Sinai and Jordan were interpreted as a 'basin-and-range' like environment by Segev *et al.* (1999).

A stable 'platformal stage' was established ~530 Ma ago (Garfunkel, 2000), with the position of the Arabian/Sinai region at the passive continental margin of the Gondwana supercontinent (Stampfli and Borel, 2002). The Phanerozoic evolution of the African-Arabian region principally reflects its location at this continental margin and is characterized by long-wave vertical movements and widespread transgressions and regressions associated with the polyphase break-up of Gondwana. Whereas during Cambrian and Ordovician times the region lay to the south of the Proto-Tethys ocean, Paleo-Tethys initial spreading began in the Late Silurian along the northern margin of Gondwana (Stampfli and Borel, 2002).

With the fragmentation of the Pangea supercontinent that started at the beginning of Mesozoic times with the opening of the Neo-Tethys, tectonic and paleogeographic conditions changed fundamentally in the Tethyan realm (Dewey *et al.*, 1973; Guiraud and Bosworth, 1999). The eastern Mediterranean basin developed by thinning of the continental crust, probably even break-up and spreading (Guiraud and Bosworth, 1999; Ginzburg *et al.*, 1979; Makris *et al.*, 1983; Ben-Avraham *et al.*, 2002; Garfunkel and Derin, 1984). At the same time the Levant was affected by uplift and magmatism, probably related to the Permo-Carboniferous Variscan tectonism. Various acid and basic igneous rocks were dated between 240 and 288 Ma in Israel and central western Sinai (Steinitz, 1980; Steinitz *et al.*, 1992), but the extent of magmatism during this period is unknown (Garfunkel, 1989).
The Jurassic as a period of major lithospheric extension is characterized by rifting in several regions around Gondwana (e.g. the opening of the central Atlantic Ocean in Early Jurassic times). Whereas open ocean conditions prevailed to the N and NE of the Levant and the Arabian peninsula, a shallow marine platform existed over large parts of the Middle East, with an uplifted, permanent continental area to the S and SE, resulting into predominantly NE–SW striking facies belts (e.g. Flexer, 2001; Garfunkel and Derin, 1984). Intraplate alkaline magmatism is

recorded in drillholes of central and northern Israel (Baer *et al.*, 1995; Segev *et al.*, 1996). Lithospheric extension and magmatic activity at the Levant margin (eastern Mediterranean), associated with strong uplift of southern Israel, continued in Early Cretaceous times (e.g. Garfunkel, 1992) and was followed by the two-phase 'Syrian Arc deformation'. The first compressive event was of Santonian to Senonian age and was caused by the beginning closure of the Neo-Tethys at this time (Walley, 1998). The second deformation phase began in the Late Eocene and probably ended in the Late Oligocene (Walley, 1998) and reflects the plate interior effects of the collision of the Arabian and Eurasian Plates and the formation of the Bitlis Suture zone (Hempton, 1985). These two mild compressional events resulted in the formation of the Central Negev–Sinai (Transjordan) shear belt — ENE to NE trending folds and E–W trending faults and folds, associated with some right lateral shearing — extending across Sinai and the Central Negev to 200 km east of the Dead Sea (Bartov, 1974, Fig. 2.1). Apart from some local relief produced by the Syrian Arc deformation, much of the Dead Sea region remained low and was covered by shallow-water marine sediments until late Eocene times (Garfunkel, 1997; Flexer, 2001).

With the Cenozoic continental break-up and the opening of the Red Sea in the Oligocene, the Arabian plate was separated from the African plate. The whole region, especially near the new plate boundaries and in particular the Arabian Shield, was uplifted and widespread igneous activity took place (Garfunkel, 1997). One of the newly forming plate boundaries was the Dead Sea Transform between the Sinai subplate to the W and the Arabian plate to the E.

2.1.2   History of the Dead Sea Transform and Related Structures

The Dead Sea Transform was activated after initiation of rifting along the Red Sea–Gulf of Suez trend (Garfunkel, 1981). Its total left-lateral offset of 105 km was determined by matching the known features of the Pan-African basement, the facies and thickness variations within the Phanerozoic sediments, as well as tectonic structures across its trace (Quennell, 1959; Freund, 1965; Freund *et al.*, 1970). Especially the lineaments of the Central Negev-Sinai shear belt (Bartov, 1974, Fig. 2.1) as well as magnetic anomaly patterns (Hatcher *et al.*, 1981) can be rather accurately matched by the restoration of 105 km relative plate motion. The beginning of the motion is constrained by a system of northwest trending dikes and small intrusions along the Red Sea and Gulf of Suez, which formed 25–20 Ma ago and which are displaced by the entire transform offset.

After previous plate kinematic studies by Quennell (1959), Freund *et al.* (1970) and Le Pichon and Francheteau (1978), Garfunkel (1981) interpreted the southern part of the DST as 'leaky' because of a small component of transverse, i.e. E–W, extension. By structural analysis two distinct phases of slip were determined (see Fig. 1.1 for the Eulerian poles), with ∼30 km displacement during the late phase (0–5 Ma), in which transverse extension has probably been much more dominant than in the early phase (Garfunkel, 1981; Joffe and Garfunkel, 1987).

The estimated slip rate along the southern DST varies between 1–10 mm/a. Whereas Joffe and Garfunkel (1987) came to a value of 6–10 mm/a from the analysis of plate kinematics, Klinger *et al.* (1999, 2000b) determined a rate of 4±2 mm/a from offset sediments in the Arava Valley. Looking at translocated Pliocene drainage systems also located in the Arava Valley, Ginat *et al.* (1998) found a 3–7.5 mm/a slip rate. A GPS based estimate of the current plate motion of 2.6±1.1 mm/a (Pe'eri *et al.*, 2002) is in agreement with the 1–3.5 mm/a rates derived from short term and historic seismicity (Ben-Menahem and Aboodi, 1981; Salamon, 1993).

At the northern half of the transform, in Lebanon and further northward, transverse compression dominates and the transform margins are supposed to act non rigidly (Garfunkel, 1981). The amount of sinistral offset has been controversially debated in the literature, probably due to the fact that older, pre-Mid Cenozoic, geological features are not orthogonally crossed by the DST but rather strike subparallel to it (Khair, 2001). Nonetheless the total left-lateral displacement is considerably less than along the southern half of the transform, with suggested values

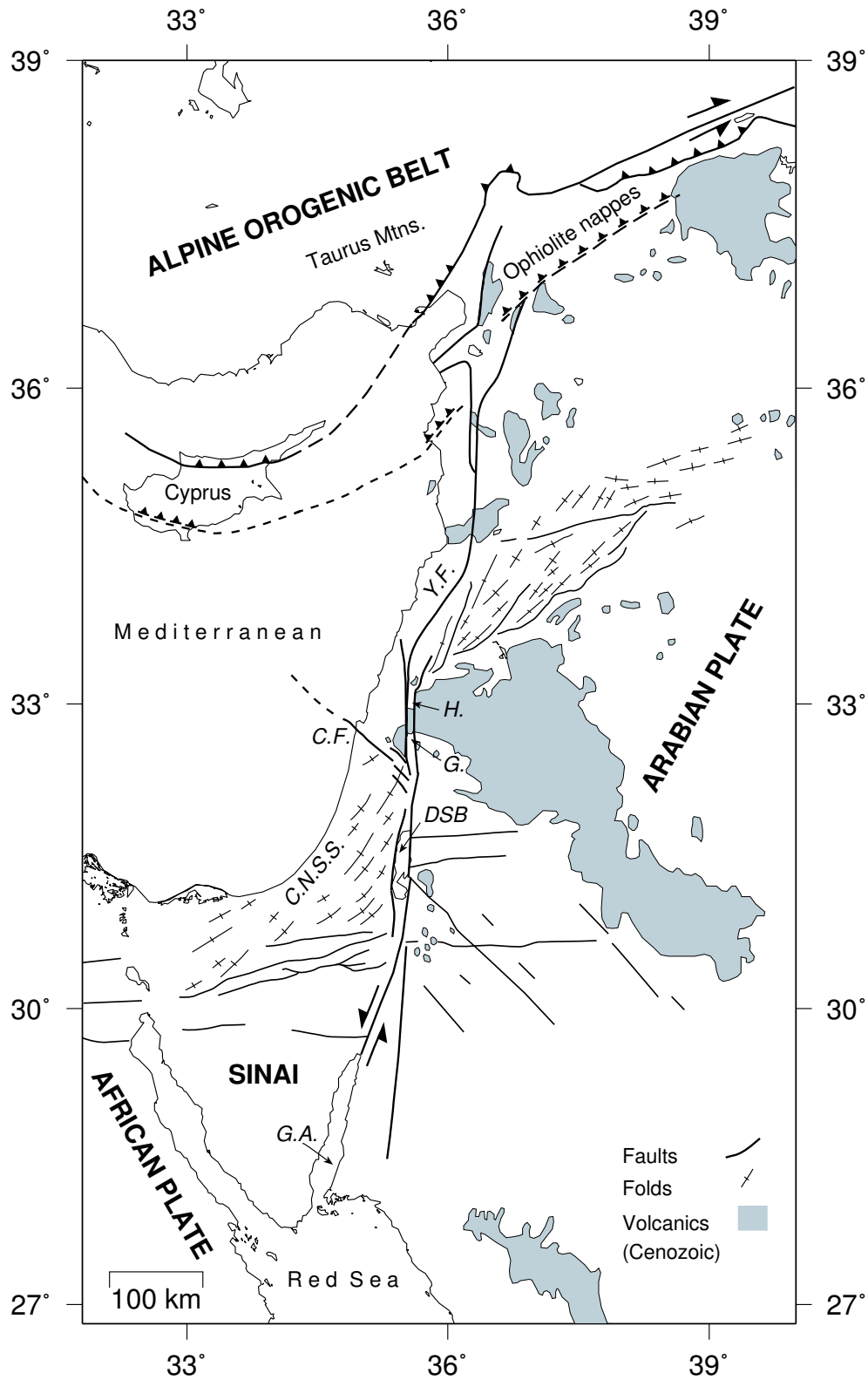Figure 2.1: Setting of the Dead Sea Transform; after Garfunkel (1981).
C.F.: Carmel Fault; *C.N.S.S.:* Central Negev-Sinai shear belt; *DSB:* Dead Sea Basin; *G.:*
Sea of Galilee; *G.A.:* Gulf of Aqaba; *H.:* Hula Valley; *Y.F.:* Yammouneh Fault.

around 10–30 km (Quennell, 1984), 50 km (Walley, 1998), 60 km (Khair, 2001) and 70 km (Freund *et al.*, 1970). An unknown part of the deformation is probably taken up by shortening in the Palmyrides and vertical and lateral tectonism along several faults in Lebanon and Galilee (Walley, 2001).

Between the Sea of Galilee and the Dead Sea Basin numerous NW–SE trending small faults branch out from the Jordan Valley, being part of the Carmel fault zone, that continues off-shore into the Mediterranean (Ginzburg and Ben-Avraham, 1987; Hofstetter *et al.*, 1996, Fig. 2.1). This seismically active zone has a complex history of strike-slip faulting, rigid block rotations and normal faulting and was probably created as a continental failed rift at the Triassic–Jurassic rifting event of the Neo-Tethys (Achmon and Ben-Avraham, 1997, and references therein).

2.1.3   Morphology of the Dead Sea Transform

In Lebanon the DST bifurcates into several fault branches, the most prominent being the Yammouneh and the Roum faults (e.g. Butler *et al.*, 1997; Garfunkel *et al.*, 1981; Khair, 2001; Walley, 1988, 1998, Fig. 2.1). At a major bend to the right, the left-lateral displacement has generated considerable compression and has produced a large uplift of the region (Quennell, 1959; Freund, 1965).

At its southern part the DST is dominated by transtensional features, resulting from left steps of the main fault trace. Both the Dead Sea Basin, the Sea of Galilee and the Hula Valley are interpreted as pull-apart basins, with the Dead Sea Basin (over 130 km long, 7–18 km wide and with a more than 10 km thick sedimentary fill of Neogene to Quaternary age) being the most prominent (e.g. Garfunkel *et al.*, 1981; Garfunkel, 1997; Garfunkel and Ben-Avraham, 2001). Also the southern extension of the DST in the Gulf of Aqaba is defined by three rhomb-shaped pull-aparts (Ben-Avraham *et al.*, 1979; Ben-Avraham, 1985) and might represent a transition between the Red Sea spreading centre and the DST.

The DST in the Arava Valley   The Arava Valley between Red Sea and Dead Sea is characterized by a relatively narrow, 10–20 km wide valley, that is bordered by marginal normal faults and elevated flanks. Whereas at first sight it might resemble a classical rift valley, its morphology can generally be explained by left-lateral transform motion (Garfunkel, 1981; Sobolev *et al.*, 2004).

The primary active fault of the southern DST is the Arava Fault (AF). Where it
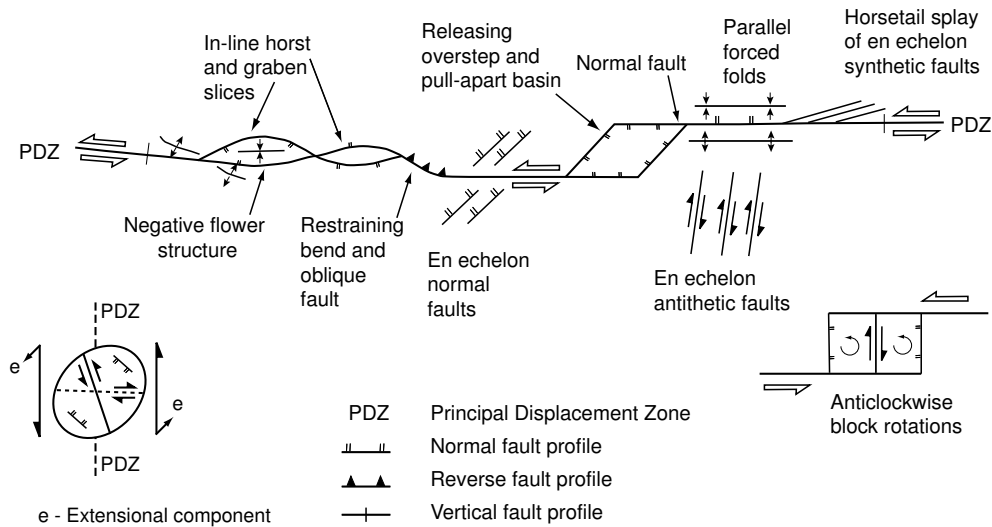
Figure 2.2: Schema of structures associated with divergent strike-slip faults (top) and simplified strain ellipse (bottom left) for sinistral strike-slip deformation. The assemblage is a composite of features that can be developed along strike-slip faults and that may be combined in various ways; modified after Harding *et al.* (1985).

is not covered by sand dunes or recent alluvial surfaces, the fault shows a sharp morphological discontinuity and can easily be traced across the alluvium (e.g. Garfunkel *et al.*, 1981; Klinger *et al.*, 2000a). Especially on satellite images and aerial photographs its surface trace is quite pronounced (see also chapter 4). At small left and right steps or bends of the fault trace, tensional and compressional features are developed on various scales (e.g. Garfunkel *et al.*, 1981; Klinger *et al.*, 2000a, Fig. 2.2). This and also the rather straight, N18°E striking AF are consistent with predominantly strike-slip motion (Garfunkel *et al.*, 1981). There are, however, numerous other subparallel faults flanking the Arava Valley that also show evidence of dip-slip motion and thus exhibit a small component of transverse extension (e.g. Garfunkel *et al.*, 1981; Bartov *et al.*, 1998). Garfunkel (1981) estimated the amount of transverse extension to be in the range of 3–4 km in the southern Arava. This value is also supported by thermo-mechanical modelling of this area (Sobolev *et al.*, 2004).

In consideration of 15–12 Ma old marine beds on the western side of the transform and some evidence from the eastern flank of the Dead Sea Basin, most of the uplift along the Arava Valley seems to have occurred in post-Miocene times (Garfunkel, 1997).
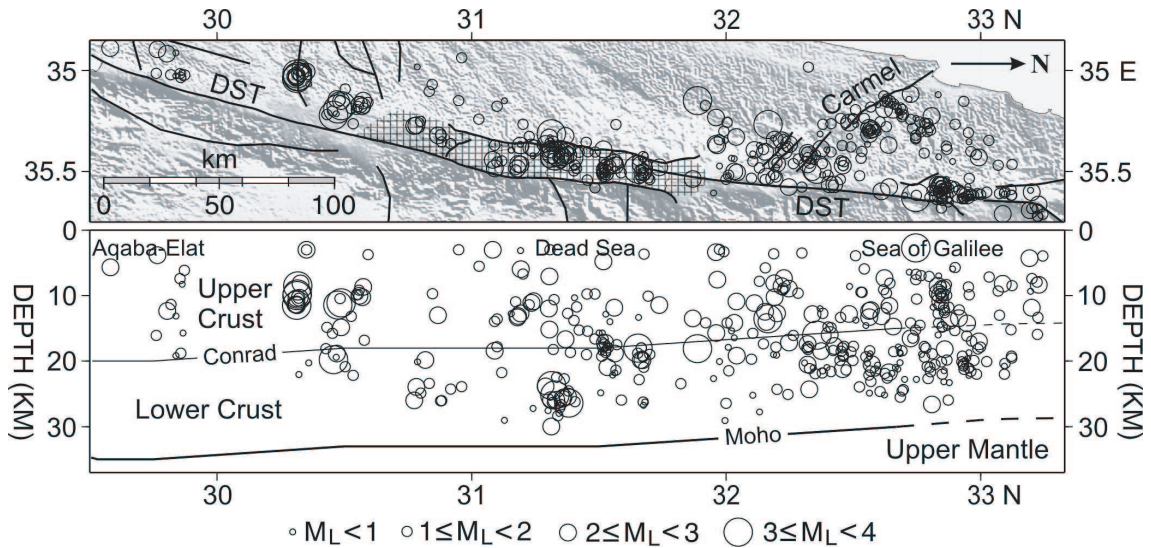
Figure 2.3: Microseismicity of the Arava Valley; depth section of 410 well-constrained earthquakes (1984–1997) recorded by short-period stations of GII (Israel) and JSO (Jordan); from Aldersons *et al.* (2003).

2.1.4 Seismicity

The Dead Sea Transform is a seismically active plate boundary at which large historical earthquakes with recurrent magnitudes of M 6–7 have occurred (Abou Karaki, 1987; Ambraseys *et al.*, 1994). But whereas in the fault segment north of the Dead Sea Basin a minimum of ten such earthquakes are thought to have occurred in the last 1000 years (Abou Karaki, 1987; Ben-Menahem, 1991), along the 160 km long Arava Fault segment only four events are reported during the same time period (Abou Karaki, 1987; Ambraseys *et al.*, 1994; Klinger *et al.*, 2000a; Zilberman *et al.*, 1998), in spite of its significant slip rate (see above). This may suggest a particular seismic behaviour, possibly with infrequent, very large earthquakes, aseismic creep or time clustering (Ambraseys *et al.*, 1994; Marco *et al.*, 1996). On the base of offset geomorphic features Klinger *et al.* (2000a) infer, that earthquakes with a moment magnitude of M_w ~7 should occur along some fault segment in the Arava Valley every 200 years. They do not rule out, however, the possibility of time clustering of earthquakes over longer timespans or an alternative seismic behaviour with M_w ~7.6 earthquakes about every 600 years and M_w ~7 earthquakes about every 250 years.

The last big (M_w=7.3) earthquake occurred in the Gulf of Aqaba and is probably related to three swarms that were documented in the same region in 1983, 1990 and 1993 with magnitudes reaching at most M_w=6.1 (Klinger *et al.*, 1999).
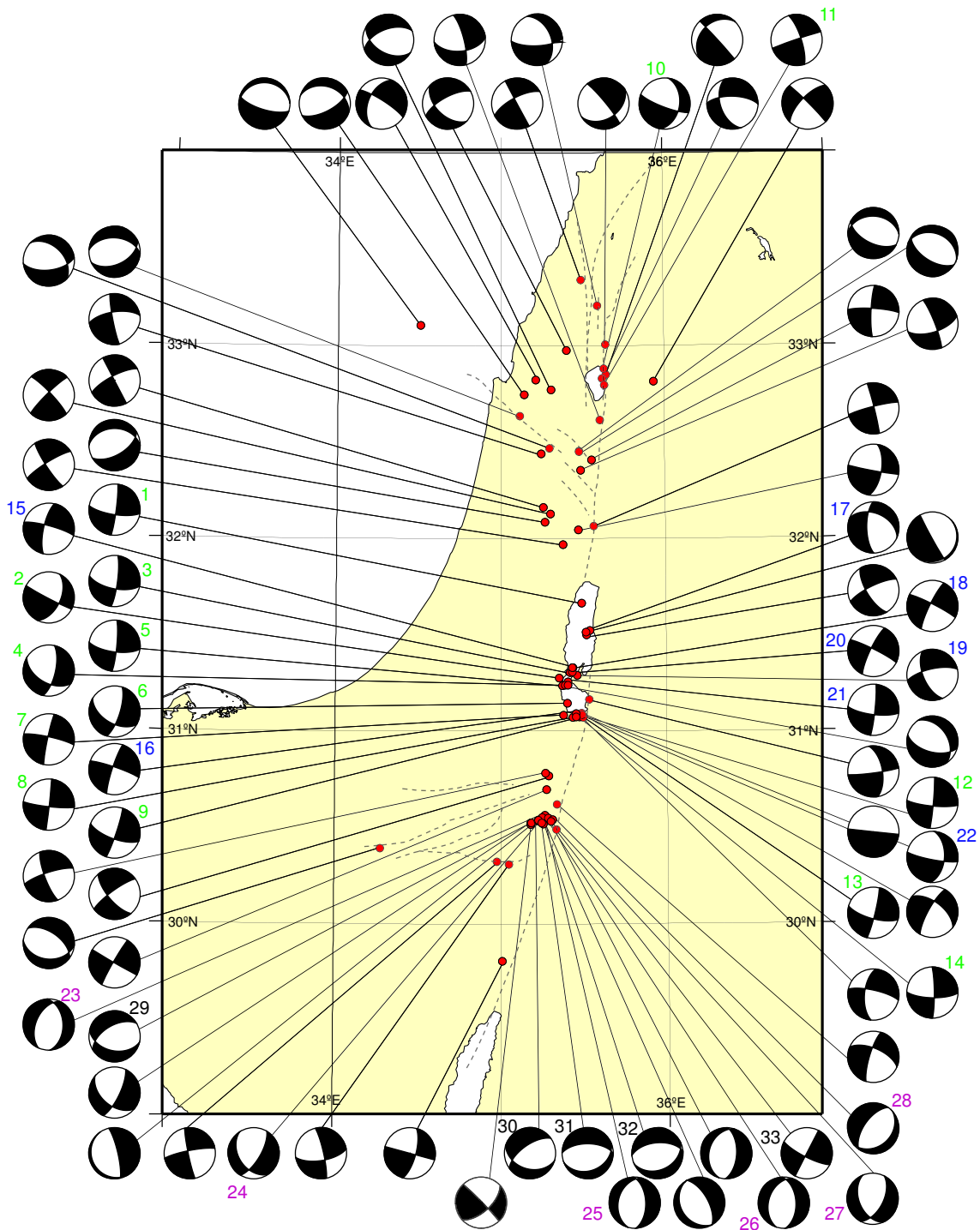
Figure 2.4: Focal mechanisms in the Arava Valley that were derived from inversion of 78 microearthquakes recorded between 1987 and 1996, with a threshold magnitude $M_L \sim 2$. Note that not the entire microseismic activity is presented in the figure, but only these events that satisfy both localization and polarity tests; from Klinger (1999). See text for details.

Microseismicity   Despite the already mentioned lack of recent strong earth-
quakes, some clear microseismic activity has been recorded along the southern half
of the DST in the last two decades (van Eck and Hofstetter, 1990; Aldersons *et al.*,
2003, Fig. 2.3). These studies show, that most of the seismic acticity is related
either to the DST or to the Carmel fault zone. Earthquake epicentres along the
DST seem to cluster in space and could be associated with left steps of the DST
(van Eck and Hofstetter, 1990). Fault plane solutions reveal mainly strike-slip fault-
ing along the southern DST (Klinger, 1999, Fig. 2.4). Whereas several events exhibit
left-lateral movement along ∼N–S trending faults (15–22 in Fig. 2.4), other focal
mechanisms suggest right-lateral movement along ∼E–W trending faults (1–14 in
Fig. 2.4) (Klinger, pers. comm., 2003). These antithetic dextral faults are in
accordance with deformation mechanisms in sinistral strike-slip regimes and could
accomodate anticlockwise block rotations between overlapping strike-slip faults (Fig.
2.2).

Another prominent microearthquake cluster is located in the Paran/Zofar area
(∼30.5°N) and lies ∼5–10 km west of the Arava Fault (Fig. 2.3; see also Fig. 2.5).
Compared to the events at the DST, the focal mechanisms of this area show a
greater variability (Fig. 2.4): events 29–32 are related to normal faulting along E–
W striking fault planes; one earthquake (event 33) is associated with right-lateral
strike-slip motion; other focal mechanisms (events 23–28) include left-lateral strike-
slip faulting and normal faulting along ∼N–S trending fault planes (Klinger, pers.
comm., 2003). The complex microseismicity pattern of this area might result from
an interaction of (older) faults of the Central Negev–Sinai shear belt (e.g. Paran
and Ramon faults; Fig. 2.5) with the DST faults (e.g. Baraq and Zofar faults; Fig.
2.5).

Aldersons *et al.* (2003) showed, that 60% of the microearthquakes between 1984
and 1997 with a local magnitude $M_L \leq 3.2$ nucleated at a depth of 20–32 km,
whereas the upper mantle seemed to be aseismic (Fig. 2.3). They concluded that
a cool and brittle lower crust would be consistent with the low heat flow of 40
mW/m². Contrary to a brittle lower crust, Al-Zoubi and ten Brink (2002) and
ten Brink (2002) suggested lower crustal flow as viable deformation mechanism in
the lower crust of the Dead Sea Basin.

2.1.5 Stress Field

The determination of orientation of a paleostress field is often based on the analysis of fold axes, faults, tabular magmatic intrusions, volcanic lineaments, joints, veins, and tectonic stylolites, whereas the recent to subrecent stress field is usually defined by stress indicators like focal plane solutions of earthquakes, hydraulic fracturing, borehole breakouts and young geological features (Zoback, 1992). Looking at recent stress data from the Sinai subplate, Badawy and Horváth (1999) determined the average direction of maximum horizontal stress (S_H) to be NW (N54°W). This is generally in agreement with other studies (e.g. Garfunkel *et al.*, 1981; Zaineldeen, 2000; Reinecker *et al.*, 2003).

A more complicated picture of stress field fluctuations along the DST was given by Eyal (1996). Also taking into account the results of an earlier study (Eyal and Reches, 1983), he came to following conclusions:

(1) WNW shortening and NNE extension, beginning in the Turonian, is associated with the development of the Syrian Arc fold belt and attributed to the Syrian Arc stress field (SAS).

(2) Middle Miocene to recent NNW shortening and ENE extension is associated with the opening of the Red Sea and the sinistral displacement along the DST and is attributed to the Dead Sea stress field (DSS).

(3) The DSS is thought to be a short-term, time-limited stress field that is occasionally superimposed on the long-term, background, plate-scale SAS stress field.

2.1.6 Recent Magmatic Activity

Coeval with the separation of Arabia from Africa was widespread basaltic magmatism that can broadly be divided into two main stages (Garfunkel, 1989). During the first stage extensive Oligocene flood volcanism occurred at the Afro-Arabian triple junction in Yemen, Ethiopia, Eritrea and Djibouti, associated with continental extension and the presence of a mantle plume in the Afar region (e.g. Camp and Roobol, 1992; Baker *et al.*, 1996). Also the latest Oligocene to Early Miocene Red Sea dike system might be connected to these volcanics. The second, Miocene to recent phase, produced numerous intraplate volcanic fields along the western margin of the Arabian Peninsula (in Israel, Jordan, Saudi Arabia, Syria

and Yemen; Fig. 2.1). Although being extensive, this Late Cenozoic intraplate vol-
canism is volumetrically insignificant compared to Oligocene flood basalts in Yemen
and Ethiopia (12,000 km^3 versus 350,000 km^3, Shaw *et al.*, 2003). Regarding magma
genesis and geodynamic implications of volcanism in NW Arabia the situation is less
clear than in the Afar region (Camp and Roobol, 1992; Shaw *et al.*, 2003). Whereas
Camp and Roobol (1992) suggested that a part of the Afar plume might have been
channelled northwards, Shaw *et al.* (2003) recognized subtle chemical and isotopi-
cal differences between volcanism in Yemen and Jordan. Therefore they proposed
melting of lithospheric mantle in response to lithospheric extension as the source of
Jordanian intraplate volcanism. If lithospheric extension is a relatively young phe-
nomena, it would not be reflected in high heat flow anomalies yet (e.g. Stein *et al.*,
1993, and S. Sobolev, pers. comm., 2003).

Lithospheric thinning beneath Arabia has also been put forward on the basis of
geophysical data. With a receiver function study Hofstetter and Bock (2003) deter-
mined the lithospheric thickness beneath the DST to be in the range of 60 km. This
is in accordance with the results of thermo-mechanical modelling by Sobolev *et al.*
(2004) who suggest that young (< 20 Ma) thinning of the lithosphere by thermal
erosion or delamination might be responsible for the uplift of the Arabian plate.
Whether or how this lithospheric thinning is related to the DST remains unclear.
It was suggested by Garfunkel (1981), that a thinner lithosphere beneath Arabia
could have been the reason, why the Arabian-African plate boundary developed at
its recent location along the DST and did not continue as straight spreading cen-
tre from the Red Sea along the Gulf of Suez. The Gulf of Suez was already well
developed in Early Miocene times.

2.2   Geology Along the NVR Profile

The wide-angle seismic refraction/reflection (WRR) experiment, in which the near-vertical seismic reflection (NVR) experiment was embedded, extended from the Jordanian highlands beyond Ma'an in the SE to the Mediterranean coast at the Gaza strip in the NW (Fig. 1.2). There is a gradual transition from the continental crust of the ANS with thicknesses of 35–40 km (El-Isa *et al.*, 1987; Makris *et al.*, 1983; Al-Zoubi and Ben-Avraham, 2002) to the crust of the eastern Mediterranean, that is assumed to be partly underlain by typical oceanic crust with thicknesses smaller than 10 km (Ginzburg *et al.*, 1979; Makris *et al.*, 1983; Ben-Avraham *et al.*, 2002). On top of the Precambrian basement usually follows an Infracambrian to Early Cambrian volcano-sedimentary succession of variable thickness. Whereas coarser clastics (Saramuj and Elat conglomerate) are restricted to fault-bound basins along the Arava Valley, finer clastics, mostly consisting of arkosic sandstones and associated volcanics (Zenifim Formation, Haiyala Volcaniclastic Unit and equivalent rock units) have been found in large parts of the Israeli and Jordanian subsurface (Weissbrod and Sneh, 2002). In boreholes close to the WRR and NVR profiles the Zenifim Formation was determined to be several hundreds of metres thick (>500 m in Maktesh Qatan, and >2500 m in Ramon-1; Fig. 2.6), though its base has not been encountered in any of the Israeli boreholes. The position of the study region at the northwestern edge of the ANS, i.e. at a passive continental margin since early Paleozoic times, is reflected in facies changes and varying sedimentary thicknesses along the seismic reflection/refraction profiles (Fig. 2.6 and Fig. 2.5). Thus the Phanerozoic along the northwestern part of the profile is dominated by Cretaceous and Tertiary rocks underlain by Jurassic, Triassic and Permian sequences that thin out towards the east. East of the Dead Sea Transform, however, Permian to Triassic strata is missing and Lower Cretaceous rocks unconformably overlie Ordovician and Cambrian sandstones. The crystalline basement rocks (rhyolites and calc-alkaline granitoids) cropping out in the Jebel Humrat Fiddan area east of the DST are thought to be equivalent to the basement rocks of the Timna region in Israel.

Apart from the Arava Fault and related structures, some major faults of the Central Negev–Sinai shear belt are either crossed by or close to the NVR profile (Fig. 2.5). Whereas the character of the Sa'ad Nafha Fault is not clear, the Ramon and Paran faults are both dextral strike-slip faults, that are probably still active (Bartov, 1974, Bartov, pers. comm., 2003). In Jordan the Salawan Fault constitutes the southern limit of the 'Dana Horst' (Fig. 2.5). It is a major, steeply dipping
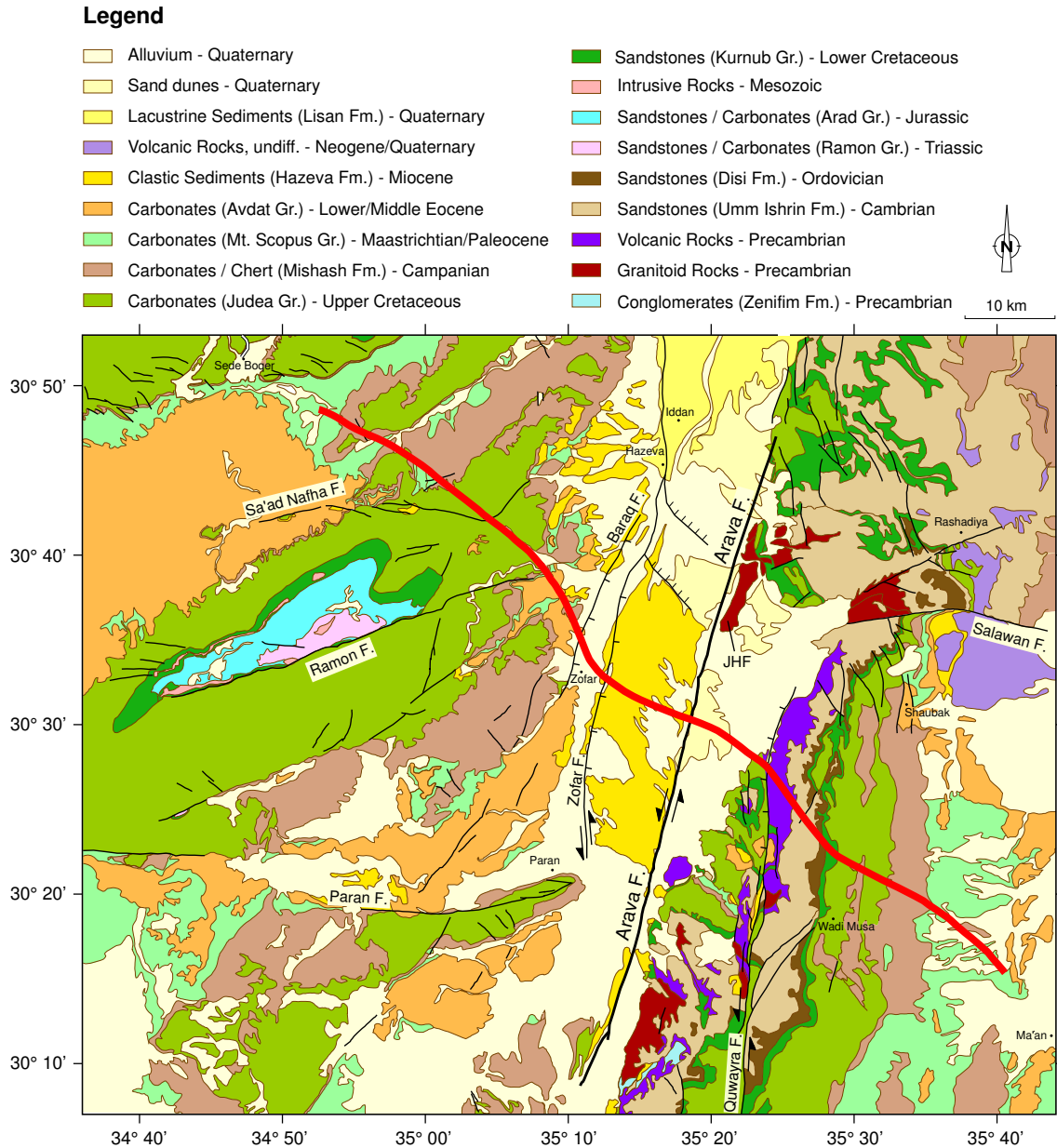
Figure 2.5: Geological map of the NVR profile area (compiled after Sneh *et al.*, 1998; Bender *et al.*, 1968; Frieslander, 2000). Given in red is the NVR common depth point line; JHF: Jebel Humrat Fiddan.
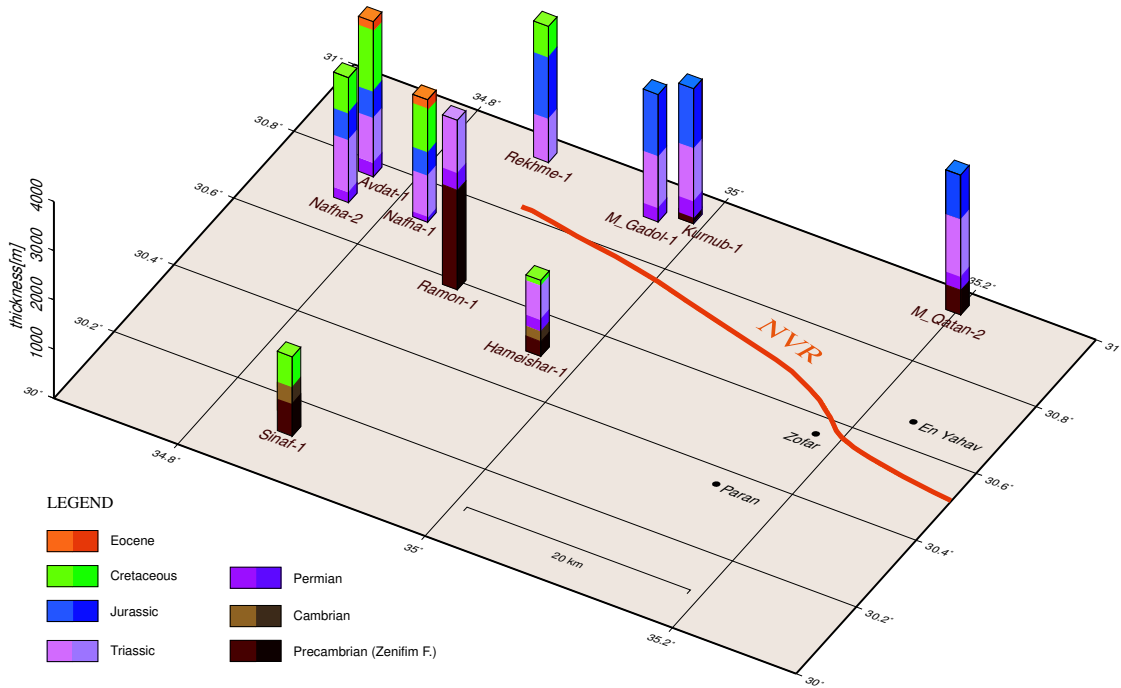
Figure 2.6: Compilation of Israeli deep wells in the vicinity of the NVR profile. Data from Fleischer and Varshavsky (2002).

fault with a vertical displacement of up to 900 m (downthrow to the south) and a suggested dextral movement of ∼7 km since the Tertiary (Barjous, 1992). Toward the east it continues in an ∼E–W direction over hundreds of kilometers into Saudi Arabia, where it is also known as Salawan–Zakimat al Hasa Fault. Barjous (1992) gave some evidence that this fault already existed as weakness zone during Precambrian times and was later rejuvenated, showing activity during the Neogene. The Salawan Fault seems to be the eastern extension of the E–W striking Themed Fault in southern Israel (Bartov, pers. comm., 2003). This gets obvious by restoring the 105 km left-lateral movement along the DST.

North of the Ramon Fault the 'Maktesh Ramon' represents an erosional valley ('crater'), that formed along an anticlinal axis. Its main incision is thought to have occurred during the Pliocene (Ben-David *et al.*, 2002).

3 The Near-Vertical Seismic Reflection Experiment (NVR)

3.1 The Seismic Reflection Method

The essence of the seismic reflection technique is to measure the time a seismic wave requires to travel from a source (at a known location at or near the surface) down into the ground where it is reflected back to the surface and detected at a receiver which is also at or near the surface at a known position (Reynolds, 1997). This time is known as two-way travel time (TWT). In seismic reflection surveys a seismic wave is usually generated by an impulsive source (e.g. explosive, airgun) or by a time-distributed source (e.g. hydraulic vibrator) and detected by geophones or hydrophones[*] . For a seismic wave to be reflected back to the surface, there has to be a subsurface interface across which there is a contrast in acoustic impedance $Z = v\rho$ (where v is the seismic velocity and ρ is the density of the layer).

The amplitude of the reflected wave depends on the impedance contrast between two layers and is described by the reflection coefficient R. For normal and low angles ($< 20°$) of incidence is:

$$R = A_1/A_0 = (Z_2 - Z_1)/(Z_2 + Z_1) = (v_2\rho_2 - v_1\rho_1)/(v_2\rho_2 + v_1\rho_1)$$
$$|R| \leq 1.$$

where A_1 is the amplitude of reflected ray, A_0 the amplitude of the transmitted ray, Z_1 the acoustic impedance of layer 1 and Z_2 the acoustic impedance of layer 2. Typical values of R are between <0.1 (weak reflection), 0.1–0.2 (moderate reflection), and >0.2 (strong reflection). The reflection raypaths over a single horizontal

---

[*]Geophones convert ground motion into electrical voltage by the relative motion between a sprung coil and a magnet. As only P (compressional) waves are of interest in standard seismic acquisition, the geophones ideally only record vertical particle motion. Hydrophones measure variations in water pressure as changes in voltage by means of two matched piezo electric crystals.
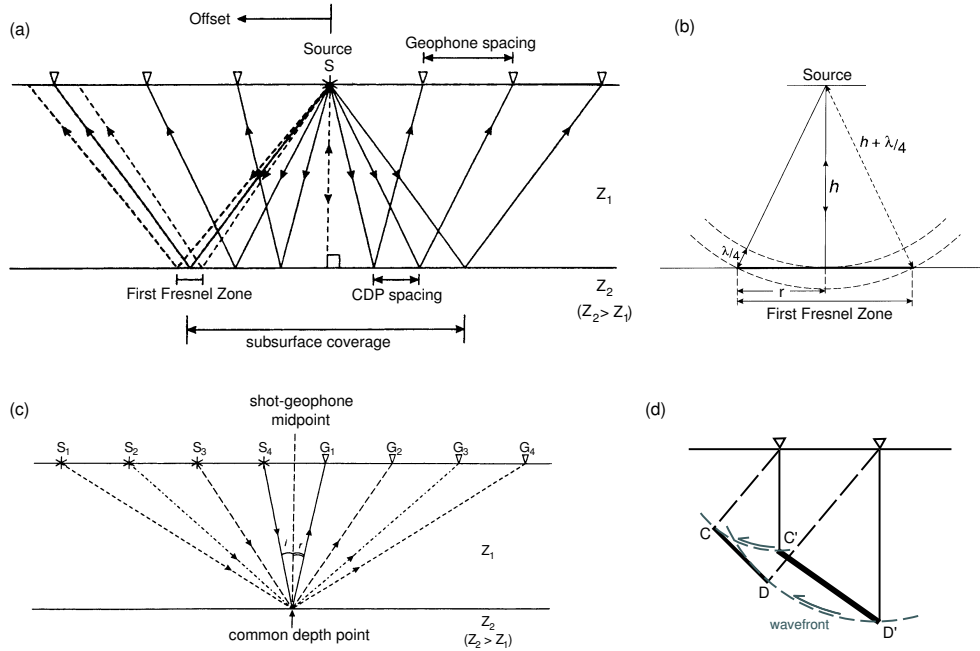
Figure 3.1: Principles of seismic reflection method. (a) Schema of reflection raypaths over a single horizontal interface; (b) First Fresnel zone on a reflector at a depth h; (c) Common depth point principle; (d) Principle of migration: The reflection segment C'D' in time section is moved updip, steepened, shortened and mapped onto its true subsurface location CD; modified after Reynolds (1997) and Yilmaz (1987).

interface are shown schematically in Fig. 3.1a.

Although seismic interfaces can most of the time be correlated with geological boundaries, they might also result from an impedance contrast within the same lithological unit. At the same time a change in stratigraphy will not cause a seismic reflection if it is not concurrently related to an impedance contrast.

The lateral resolution depends on both the depth of the reflector below the source (h) and the wavelength of the incident wave (λ) and is generally given by the size of the first Fresnel zone (e.g. Sheriff and Geldart, 1986, , Fig. 3.1b). Following Huygen's principle, the two elemantary waves emanating from the source foot point (i.e. the point directly below the source) and from a point located at a distance r from this footpoint interfere constructively, if their phase difference equals π. As two-way travels times are considered, the path difference must equal $\lambda/4$ instead of $\lambda/2$, leading to $r^2 = \lambda h/2 + \lambda^2/16$ (Fig. 3.1b). For $\lambda \ll h$ the radius of the first

Fresnel zone is given by

$$r \approx (h\lambda/2)^{1/2} = (v/2)(t/f)^{1/2}$$

where h is the depth of the reflector, λ the dominant wavelength, f the dominant frequency of the incident wave, v its propagation speed and t the two-way travel time. This implies that the lateral resolution decreases with depth as the radii of the Fresnel zones get larger.

A seismic survey comprises a line or spread of recording stations that are set at regular distances away from the source. If more than one source location is used, reflections from the same point on a subsurface interface are detected at different receiver locations (Fig. 3.1c). This common point of reflection is known as the common depth point (CDP). Its equivalent at the surface is the shot-geophone midpoint, the common midpoint (CMP). Usually all recorded traces are sorted by CDPs, corrected for time and amplitude, and displayed as a single stacked trace. The number of traces imaging the same CDP is known as the fold of coverage. During stacking it is assumed that the reflection is derived from a point directly below the receiver. This, however, is not true for dipping or curved events, as shown in Fig. 3.1d. It is the objective of seismic migration to shift reflections to their true position. This leads at the same time to a higher spatial resolution, as migration tends to reduce the Fresnel zone to approximately the dominant wavelength (Stolt and Benson, 1986, for a detailed discussion of this issue see e.g. Yilmaz, 1987).

For digital recording of seismic signals, which are originally continuous in time, the sampling rate is a crucial point, i.e. the (constant) time interval between amplitude measurements of the signal. If a signal is insufficiently sampled, high-frequency components present in the originally analog signal may be lost. Aliasing, i.e. the occurrence of artificially low frequencies, is a direct consequence of undersampling. The frequency below which aliasing does not occur is termed Nyquist frequency and is the reciprocal of one half of the sampling rate. In most seismic reflection studies sampling intervals range between 1 and 5 ms. For a sampling rate of $\Delta t = 5$ ms, the highest frequency that can be reproduced without distortion is $f_{Nyquist} = 1/(2\Delta t) = 100$ Hz. To eliminate distorted frequencies from the data, a high-cut anti-aliasing filter is applied before analog-to-digital conversion of a seismic signal occurs. Typically this filter has a cut-off frequency that is three quarters to half of the Nyquist frequency (Yilmaz, 1987).

The various processing steps required in seismic reflection surveys will be illustrated on the basis of the NVR data in the following.

3.2 The Near-Vertical Reflection Study within DESERT

3.2.1 Experiment Set-up

The near-vertical incidence reflection experiment was carried out during March 2000. The profile line is located between Sede Boqer/Israel and Ma'an/Jordan and coincides with the inner 100 km of a wide-angle reflection/refraction profile (Fig.1.2). Whereas a vibroseis survey with good energy penetration, dense CDP spacing and high subsurface coverage was aimed to image the entire crust, a few explosive shots, with a single-fold coverage along the line, should yield reflections from the deeper crust and the upper mantle.* Due to the rough terrain, poor infrastructure, natural and military protection areas and only a few locations at which border crossing was possible, a straight profile line was not attainable. However, with a general NW-SE trend of the line, the Arava Fault as the main fault of the southern DST system was crossed almost perpendicularly (Fig.3.2).

Compared to the conventional method of seismic reflection surveying with multi-channel recording systems controlling both sources and receivers along the entire line, the DESERT NVR experiment availed itself of a different technique: A large number of digital seismic recorders built the seismic line and recorded permanently during source activities. Continuous GPS monitoring of both sources and receivers allowed exact time control. In a 'roll-along' procedure the 18 km long active spread was shifted 3.6 km along the line per day. The measurements were carried out during the afternoon and night, with six vibrators from the Geophysical Institute of Israel (GII) acting as sources along the inner 7 km of the spread. The detailed acquisition parameters are shown in Table 3.1.

3.2.2 Data Processing

Using the absolute GPS shot times, the seismic traces with the desired recording length were cut from the continuously recorded time series. Thus, uncorrelated, ver-

---

*Compared to the vibroseis data, the quality of the explosive shot data was extremely poor, with no clear reflections from the lower crust, the crust/mantle boundary or the upper mantle. The very dry ground and highly scattered energy in the shot holes are a possible explanation for the poor data quality. In consideration of its very limited potential regarding interpretation, the NVR explosive shot dataset will not further be mentioned.
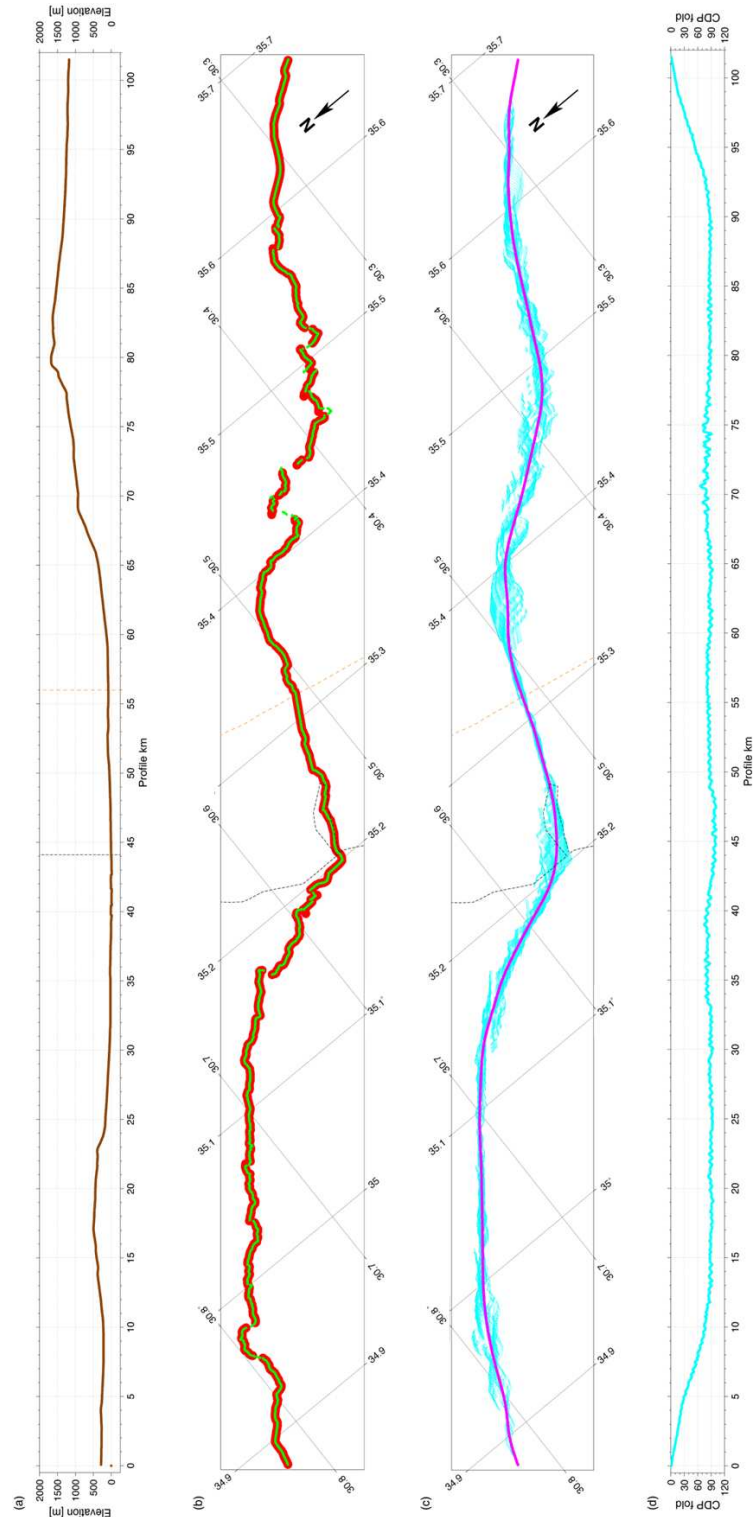
Figure 3.2: Geometry of the DESERT NVR line. The AF is represented as dashed orange line, the Israeli/Jordanian border as dashed black line. (a) Elevation profile with a length-to-height exaggeration of 1:3; (b) Source/receiver geometry. Geophone locations are displayed in red, vibrator locations in green; (c) More than 300'000 subsurface CMP points (cyan) are projected onto a smoothly curved CDP line (magenta); (d) CDP coverage along line.

Recording Parameters		**Source specifications**	
Recording period	1st March – 2nd April 2000	**Vibroseis** (Geophysical Institute of Israel, Lod, Israel)	
Recording area	Sede Boqer (IL)→Ma'an (HKJ)		
Recording systems	30 Teledyne PDAS-100	Number of vibrators	5 - 6 (260,000 lbs total peak force)
	seismological recorders	Recording length	24 s sweep + 18 s listening time
	(6 channels + GPS-clock,	Sweep range	10 - 48 Hz linear
	1 GigaByte hard disk)	Configuration	asymmetrical split-spread
Sample rate	5 ms, continuously recording		(-9 km...[-3.4 km...VP...3.4 km]...9 km)
		Vertical fold	10 vibrations/point, 100 m pattern
Deployment/Data collection	8 – 14 o'clock	Source spacing	50 m
Shooting/Vibrating	14 – 24 o'clock	Number of source points	1,734 (70 VPs per day)
		Subsurface coverage	90 fold
Profile length	125 km along geophone line,	Data amount	17,260 sweeps x 180 channels x
	102 km along CDP line,		8,600 samples = 3.1 million traces
	99 km as the crow flies		= 106.8 GByte
Profile direction	NW → SE		
		Explosive (Site Group, Chemical & Mining Ind., Amman, Jordan;	
		Geophysical Institute of Israel, Lod, Israel)	
Receiver Specifications			
		Charge	100 kg per shot in 30 m depth
Number of channels	30 units $\times$ 6 channels	Recording length	60 s
Geophone type	Sensor SM 6, 4.5 Hz, vertical	Configuration	asymmetrical split-spread shooting
Receiver array	6 per group,		(2:3, 3:2)
	linear pattern 15 m in-line	Shotpoint spacing	alternating 7.2 km and 10.8 km
Group spacing	100 m	Number of shots	10
Block move-up	3.6 km per day	Subsurface coverage	single fold
Spread length	18 km	Data amount	10 x 180 channels x 12,000 samples
Number of stations	1,008		= 87 MByte

Table 3.1: Acquisition parameters of the NVR experiment.

tically unstacked, shot-sorted traces were produced in standard segy format. Further processing was then carried out using Landmarks's ProMAX software. The most important steps of the principal processing sequence, that is shown in Table 3.2, will now be further explained. First of all a Common Depth Point (CDP), crooked-line geometry was constructed. Due to the laterally strongly scattered CMP distribution, caused by the non-linear course of the NVR line, the more than 300'000 traces were projected onto a smoothly curved 'reflection line' (Fig. 3.2). Prior to this, the 10 individual vibration point (VP) gathers per location had to be cross-correlated with the pilot sweep and vertically summed. This was done with a diversity stacking algorithm, which weights the sum with respect to the individual trace similarities and yields efficient noise reduction. The final horizontal subsurface coverage is 90-fold, with a CDP trace spacing of 25 m.

Handling of Noise   Various (source-generated and other) noise amplitudes/wave trains produced numerous bad or partly disturbed traces. Due to the large amount of data a pre-first-break/post-first-break energy threshold was used to automatically distinguish between 'good' and 'bad' traces. This resulted in an elimination of 20%

of the traces. Fig. 3.3 shows two receiver gathers before and after this process. As most of the sweeps generated a strong air blast wave that was visible along the entire spread (Fig. 3.3), a sharp 'surgical muting' was done manually.

Band-pass Filtering Time- and space-variant zero-phase band-pass filters were determined and applied to restrict the amplitude spectra to the signal frequencies between 10 and 50 Hz. For the reflected wavefield, however, the main signal frequencies are in average between 10 and 30 Hz, on rocky ground up to 40 Hz and on sandy ground only up to 20 Hz. The main signal frequencies along the NVR profile (Fig. 3.4) seem partly to be connected to the geology and near-surface conditions. The highest frequencies are found about 20 km west of the AF, where Eocene limestones and chalk crop out at the surface, whereas the lowest frequencies occur in the region around the AF in an area covered by sand dunes and alluvium.

Amplitude Corrections Mathematical corrections are generally necessary on each trace sample to compensate for various physical conditions affecting the amplitude of seismic waves (like spherical divergence, absorption and scattering or transmission losses). Moreover, noise amplitudes should be suppressed and relative amplitude dynamics should be preserved. The basic stacking condition — summing only similar and equivalent traces — was met only after various corrections were applied on the NVR data (falling in the categories 'energy decay compensation' and 'amplitude equalization' in Table 3.2).

Static Corrections Static (travel time independent) corrections are applied to account for irregular or changing topography and for near-surface velocity variations of the travel times. Near-surface conditions (like the thickness of a low-velocity weathering layer, sand dunes etc.) are usually only resolved by accompanying short refraction lines. As such additional measurements were not carried out within the NVR experiment, only elevation-based static time corrections were calculated. Using a correction and replacement velocity of 3.5 km/s the actual source and receiver positions were adjusted to a common datum. Due to the large elevation differences of 1750 m an intermediate 'floating datum', following the smoothed topography, was applied first. Only after CDP stacking the data was shifted to the final sea level datum.
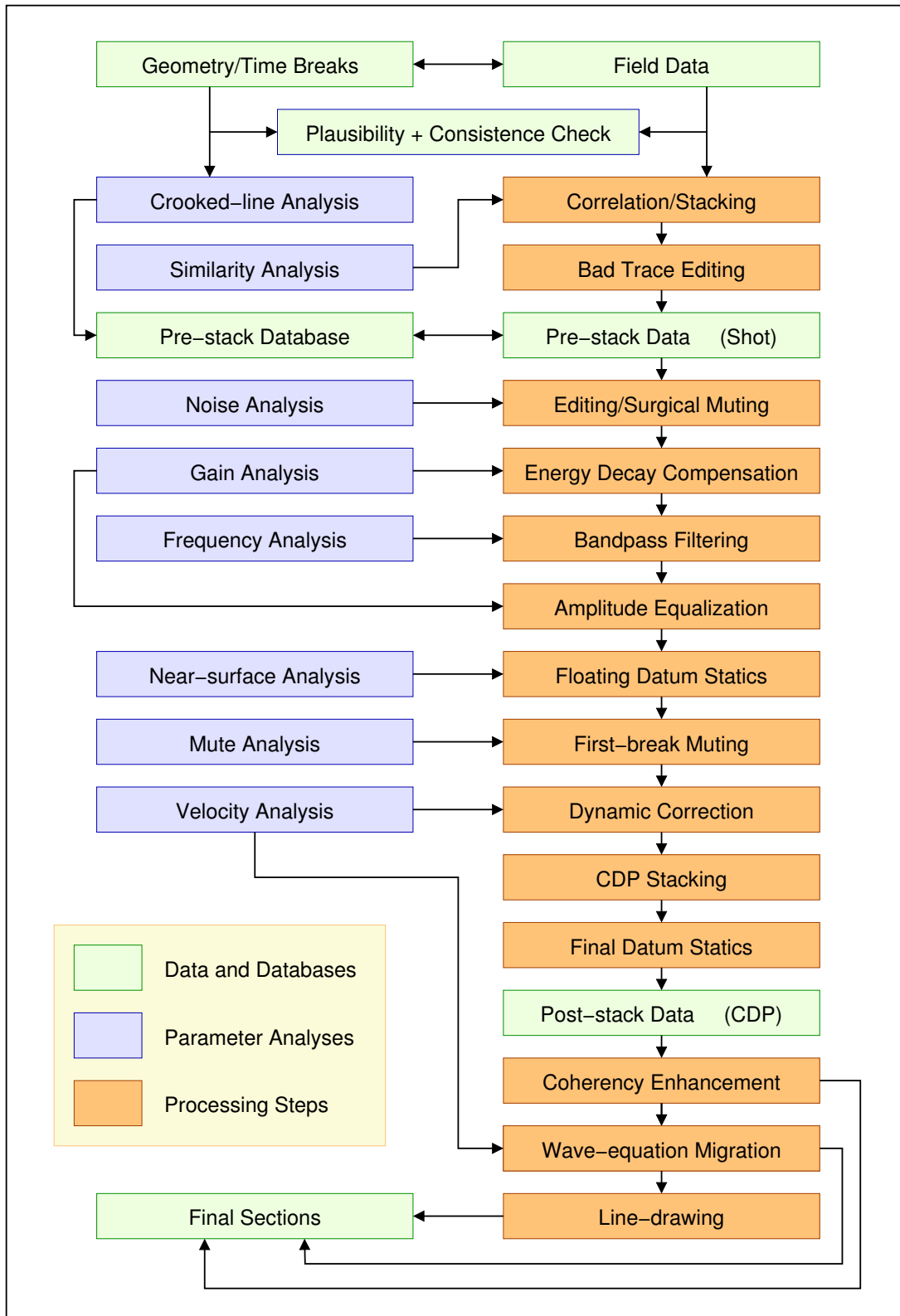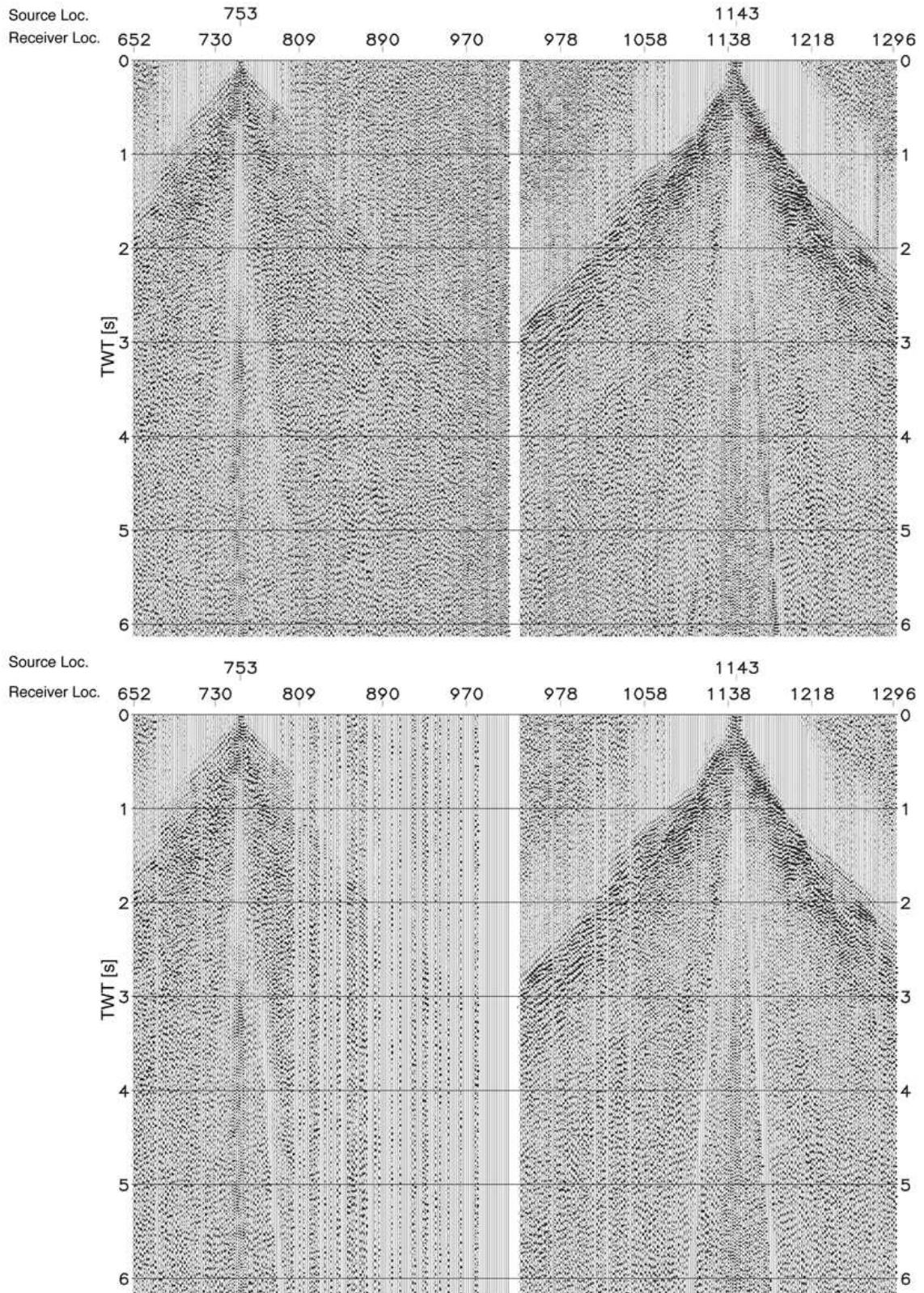
Table 3.2: Processing plan of the NVR dataset.

Figure 3.3: Two data examples before (top) and after (bottom) automatic bad trace zeroing. The strong air blast wave seen in shot 1143 (top right), was manually removed by 'surgical muting'.

Dynamic Corrections and Stacking   Before traces that image the same CDP can be stacked, dynamic (travel time dependent) corrections are required. This results from the fact, that travel times associated with geophones at large offsets are greater than those at short offsets, independent from the subsurface velocity. If a CDP gather is plotted with increasing offset, a primary reflection will have a hyperbolic shape. In the case of a horizontal reflector, the difference in travel time at the largest offset from the normal incidence is known as the normal moveout (NMO). It is crucial to analyze for optimum NMO velocities as accurately as possible to achieve a constructive stacking result. Usually the weighted-average velocity, which is termed root-mean-square velocity (v_{rms}), is used as NMO or stacking velocity for horizontal layers. For dipping reflectors a so-called dip moveout can be necessary (for more details see e.g. Yilmaz, 1987).

For the NVR data a v_{rms}–TWT background model was derived from turning-ray tomographic inversion for the upper time range and from the wide-angle data along the WRR line for the lower time range to find the most appropriate NMO velocities. After NMO correction the zero-offset traces were stacked, assuming an alignment of signals with an error less than half of the dominant wavelength. Whereas at some places the stacking result is convincing and shows a good signal-to-noise (S/N) enhancement (Fig. 3.5), the result remains unsatisfactory in other regions (Fig. 3.6). Reasons for this might be found in the strong lateral scattering of the CMPs (Fig. 3.2) and in insufficient static corrections accounting for near-surface effects. On a lower level, the relatively small frequency range of the data in some regions of the profile (Fig. 3.4) might further reduce the S/N ratio.
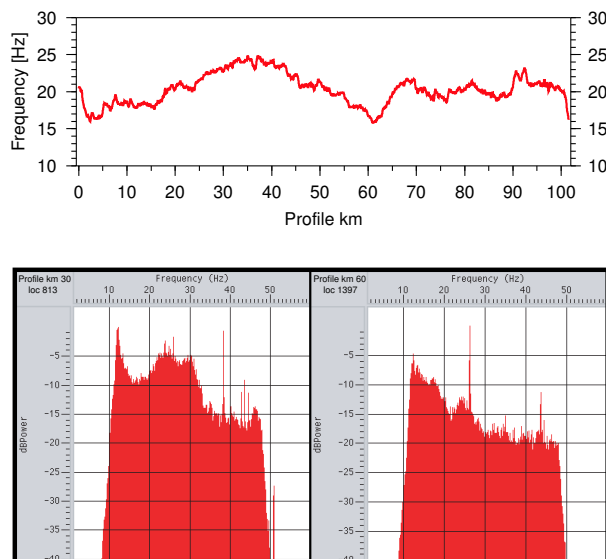

Figure 3.4: Frequency spectra. Top: Main signal frequencies along the NVR profile; bottom: The left spectra belongs to a shot gather from profile km 30, where the average frequencies are relatively high, whereas the right spectra is from a station located at profile km 60, where average frequencies are low.
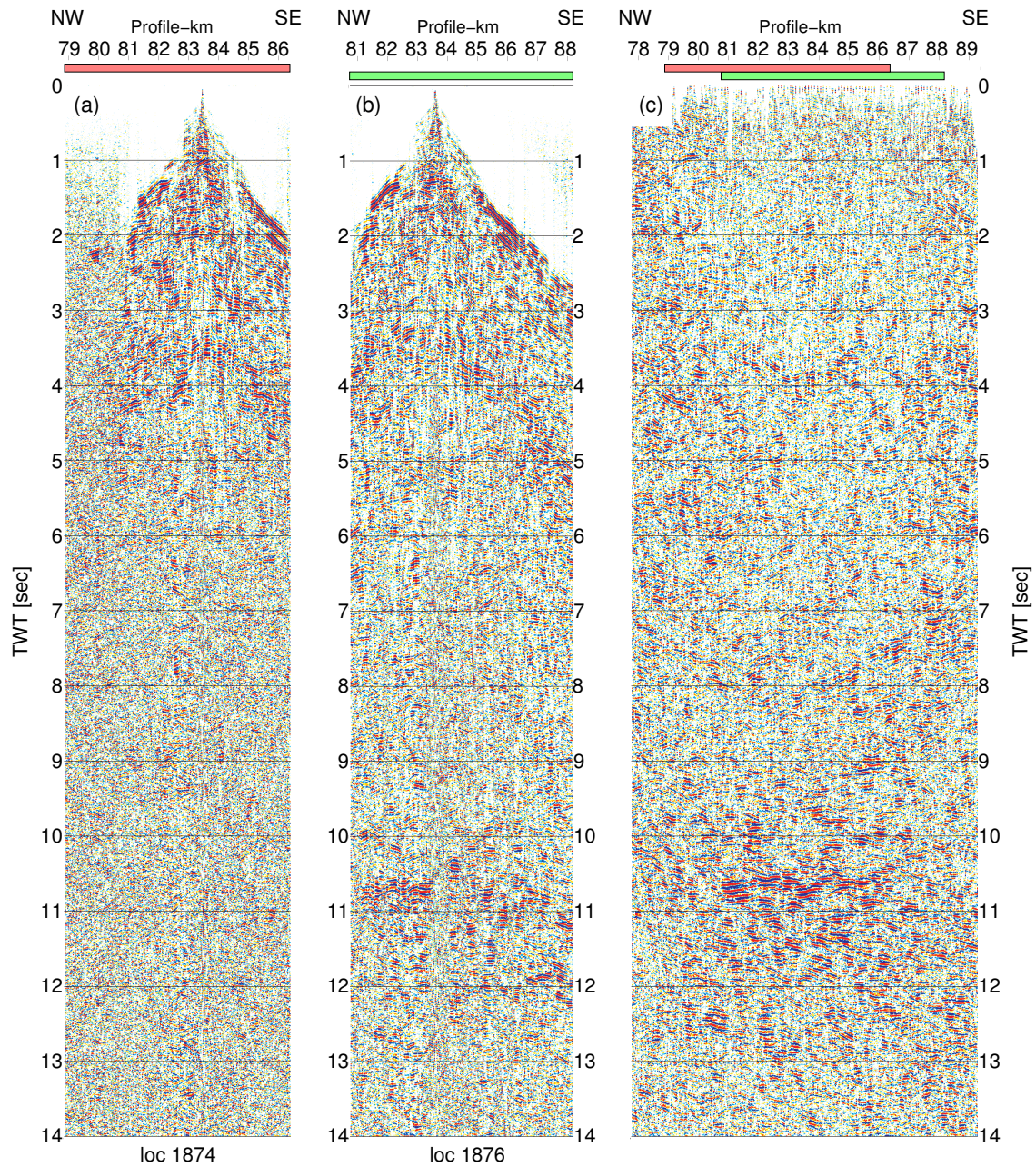
Figure 3.5: Data examples of the CDP section. (a) Common Receiver Gather (CRG) at profile km 83.4 with bad S/N ratio; (b) CRG at profile km 83.5 with good S/N ratio; (c) Final CDP stack from profile km 78 to 89. The respective locations of the CRGs are marked at the top of the stack.

Migration   As already mentioned in section 3.1 the aim of migration is to obtain a spatially true image of the subsurface showing all reflections with the correct dip at the correct depth. Generally three wave-equation migration methods are used: frequency-wave number (F-K), finite-difference (FD), and Kirchhoff summation schemes. With each method having its pros and cons (for a detailed explanation see e.g. Stolt and Benson, 1986; Yilmaz, 1987), all methods were tested on the NVR data, using different parameters. Finally a $50°$ FD depth approach with a smoothed interval velocity depth model calculated from the WRR velocities turned out to be the best compromise between clear and robust imaging and minimum 'smile'-like artifacts (DESERT Group, 2004). Smiles can be produced by the migration process if the used velocity model is not representative for a special region or if the boundary conditions (e.g. input is a true, noise-free zero-offset section) are not fulfilled. If the applied velocities are too slow, a point diffractor, e.g. a single burst of noise, will have an upward curvature ('smile'), if the velocities are too fast, the curvature will be downward. Smiles occur always at the margins of a section due to missing data. The resulting depth-migrated section is shown in Fig. 3.7.
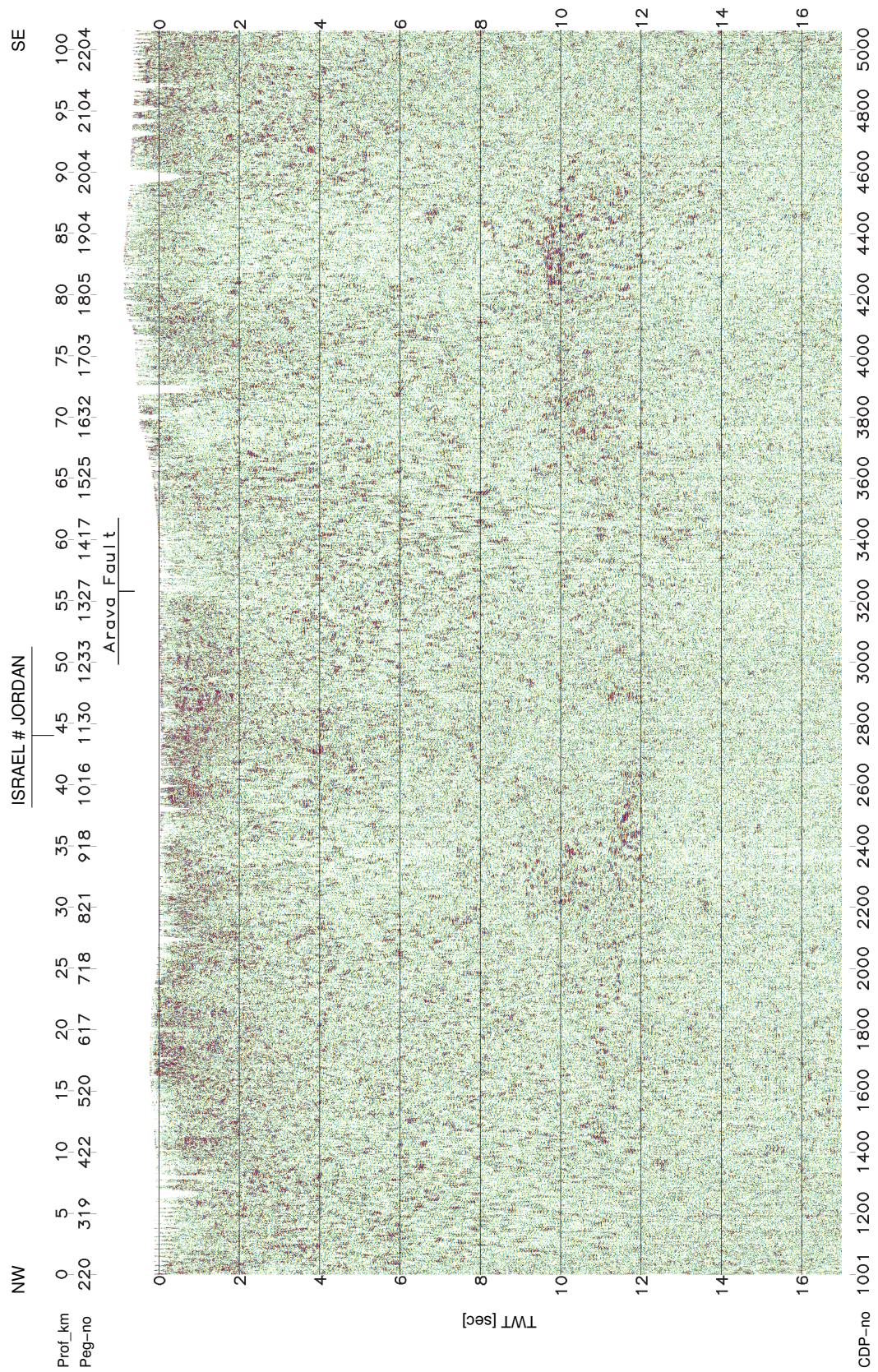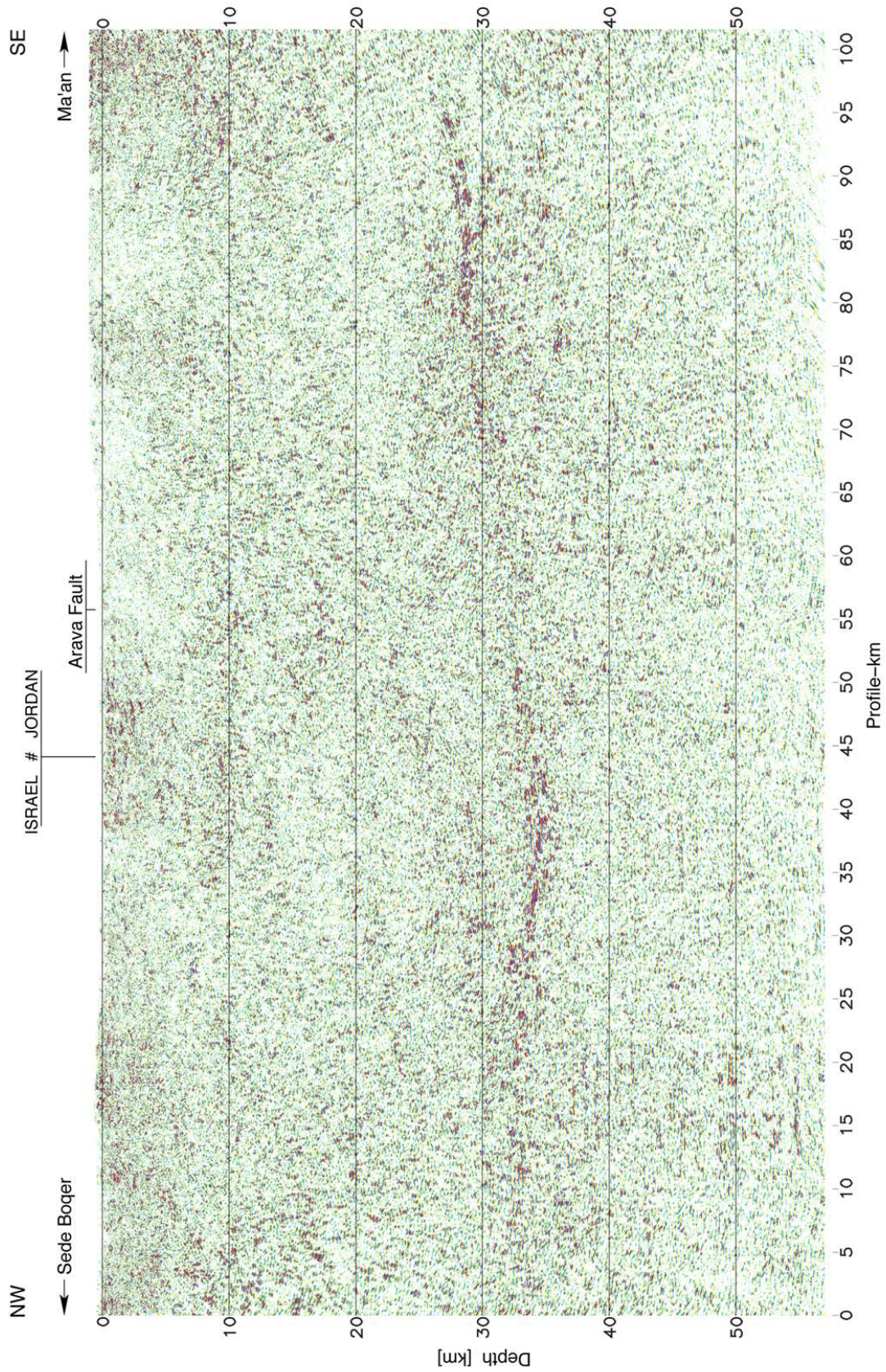
Figure 3.6: Unmigrated final CDP stack of NVR data

Figure 3.7: Depth migrated CDP stack.

3.3 Interpretation of the NVR Data

3.3.1 General Aspects

Near-vertical seismic reflection methods are important tools in imaging subsurface
structures, although the interpretation of the data is certainly not unambiguous and
processing results are nonunique. Though basic processing routines might be the
same, the final results of processed data can look rather different — depending on
the choice of parameters at the various stages of processing. This might result in
both a different frequency content and signal-to-noise ratio of the final data, and
also the form of display may focus one's attention on to specific features within the
data.

Another generally critical point is the translation of two-way travel time into
depth. Despite careful consideration of parameters and comparison of the results
of different migration techniques, artifacts might still be present just due to an
inadequate velocity model (see also section 3.2.2). 'White' or only diffusely reflec-
tive zones might be characteristic for some parts of the continental crust (e.g.
Mooney and Brocher, 1987), but could as well represent zones where energy did
not penetrate far enough into the ground, possibly caused by insufficient coupling
of the geophones or by thick weathering layers.

A major challenge of continental crustal studies is to determine the origin of deep
crustal reflections. There are various factors that can result in impedance contrasts
between adjacent rocks and are thus sources of crustal reflectivity. According to
Mooney and Meissner (1992) the main reasons are:

- (sill-like) mafic intrusions within crustal rocks of differing physical properties
  or igneous cumulate layering,

- faults that juxtapose different rock types,

- localized ductile shear zones where reflections originate because of seismic
  anisotropy within the shear zone, metamorphic recrystallization within the
  shear zone that is absent outside the zone, constructive interference from
  enhancement of lithologic layering related to high strain or the complex inter-
  action of all these effects,

- local zones containing fluids under high pore pressure,

- pervasive ductile flow in the deep crust that enhances layering, anisotropy and constructive interference,

- molten or partially molten bodies in the lower crust.

In contrast to an often highly reflective lower crust and to well-resolved sedimentary reflections, few reflections are generally observed in the upper part of the crust beneath the sedimentary cover (e.g. Mooney and Brocher, 1987). Mooney and Brocher (1987) propose two possible explanations:

- As the reflection strength is a strong function of a reflector's geometry and scale, the velocity perturbations in the upper crust are probably neither well laminated nor of long scale length. Due to the nonductile behaviour of the upper crust, brittle extension and compression occur, producing short features with steep dips that are not well imaged using conventional seismic profiling methods.

- Partially, the transparency of the upper crust might be an artifact of the seismic reflection method itself. For example, after muting of the first arrivals, CDP folds are significantly lower for the first 5 s TWT of the section, resulting in lower S/N improvement during stacking. Also the near-source data, that provide information especially on the upper crust, are most frequently contaminated by source-generated noise.

However, in view of the rapid onset of the reflective lower crust in deep seismic sections, good images of sedimentary basins, and also a transparent upper crust in marine data, that are usually less hampered by surface noise problems, the second reason is interpreted as being of minor importance.

Looking at a seismic image of continental crust we just see a (two-dimensional) snapshot of a piece of crust that often underwent a complicated geologic history. It is not necessarily known to what extent older events are 'preserved' in the crustal image and how the recent geology (recent stress field, active structures we observe at the surface) has 'overprinted' older structures. Whereas the truncation or crosscutting of reflectors by other diversely dipping reflectors sometimes might hint at the relative age of these structures, it is often not possible to derive even a relative chronology of 'events'. Moreover, a 2-D section always leaves open the question regarding the true orientation/dip of certain structures.

One will never be able to make allowances for all these afforementioned effects to their full extent, but they should still be taken into account when interpreting seismic reflection data. It is crucial therefore to consider independent data, both geological and geophysical, to come to a comprehensive and geologically reasonable interpretation. Solely on the basis of near-vertical seismic reflection data, that only contain information about the seismic wavefield over a limited range of frequencies and incidence angles, this is not possible.

3.3.2 Deep Crustal Structure

A large number of near-vertical seismic reflection profiles have shown that a reflective lower crust and a mainly transparent upper crust are typical for the continental lithosphere (see e.g. Mooney and Brocher, 1987). Also in the CDP section of the DESERT NVR profile a highly reflective lower crust can be recognized along the whole profile except in a ∼15 km wide zone beneath the DST (see below). In addition, the upper crust is generally transparent along the entire line. There is, however, a change in the overall appearance of crustal reflectivity west and east of the transform. After a description of the nature of the crust/mantle boundary, a discussion of this general crustal reflectivity pattern will follow.

Crust/Mantle Boundary

In deep crustal reflection data the crust/mantle boundary or Mohorovičić discontinuity (usually termed 'Moho') is commonly defined as the break-off of lower crustal reflectivity. With slight variations lower crustal reflectivity terminates between 33 and 36 km depth along the NVR profile (Fig. 3.7). However, whereas northwest of the DST there is a rather abrupt termination of relatively strong lower crustal reflectors, southeast of the transform the distinction between reflective lower crust and non-reflective mantle is somewhat blurred. The very conspicuous zone of lower crustal reflectivity at 28 to 30 km depth between profile km 75 and 92 might lead to the conclusion of a Moho at 30 km depth. There are, however, numerous laterally discontinuous reflectors below this coherent band of reflections, pointing to an actual Moho depth of ∼36 km.
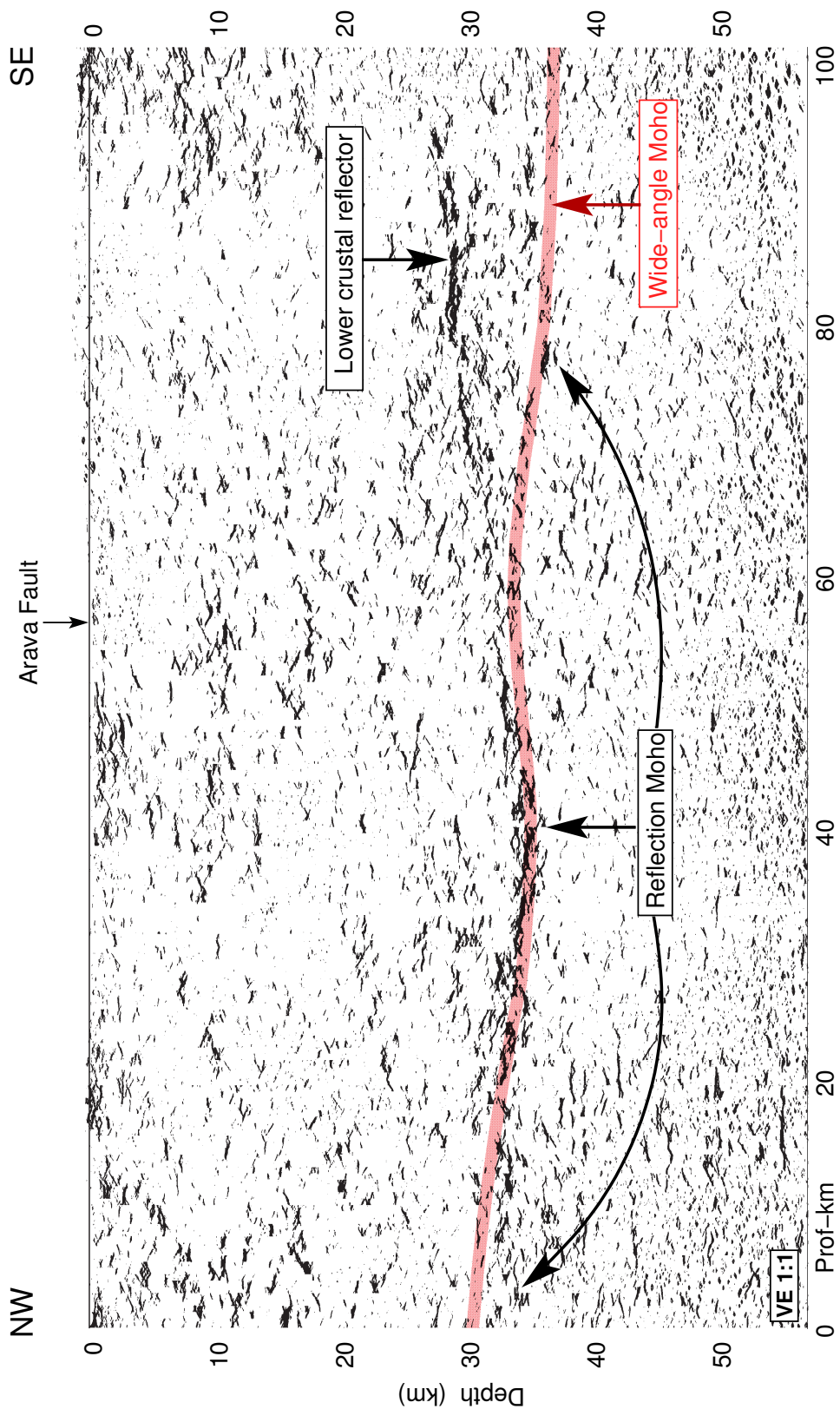
Figure 3.8: Automatic line drawing of the depth–migrated seismic CDP section of the
NVR experiment. The red band indicates the location of the Moho as derived from the
WRR data.

The increase in Moho depth from ∼30 to 38 km beneath the NVR profile, that is observed in the WRR data (Fig. 3.8), is more or less in accordance with the NVR results. A few small discrepancies between the reflection and refraction seismic data as, for example, at the western end of the NVR line, are not unusual for coincident seismic reflection/refraction surveys (e.g. Mooney and Brocher, 1987). They might result from the different imaging techniques, different dominant frequencies of the two methods (12–13 Hz in the NVR data in contrast to 6–7 Hz in the WRR data) and general measurement uncertainties, that are in the range of ± 2–3 km for the WRR experiment (DESERT Group, 2004).

The results of the NVR experiment are also in good agreement with other geophysical studies in the region. Combining seismic refraction data, teleseismic-based profiles and gravity anomalies, Hofstetter *et al.* (2000) compiled a 'reference Moho' for the eastern Mediterranean and Israel, which shows a general increase of crustal thicknesses to the SE and Moho depths of around 33–34 km under the NVR line. According to a seismic refraction study reported by Ginzburg *et al.* (1979) the Moho depth beneath the NVR profile should be ∼35 km. On the Jordanian side of the transform the Moho depth was determined to be around 33 km in a seismic refraction study by El-Isa *et al.* (1987). In the light of new seismic and receiver function data, however, this value seems to be too low (DESERT Group, 2004). The receiver function study (A. Mohsen, pers. comm., 2003) defined the crust/mantle boundary at 35–38 km depth beneath the Jordanian highlands in the region of Ma'an. An analysis of potential field data by Al-Zoubi and Ben-Avraham (2002) also resulted in the determination of crustal thicknesses of around 35–36 km here. However, there seem to be some 3-D variations in Moho depth in the vicinity of the DESERT seismic profiles, evident in receiver function data (A. Mohsen, pers. comm., 2003) and also in gravity data (R. El–Kelani, pers. comm., 2003). These datasets indicate a ∼30–70 km wide, NW–SE trending 'Moho trough' east of the AF, parallel to the WRR and NVR lines, with Moho depths clearly below 35 km. NW–SE striking tectonic elements such as e.g. the sinistral Najd fault system in Saudi Arabia and a proposed subduction zone at the Gondwana margin in Late Proterozoic times (see section 2.1.1) are known from the literature (e.g. Husseini, 1989; Stern, 1994; Jarrar, 2002) and might be linked to this feature.
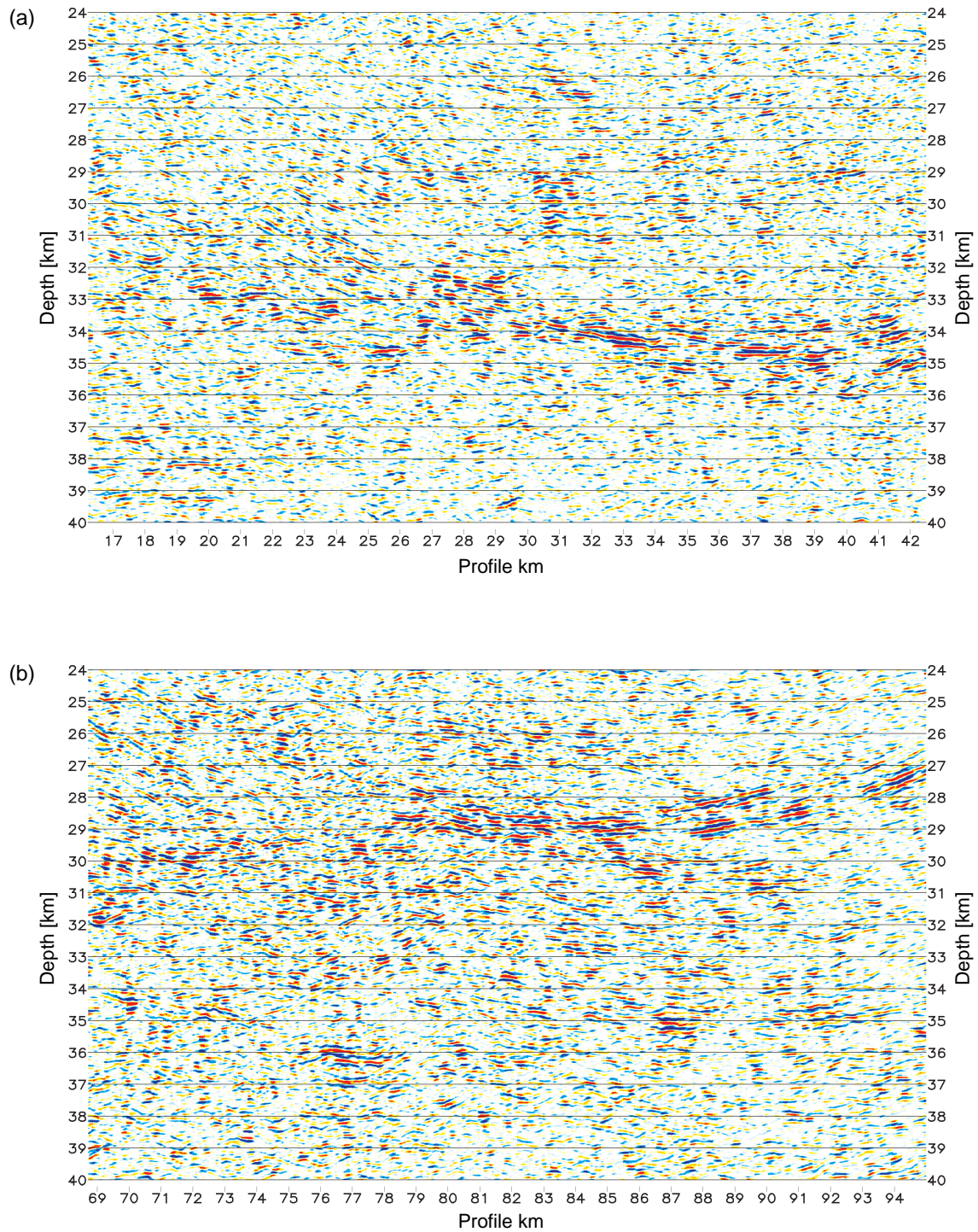
Figure 3.9: Zooms of the depth-migrated CDP section at Moho depths. (a) Lower crustal reflectivity west of the DST; (b) Lower crustal reflectivity east of the DST.

Crustal Reflectivity West of the DST

Northwest of the DST strong, rather continuous reflections are found at the base of the crust along a delimited band of ∼3 km thickness (Fig. 3.7 and Fig. 3.9a). The reason for their weaker amplitude at the very northwestern end of the profile might lie in the lower subsurface CDP coverage or a stronger attentuation of energy in the upper crust here. The apparently southeasterly dipping reflectors, that can be delineated between profile km 16 and 26 at 30 to 34 km depth, seem to partly crosscut these subhorizontal reflectors, meeting them at Moho depth. They are thus interpreted as younger fabrics, maybe representing a low–angle lower crustal shear zone. However, because a connection of these dipping reflectors to structures in the middle or upper crust cannot be made out in the reflection image, their interpretation remains speculative. The origin of this structure might be connected with the Tethys rifting events in Triassic and Jurassic times or with the 'Syrian Arc' compressional event (see section 2.1.1). Due to its apparent extension towards the NW, it does not seem to be related to the transform motion along the DST.

The region between profile km 25 and 43 is characterized by relatively strong, but discontinuous subhorizontal reflectors between 25 and 30 km depth. These might result from heterogeneities/compositional layering or metamorphic fabrics in the lower crust. As this zone is not marked in the refraction data by distinct features in P and S wave velocities and also due to a lack of studies on Israeli xenoliths, its further characterization is not possible.

Within a mainly transparent upper crust, a reflective zone between profile km 20 and 50 at depths between 8 and 11 km is apparent (Fig. 3.7). This zone extends from beneath the surface trace of the Ramon Fault to the Arava Fault and underlies the Zofar and the Baraq faults, that are subparallel to the Arava Fault (Fig. 2.5). An attractive interpretation of the reflectors' origin would therefore be a detachment horizon/subhorizontal shear zone, linking the various faults and accommodating at least part of the deformation. The observation, that east of a less reflective zone from profile km 48 to 51 some reflective elements occur at the same depth below the surface trace of the Arava Fault, would support this hypothesis. Yet it should be taken into account, that a possible shear zone at this crustal depth does not necessarily have a relation to the recent geologic history, i.e. the strike-slip motion along the DST. The rather abrupt termination of the reflectors beneath the surface trace of the Ramon Fault — a dextral strike-slip fault — could favour an interpretation of an older shear zone, the western extension of which is not
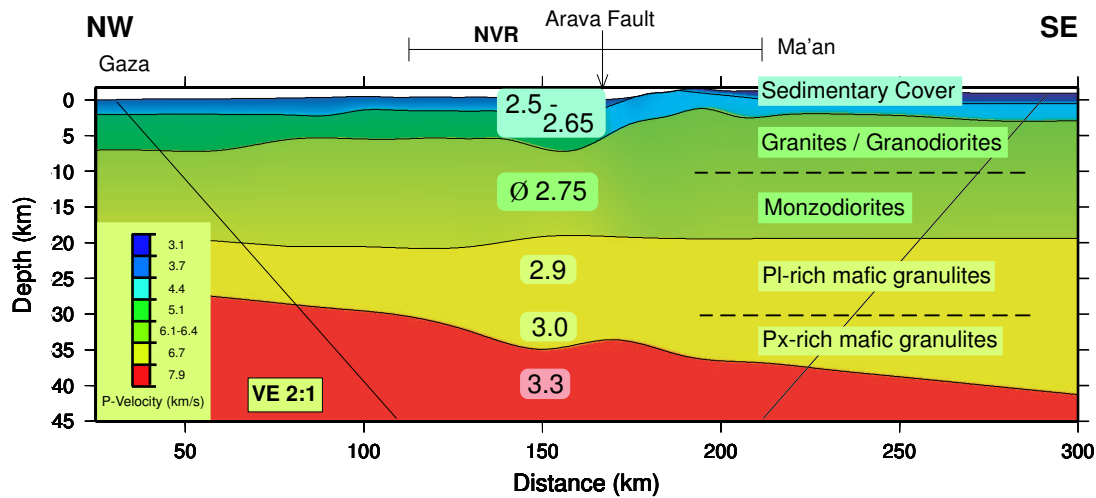
Figure 3.10: Crustal model along the WRR profile; the WRR P velocities are colour-coded (DESERT Group, 2004), the numbers represent density values in g/cm^3 from gravity modelling (El-Kelani *et al.*, 2003). The petrology is after H.–J. Förster (pers. comm., 2003)

imaged in the NVR data because of the (Cretaceous to Tertiary) displacement along the Ramon Fault. The fact, that the reflective zone has no obvious continuation at shallower depth would also support the latter view. Looking at the character of the reflections it appears, that laterally long, continuous reflectors are missing. Therefore, a possible shear zone, regardless of its age, should assumedly not be a distinct single fault plane but rather a broader zone where shear deformation is taken up. At the same time this zone might coincide with a compositional transition from more silicic to more basic granitoid rocks or rocks with a metamorphic layering.

The reflectivity pattern that is observed in the NVR data west of the DST is in agreement with the eastern part of a ∼90 km long NW–SE trending deep seismic reflection line in central Israel between the Mediterranean and the Dead Sea (Yuval and Rotstein, 1987; Rotstein *et al.*, 1987). This survey also showed a reflective lower crust and a mainly transparent upper crust towards the Dead Sea Basin. There is also a good correlation between the refraction Moho and the termination of lower crustal reflections here. Interestingly, in the immediate vicinity of the Dead Sea Basin, there are also some reflections at 3–4 sec TWT, comparable to the reflectors described above. These reflections were interpreted to be related to the recent extension at the Dead Sea without any further, more detailed interpretation.

Crustal Reflectivity East of the DST

To the east of the Arava Fault, the most conspicuous feature is the strong lower crustal reflectivity at ∼28 km depth beneath the Jordanian highlands between profile km 78 and 92 (Fig. 3.9b). A possible intra–crustal reflection (Pi2P) from around 30 km depth might also be evident in the wide-angle reflection/refraction data east of the AF, but this is not unequivocal (DESERT Group, 2004).

One possibility for the origin of this high reflectivity could be a zone of localized strain close to the base of the crust. This is in agreement with mechanical modelling results of Sobolev *et al.* (2004), who show a zone of high shear deformation and possible lower crustal flow east of the transform. Also in general models of lower crustal reflectivity, reflective bands have been correlated with zones of mechanically weak, high-strain zones (Meissner, 1989).

Alternatively, the reflector might represent a lithological contrast, an interpretation that is supported by the following considerations. Based on the study of xenoliths in Jordanian Cenozoic basalts, two major groups of lower-crustal rocks were distinguished (H.–J. Förster, pers. comm., 2003), namely plagioclase-rich mafic granulites and two-pyroxene mafic granulites. The modelled P velocity for the lower crust is 6.7 km/s, which is in good agreement with the densities of plagioclase-rich mafic granulites, if the density-velocity conversion method by Sobolev and Babeyko (1994) is used (H.–J. Förster, pers. comm., 2003). For two-pyroxene mafic granulites densities of ∼3.05 g/cm^3 and higher would be expected (see Table 3.3), which would in turn result in P velocities of around 7.1–7.3 km/s. Considering these differences, a predominance of plagioclase-rich mafic granulites in the lower crust of Jordan is assumed. Two-pyroxene mafic granulites might occur, however, at the very base of the crust, in a kind of 'lower crustal wedge' below 30 km depth east of the DST (Fig. 3.10). P velocities of ∼7.15 km/s within this suggested 'wedge' are still in accordance with the seismic refraction data and would only have a small influence on the estimated Moho depth, moving it 1–3 km deeper (DESERT Group, 2004, , J. Mechie, pers. comm., 2003). A two-layer lower crust beneath Jordan is also compatible with 3-D gravity models (El-Kelani *et al.*, 2003), suggesting higher density values of ∼3.0 g/cm^3 beneath 30 km depth.

In the receiver function study, in which P to S conversions at subsurface boundaries are observed, a multiple from a lower crustal discontinuity is clearly seen at

	density ρ [g/cm^3]	V_P [km/s]
Plagioclase-rich mafic granulites	2.91 – 3.04	6.69 – 6.84
Pyroxene-rich mafic granulites	3.09 – 3.13	7.09 – 7.29
DESERT Ø	2.9 – 3.0	6.7 ± 0.2

Table 3.3: Densities and P velocities of (Jordanian) lower crustal rocks, calculated for T=600 °C and P=1 GPa. The black values represent the measured values, whereas the blue numbers are the calculated values, using the density-velocity conversion method by Sobolev and Babeyko (1994). After H.–J. Förster, pers. comm. (2003).

some stations in Jordan (Mohsen *et al.*, 2004, Fig. 3.11). With depths of ∼28–30 km this discontinuity is also in accordance with the two-layer crustal model beneath Jordan. One might expect, however, that a distinct compositional boundary in the lower crust would be recognized in the P- and S-wave arrivals of the WRR data. This apparent discrepancy could be explained with the following scenario: If the velocity jump at a lower crustal boundary is only small, possible wide-angle reflections from this boundary could not necessarily be distinguished as separate reflections from the wide-angle Moho reflections (J. Mechie, pers. comm., 2004). A small velocity jump would furthermore imply only a minor compositional difference between the respective rocks of the lower crust. Therefore the lowermost crustal layer would have to become more and more mafic towards its bottom, to be in accordance with the gravity and petrology models. Such a transition zone could explain both the observed receiver function and the WRR data.

Considering the high amplitude of the strong lower crustal reflections recognized in

$\lambda/4 = v/4f$				
v [m/s]	f [Hz]$_{WRR}$	$\lambda/4$ [m]$_{WRR}$	f [Hz]$_{NVR}$	$\lambda/4$ [m]$_{NVR}$
6000	7	214	12	125
6500	7	232	12	135
6900	7	246	12	144
7100	7	254	12	148

Table 3.4: Threshold for vertical seismic resolution. After Yilmaz (1987) the vertical seismic resolution is around a quarter of the dominant wavelength.
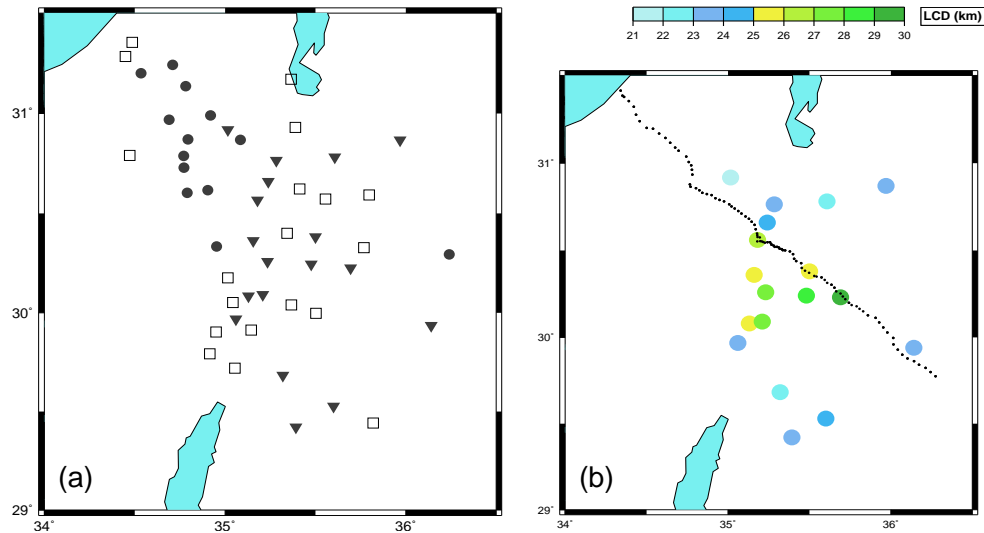
Figure 3.11: Lower crustal discontinuity (LCD) as recognized in a receiver function study. (a) Distribution of stations according to the appearance of the LCD multiple. Full circles represent stations that have one clear Moho multiple; full triangles represent stations that have a LCD multiple; open squares stand for stations that do not show multiples (neither Moho nor LCD); (b) Depth map of the LCD mainly east of the DST; the black dots indicate the stations of the WRR experiment. (Mohsen, 2004).

the near-vertical seismic reflection data, another explanation than a minor compositional difference between the adjacent rocks is necessary. It is suggested here, that they originate from sill-like mafic intrusions. If the thickness of the suggested sills is in the range of 120–180 m, they are not expected to be identified in the WRR data with dominant frequencies around 5–7 Hz, but could be seen in the NVR data with frequencies around 12–13 Hz in the lower crust (Table 3.4).

Such sills might be associated with the strong magmatic activity that occurred in the region in both Precambrian/Cambrian, Cretaceous and Neogene times. Neogene basalts crop out close to the NVR profile near Karak and Ma'an, but also Precambrian volcanics are abundant east of the Arava Fault (Fig. 2.5). The wide-spread dikes that were emplaced into the Jordanian crystalline basement between 600 and 540 Ma point to an extensional tectonic environment at this time, that could have favoured the sill-like intrusion of mafic magmas into the lower crust (e.g. Warner, 1990).

Looking at the receiver function data, especially at the location of the seismic broad-band stations that recorded a lower crustal multiple (Fig. 3.11), it seems improbable that this lower crustal discontinuity is related to the occurrence of the

'Moho trough' (see above), because it is observed at almost all of the south Jordanian stations.

Whereas compositional layering due to sill-like mafic intrusions is considered to be the main reason for the strong lower crustal reflectors observed in the NVR data, it might well be that lower crustal deformation zones, related to the lateral motion along the DST, later developed at these lithological contrasts. Based on crustal rheology, a combination of ductile flow and horizontal mafic intrusions as the origin for lower crustal reflections was also suggested by Holliger and Levander (1994).

Arava Fault

Imaging near-vertical structures by near-vertical seismic reflection techniques is difficult (e.g. Meissner, 1996). It is, however, possible to get indirect evidence of the depth continuation of steeply dipping faults by the offset of crustal reflectors or an observed change in crustal reflectivity. However, although the DST/AF is clearly recognized in satellite data as a rather straight line between the Red Sea and the Dead Sea (see also chapter 4) it cannot unambiguously be delineated in the CDP section (Fig. 3.7). There is no pronounced difference in crustal structure directly west and east of the Arava Fault and in the immediate vicinity of its surface trace sedimentary reflections are missing. The absence of sedimentary reflectors might be due to strong deformation of the rocks close to the fault, but could also be caused by the absorption of high frequencies in an area covered by sand dunes and alluvium. Whereas a possible Moho offset has been proposed for the San Andreas Fault from deep crustal seismic reflection and refraction studies (Henstock *et al.*, 1997), and for the DST north of the Dead Sea Basin from the analysis of gravity data (ten Brink *et al.*, 1990), there is no evidence for such an offset at the AF along the NVR profile. Nonetheless it is inferred that the AF reaches down to the mantle, changing into a broader deformation zone at mid-crustal level, due to the following reasons:

(a) At Moho depth an ∼15 km wide zone (profile km 54 to 70 in Fig. 3.7) beneath the surface trace of the AF is observed that lacks the strong reflectors observed farther to the west and the lower crustal reflectors observed to the east. From this it follows that the fault zone becomes broader in the lower crust. The strong reflections beneath the AF at about 18 km depth are thought to occur at the upper/lower crust boundary and are linked to a velocity jump from 6.4 to 6.7 km/s (Fig. 3.10). There is no good expression of this boundary elsewhere

in the NVR data. This is taken as an indication for a zone of localized shear strain between the felsic upper and mafic lower crust related to the transform motion along the AF. Whereas Furlong *et al.* (1989) and Brocher *et al.* (1994) interpreted a similar subhorizontal surface at 15–20 km depth below the San Andreas Fault Zone in the San Francisco Bay area as a possible detachment zone of the San Andreas Fault, linking it to the Hayward/Calaveras fault system, Holbrook *et al.* (1996) interpreted it as corresponding to the top of the lower crust, acting on the whole to accommodate shear deformation in a broad zone. Here a similar model to the one by Holbrook *et al.* (1996) is proposed for the DST.

(b) The small but visible, asymmetric topography of the Moho below the Arava Valley in the WRR model (profile km 130 to 170 in Fig. 3.10) is also consistent with the NVR data (Fig. 3.8). This is another piece of evidence for the AF cutting through the whole crust. Whereas a bending down of the Moho, or a 'Moho keel' has been put forward for some Paleozoic strike-slip regions in transpressional tectonic regimes (McBride, 1994; Stern and McBride, 1998), this coupled upward-downward structure of the Moho might be due to the transtensional character of the DST between the Red Sea and the Dead Sea. Mathematical models describe the geometric, thermal and flexural-isostatic response of the lithosphere to extension by faulting (simple-shear) in the upper crust and distributed plastic deformation (pure-shear) in the lower crust and mantle (Kusznir *et al.*, 1991; Kusznir and Ziegler, 1992). During faulting, the footwall and hanging-wall blocks are considered to behave as two interacting cantilevers. The response of these cantilevers to the isostatic forces produces footwall uplift and hanging wall collapse. To compensate for upper crustal extension the lower crust acts with plastic deformation and a change of Moho topography. Although these 'flexural-cantilever' models were constructed to explain the geometry and formation of major extensional basins, they might partly be applied to the DST as well. This will be elucidated in the following. It was already mentioned that the southern DST is characterized by some minor transverse, i.e. W–E, extension (see section 2.1.2). At the location of the NVR profile, the Al Quwayra Fault (Fig. 2.5) is a major fault, that places Precambrian rhyolites to the east next to Upper Cretaceous sediments to the west, with a fault plane dipping ∼55° to the W. The footwall is uplifted some hundred metres. With a vertical stratigraphic displacement of more than 1 km at the NVR profile, at least 8 km of left-lateral motion

along this fault have been reported (Abu Taimeh, 1988). This combined lateral and vertical displacement seems to be jointly responsible for the 3–5 km vertical offset of the 'seismic basement' across the DST in the WRR model (Fig. 3.10). In the NVR data the Al Quwayra Fault is not imaged at all and its continuation into depth remains speculative. Taking also into account the left-lateral motion along the Al Quwayra Fault, the amount of transverse extension is difficult to assess. Whereas in the models by Kusznir *et al.* (1991) and Kusznir and Ziegler (1992) the footwall uplift of a major normal fault is explained with the flexural isostatic response of the lithosphere to extension, modelling by ten Brink *et al.* (1996) and the thermo-mechanical model by Sobolev *et al.* (2004) attribute most of the observed uplift east of the DST to the transform motion. It thus remains unclear, whether the small observed Moho topography can be explained with flexural behaviour due to (a minor amount of) extension, or whether it is a 'by-product' of pure transform motion.

(c) Reflectors in the lowermost crust, at 25–32 km depth from profile km 55 to 70 (Fig. 3.7 and Fig. 3.8), that dip away from the suspected fault zone and are most pronounced east of the AF, might correspond to anisotropic fabrics developing along mylonitic shear zones, similar to the dipping reflectors beneath the Walls Boundary strike-slip fault in the northern British Caledonides (McBride, 1994).

Evidence for the continuation of the Arava Fault into the mantle, and even through the whole lithosphere, also comes from independent geophysical data. An analysis of shear-wave splitting (Rümpker *et al.*, 2003), proposes a distinct, ∼20 km wide anisotropic zone in the lithospheric mantle with fault-parallel mineral alignment suggesting subhorizontal mantle flow. Moreover, a thermo-mechanical model of the region (Sobolev *et al.*, 2004) on the basis of all available petrological, geological and geophysical data clearly defines a similar broad shear zone extending through the entire lithosphere.

3.3.3   Shallow Crustal Structure

Sedimentary structure west of the Arava Fault

Although there are no coherent upper crustal sedimentary reflections in many parts
of the NVR profile, there are some locations, where clear reflectors from sediments
are observed. As it is hardly possible to further characterize the upper crustal
reflections between profile km 15 and 25, between km 73 and 81, and between km
90 and 101 (Fig. 3.7), the following description concentrates on the Arava Valley.
Moreover, due to the vicinity to the Arava Fault, this area is of special interest,
because upper crustal deformation related to the transform plate boundary might
be recognized in the seismic data.

At the location between profile km 41 and 51, approximately 5–15 km W of
the AF, at the western edge of the Arava Valley, sedimentary reflections in the
NVR data are especially clear and coherent (Fig. 3.12). Here, the Baraq Fault
and the Zofar Fault, both seen at the surface, are rather clearly imaged. Whereas
the apparent offset at the Baraq Fault seems to be minor, the Zofar Fault shows a
vertical displacement of ∼500 m.

Both faults have also been imaged in various shallow seismic reflection lines, that
were part of an extensive high-resolution seismic reflection study in the Israeli part
of the Arava Valley (e.g. Bartov *et al.*, 1998; Frieslander, 2000). This dataset was
carefully analyzed by Frieslander (2000) who compared the recorded seismograms
to synthetic seismograms and correlated seismic reflections with stratigraphy. This
study was also backed up by borehole data of the region. Taking Frieslander's
interpretation of line GP 2150, the location of which coincides with the NVR line
between profile km 43 and 49, it was also possible to determine the boundaries of
some lithological units in the NVR data (Fig. 3.12).

The Zofar Fault has been interpreted as a major fault in the northern Arava
Valley. Its northern part is the western border fault of the southern Dead Sea
Basin (e.g. Bartov *et al.*, 1998; Frieslander, 2000). Except for the obvious vertical
stratigraphic separation across its surface trace, a sinistral strike-slip component has
also been assumed, even if any evidence for the amount of lateral displacement is
missing (Y. Bartov and Z. Garfunkel, pers. comm., 2003). An antithetic fault east
of the Zofar Fault, called 'Eastern fault' by Frieslander (2000), shows hardly any
displacement but is clearly linked to the Zofar Fault at ∼2.5 km depth, which could
not be seen in the Israeli shallow seismic study because of its limited 1.3 s recording
time, that corresponds to a depth of ∼1.5 km.
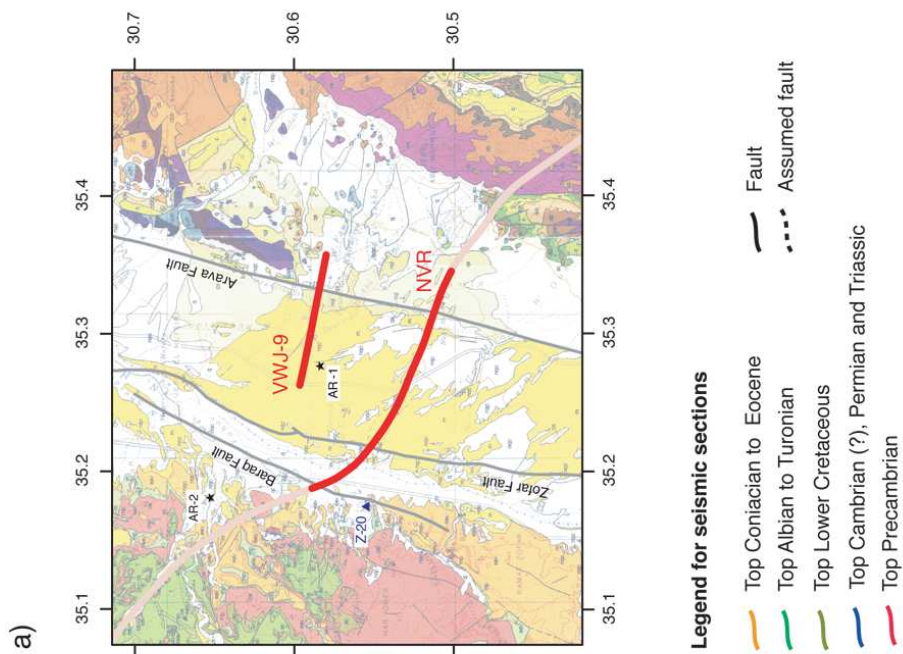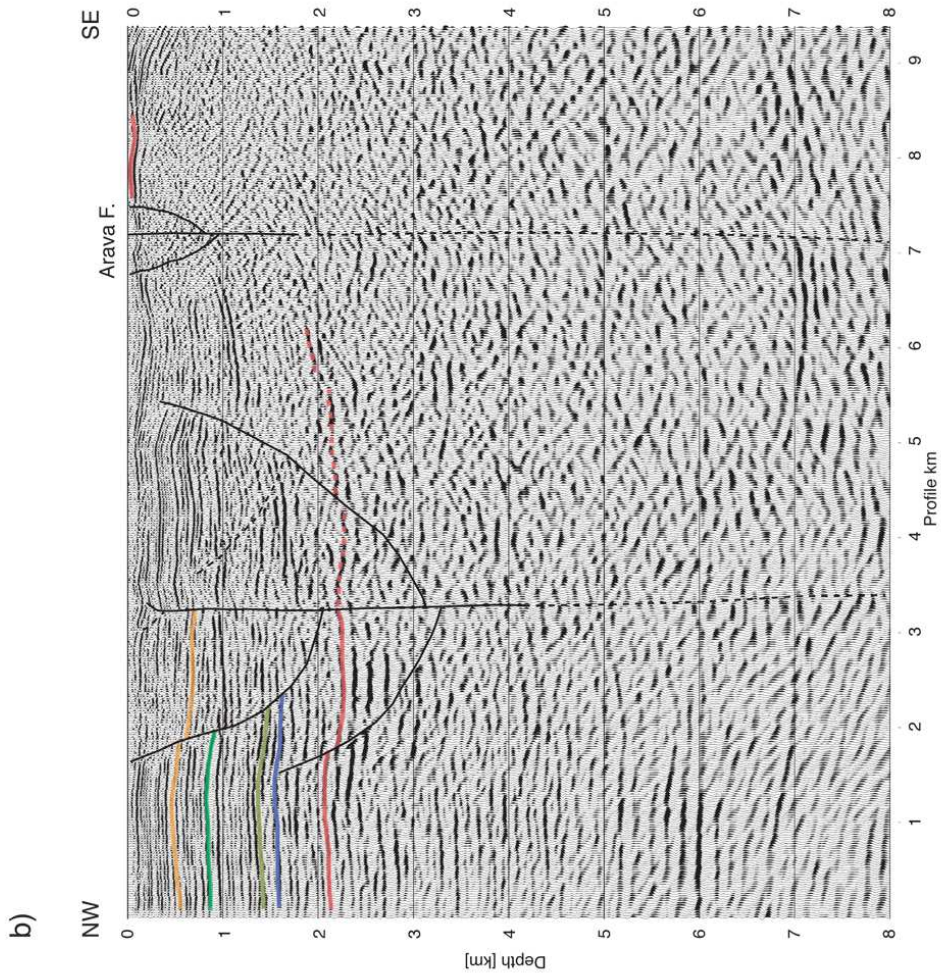
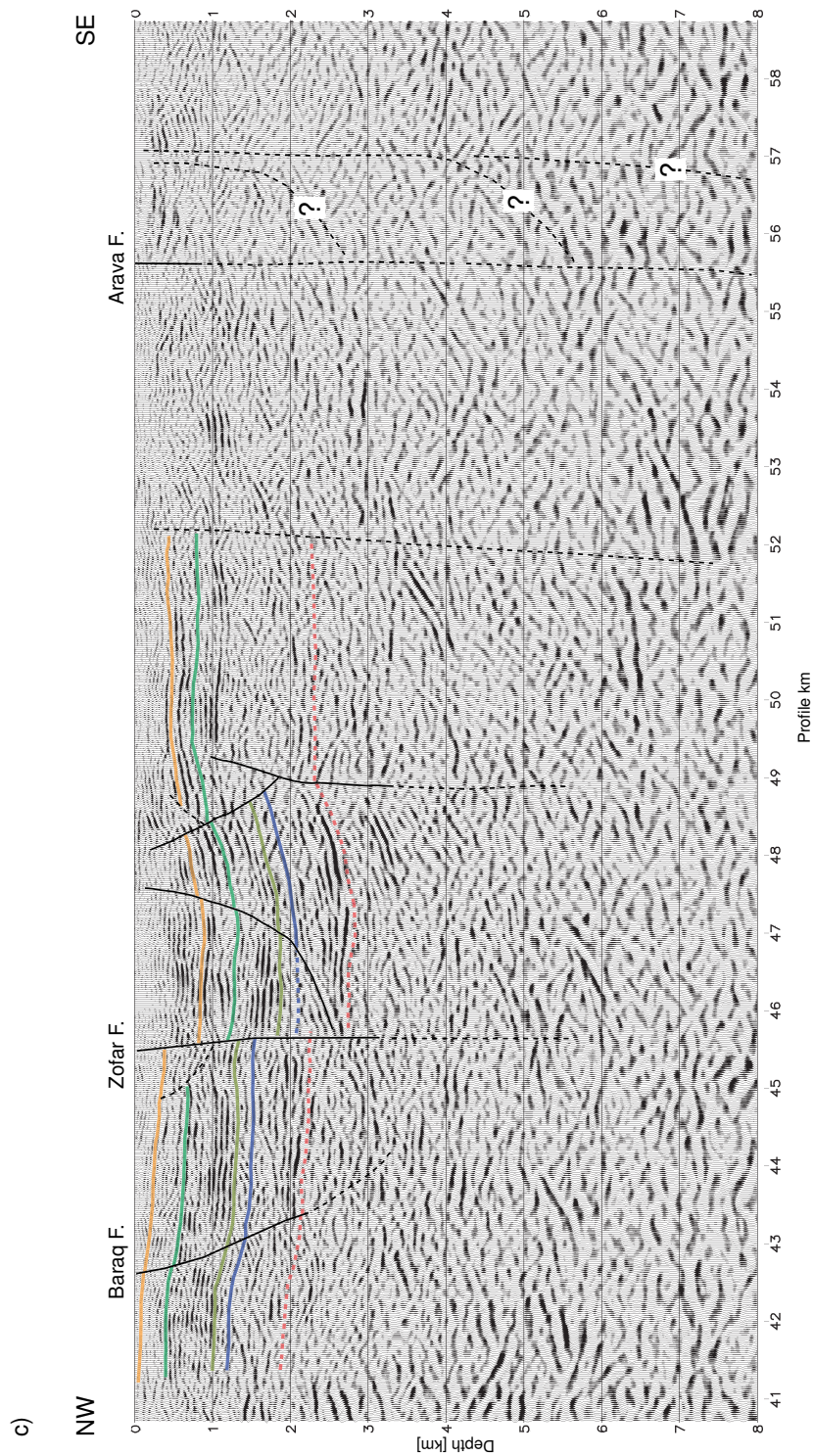Figure 3.12: Near-surface structure as seen in seismic reflection data. (a) (previous page) Location of the seismic profiles; Z-20: Zofar-20 well; AR-1 and AR-2: outcrops of Arava Formation (see text for further explanation); (b) (previous page) Depth-migrated shallow seismic reflection profile VWJ-9; (c) Upper central part of the depth-migrated NVR profile, as indicated by the dark red line in (a).
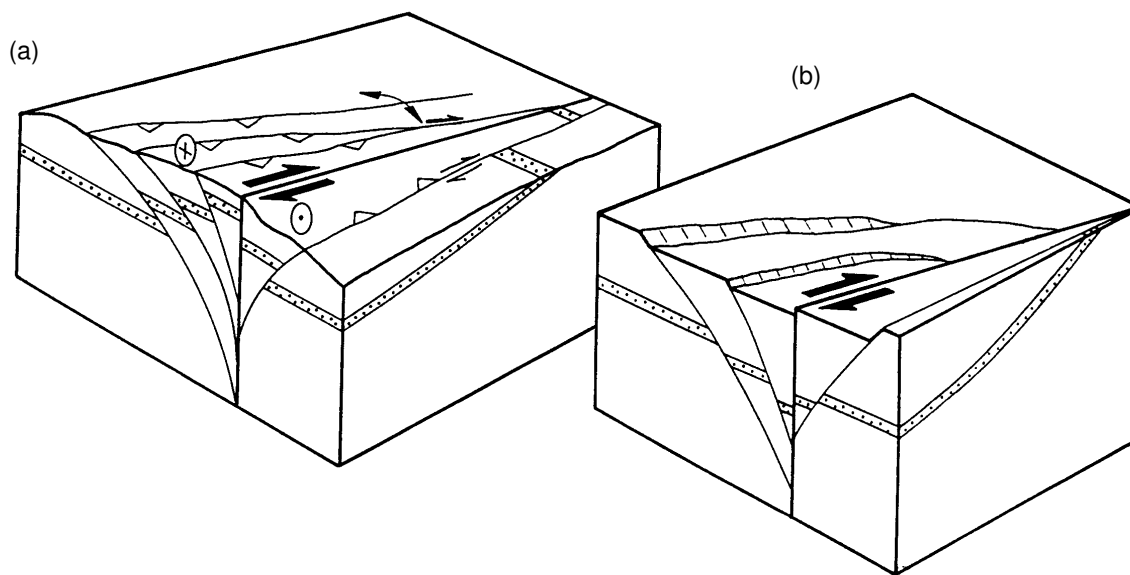
Figure 3.13: Schematic picture of a positive (a) and a negative (b) flower structure; from Eisbacher (1996).

The fault at profile km 49 (Fig. 3.12) does not seem to cut through the uppermost sediments and is not recognized at the surface. Thus it is assumed to have not been active in the recent past. There is, however, a marked contrast in reflectivity across this fault, a reason why it is considered to have had a strike-slip component. The fault's near-vertical geometry confirms this interpretation.

Another fault that is indicated at profile km 52 in Fig. 3.12c seems quite tentative just by looking at the NVR data. There is, however, a fault clearly recognizable in the seismic reflection profile VWJ-9* (Fig. 3.12b)at a similar location, around profile km 3.3. As the VWJ-9 profile is located ∼9 km north of the NVR line and runs nearly parallel to it, a comparison of these two seismic lines is possible. The obvious fault around profile km 3.3 of the VWJ-9 line represents a negative 'flower structure', a term that is used for upward and outward diverging strands of a strike-slip fault. Negative flower structures are associated with transtension and synformal structures, while positive flower structures are related to transpression and compressional features. Both are typical features of strike-slip fault zones

---

*Profile VWJ-9 is an industrial profile that was recorded in 1988 and is now property of the Natural Resources Authority (NRA) in Amman. The data, originally only available as blueprint of the time section, was scanned and digitized to segy format by Phoenix Data Solutions Ltd., London, UK. With the help of velocity analyses, that had additionally been carried out, it was then possible to migrate the data and convert them to depth.

(e.g. D'Onfro and Glagola, 1983; Harding and Lowell, 1979; Harding, 1983, 1985; Shtivelman *et al.*, 1998). The negative flower structure observed here is thought to be associated with a currently inactive strike-slip fault. At the surface there is no evidence for recent displacement. If the discontinuous reflectivity pattern around profile km 52 in the NVR line is related to the distinct strike-slip fault in profile VWJ-9, this 'old' fault would have been at a small angle to the currently active Arava Fault, running nearly N–S.

A shifting of the main active fault of the Dead Sea Transform Fault System was proposed by Rotstein *et al.* (1992) on the basis of shallow seismic reflection results of the Kinarot basin, south of the Sea of Galilee. The authors saw evidence for an extinct fault trace, approximately 2.5 km west of the active segment of the DST. However, as the Kinarot basin is located more than 200 km to the north of our study region, a direct comparison of the observed structures does not seem to be reasonable. Nevertheless there could have been a more regional cause for local changes in the structural setting of the DST. Such changes in the geometry of large transform faults are generally thought to be quite common with time. For the DST, a major shift in the direction of plate motion around 5 Ma ago was suggested by Joffe and Garfunkel (1987). Ten Brink *et al.* (1999) proposed continuous small variations in plate motion to be responsible for the observed geometry of the DST.

In order to constrain the period of time in which the proposed fault west of the Arava Fault has not been active, it is crucial to know the age of the surface sediments. However, as there are no dated young surfaces in the Arava Valley and also due to the great variety of stratigraphic studies and the often not well-defined nomenclature of the Neogene – mainly fluviatile strata – the information derived from geological maps and literature is highly ambiguous. On the Israeli 1:200 000 geological map (Sneh *et al.*, 1998) the sediments between the VWJ-9 and NVR profiles east of the Zofar Fault are mainly attributed to the Miocene Hazeva Formation/Dana Conglomerate (Fig. 2.5). This view is also supported by Calvo and Bartov (2001). Contrarily, the same sediments are marked as Pleistocene sand and gravels on the 1:100 000 (Bender, 1974) and 1:50 000 (Rabb'a, 1991) Jordanian geological maps. Horowitz (2001), too, favours an early Pleistocene age for these sediments, describing them as 'Melekh Sedom Sands'. In a detailed study on Pliocene sequences of the Arava Valley, outcrops at the same location are identified as the ∼4–2 Ma old Arava Formation (Avni *et al.*, 2001). At point AR–1 in Fig. 3.12a, an outcrop of reddish sandstone and chalky limestone, overlain by a conglomerate with mainly well–rounded pebbles of limestone, chert and igneous rocks, highly resembles the

description of an outcrop of the Arava Formation at Nahal Neqarot (Fig. 2G and Fig. 4 in Avni *et al.*, 2001), located around 5 km WSW of 'En Yahav (point AR–2 in Fig. 3.12a). This observation supports the interpretation by Avni *et al.* (2001). Taking into account these various age estimates, the period in which the assumed strike-slip fault has not been active lies between 2 and 7 Ma.

Arava Fault

As already mentioned, there is hardly an expression of the Arava Fault in the upper crust in the NVR data. The lack of coherent sedimentary reflections in the vicinity of the AF might result from intense brittle deformation of the rocks close to the fault, but could also be caused by the absorption of high frequencies in an area covered by sand dunes and alluvium (Fig. 3.2.2). There is, however, a slight change in the character of (diffuse) reflectivity across the subsurface continuation of the AF (Fig. 3.12c). Approximately 1 km to the E of the AF a rather 'white' zone might point to a second segment of the AF. This proposed segment is not visible at the surface, but is clearly seen in a study on scattered seismic waves (Maercklin *et al.*, 2004). It could therefore be a recently inactive branch of the AF, joining it at some depth. In the study by Maercklin *et al.* (2004) scattered seismic waves still occur at a depth of 4 km, 1 km east of the AF. The dashed lines in Fig. 3.12c indicate various options for a proposed eastern fault segment, which is not resolved by the NVR data. Its geometry therefore remains speculative.

Further to the north, there is clear indirect evidence of the AF in the seismic profile VWJ-9 (Fig. 3.12a). Here the AF lies between a zone with clear sedimentary reflections to the west and a purely diffusely reflective upper crust towards the east. The strong 'double reflector' close to the surface between profile km 7.5 and 8.5 is attributed to the top of the Precambrian basement. A massive block of Precambrian rocks crops out in the Fiddan area further to the north and various small outcrops of Precambrian granite are found 700 to 1200 m north of profile line VWJ-9 (Fig. 3.14). Due to the strong impedance contrast between the thin layer of surface sediments and the granites directly below, the observed second, parallel reflector is interpreted as multiple.

The AF itself is imaged as a non-reflective zone that is ~800 m wide at the surface and probably consists of at least three branches (Fig. 3.12a). This is mainly derived from surface geological data, aerial photographs, and satellite images which all show indications for subparallel fault segments. The surface appearance of the

AF between the NVR and VWJ-9 profiles will now further be discussed.

In the region west of Jebel Humrat Fidan (Fig. 3.14) the AF changes its orientation from ~13.5°E in the south to ~16.2°E towards the north. This restraining bend is clearly visible on satellite images and is responsible for the formation of a pronounced pressure ridge of Lower Cretaceous sandstones and Upper Cretaceous carbonates (delineated by a dark green line in Fig. 3.14). The main fault trace runs directly through this ridge and is associated with steeply dipping beds of limestone and some fault breccias. South of the pressure ridge the AF can be traced across the alluvium, sometimes forming small, steeply dipping scarps. A river bed, running approximately parallel to the NVR profile, shows a sharp kink towards a northerly direction, where it meets with the AF (Fig. 3.14). The scarce outcrops located along the fault are shown in Fig. 3.14 and can mainly be divided in three different types: small, strongly weathered hills of limestone fragments, (Fig. 3.15b, given in yellow in Fig. 3.14), most of them being elongated in a N–S direction; massive limestone beds (Fig. 3.15c; coloured in green in Fig. 3.14) and breccias with fragments of limestone, sandstone and granite (Fig. 3.15d and e; orange in Fig. 3.14). Whereas the breccias can clearly be attributed to the Pliocene Arava Formation (Y. Bartov, pers. comm., 2002), the massive limestone outcrops are thought to have an Upper Cretaceous age. The limestone fragments that are found on small hills might belong to the lower part of the Miocene, but an Eocene to Upper Cretaceous age cannot be ruled out for all of these occurrences. At some places small, man-made holes with standing water are found directly at the surface trace of the AF (marked in blue in Fig. 3.14).

Considering the deformation pattern of the exposed rocks, it is hardly possible to make any statement of the internal structure of the fault zone. Even the scarce outcrops located at the fault do not exhibit the typical fault zone architecture with a main gouge zone, fault related damage zone and undeformed host rock, that is well known from other fault studies (Chester and Logan, 1986; Chester *et al.*, 1993; Schulz and Evans, 1998; Faulkner *et al.*, 2003). Regarding the few outcrops it just seems to be evident, that in the region of profile VWJ-9 the AF consists of several branches, that are only partly expressed on the surface. There are indications for a fault both to the west and to the east of the limestone outcrop located at 30.587°N in Fig. 3.14. Along the western border of this outcrop the Cretaceous carbonates are extremely brecciated and at one place a steeply dipping (N20/88 ESE) fault plane is exposed in the limestone beds. To the east subvertically dipping gypsum beds and various coloured marls provide evidence of a subparallel fault. A third fault branch
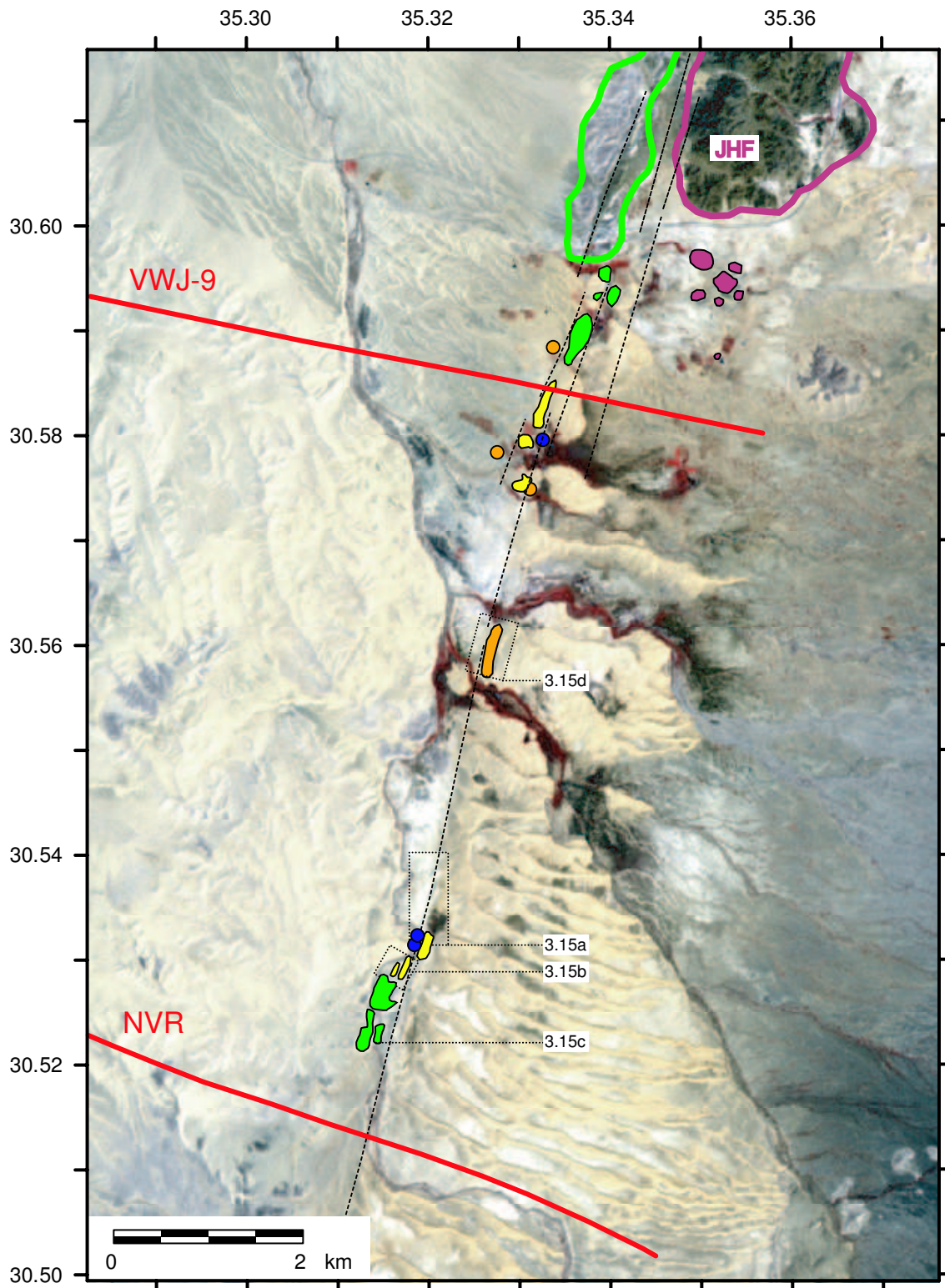
Figure 3.14: Surface appearance of Arava Fault close to NVR profile. Outcrops along the AF are overplotted in various colours on a high-resolution ASTER satellite image. Dark red: Precambrian granites; green: limestones; yellow: small hills of limestone fragments; orange: sandstones and breccias; blue: waterholes. The positions of the photographs of Fig. 3.15 are schematically indicated. See text for further explanation. JHF: Jebel Humrat Fiddan.

might be located even further to the east, displacing Cretaceous sediments against Precambrian granites.

Different subparallel fault segments are also in accordance with both shallow seismic tomography (Maercklin *et al.*, 2002) and magnetotelluric studies (U. Weckmann, pers. comm., 2003). These studies, which had the region between the NVR and the VWJ-9 profiles as target area, show a fault zone that apparently gets more complex towards the north. This is most probably related to the restraining bend of the Arava Fault in this region.

Shallow subsurface structure along the NVR line from tomography

With the NVR seismic data tomographic inversion techniques were applied to first arrival times of direct P waves to study the shallow part of the crust (Ryberg *et al.*, 2001; Ritter *et al.*, 2003). The result along the central part of the NVR profile is shown in Fig. 3.16. The uppermost crust is characterized by velocities < 3 km/s that mainly correspond to Miocene and younger sediments, at least between the Zofar Fault in the W and the AF in the E. This is inferred from the geological interpretation of the seismic reflection data (Fig. 3.12c, see above).

East of the AF the most prominent feature is a high-velocity block ($v \approx 4.8$ km/s; Ritter *et al.*, 2003) that is interpreted as horst structure of Precambrian magmatic rocks. This horst structure might even represent the southward continuation of Jebel Humrat Fiddan (see e.g. Fig. 3.14). The exact location and geometry of the indicated normal fault to its east (Fig. 3.16) is tentative, but in satellite data a clear lineament is seen at the surface (Fig. 4.2.2) that might represent the surface trace of a (now inactive) fault. Such a fault could be an antithetic fault to the Al Quwayra Fault (AQF), but could also have a strike-slip character and thus extend subvertically downward. The AQF is delineated with a (local) dip of 55° towards the W, as it was measured at an outcrop close to the NVR profile. Its continuation with depth is unknown. As the fault clearly exhibits both lateral and vertical displacement[*], a subvertical main shear zone with various fault branches might be considered.

---

[*]In an outcrop approximately 100 m west of the main fault plane, directly at the NVR profile, Upper Cretaceous sediments dip nearly vertically and show intense, subhorizontal slickensides, indicating a sinistral movement along the Al Quwayra Fault.
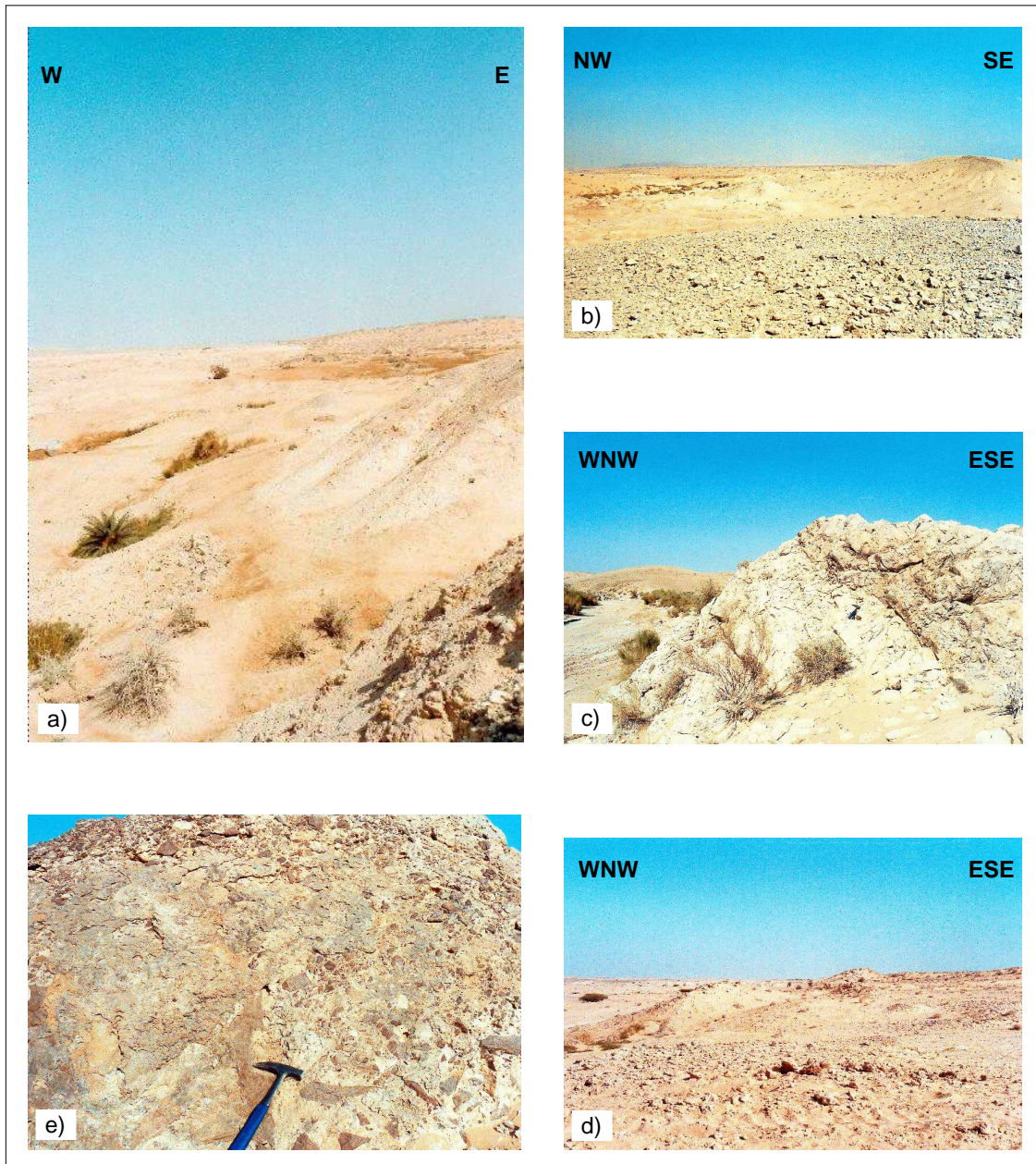
Figure 3.15: Features along the Arava Fault between the NVR and VWJ-9 profiles. (a) AF at 35.32°E, 30.531°N, looking towards the N; (b) Hills of limestone fragments at 35.315°E, 30.529°N, looking towards NE; (c) Bedded limestone at 35.315°E, 30.523°N, around 200 m west of the surface trace of the AF; (d) N–S elongated ridges of breccias at 35.328°E, 30.558°N, directly east of the surface trace of the AF; (e) breccia with sandstone, limestone and granite fragments from outcrop shown in (d), part of the Pliocene Arava Formation.
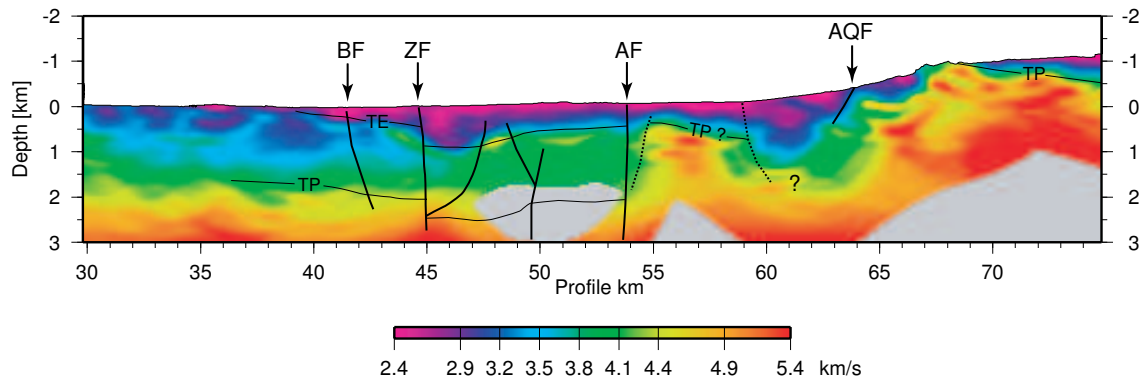
Figure 3.16: P wave tomography model along centre of NVR profile, from Ryberg *et al.* (2001). The structural interpretation is mainly derived from seismic reflection data (see also Fig. 3.12c). See text for further explanation. BF: Baraq Fault; ZF: Zofar Fault; AF: Arava Fault; AQF: Al Quwayra Fault; TE: Top Eocene; TP: Top Precambrian.

4 ASTER Satellite Images

As a complementary part to the near-vertical seismic experiment that answers questions concerning subsurface structures, ASTER (Advanced Spaceborne Thermal Emission and Reflection Radiometer) satellite images* were used to gain additional information on neotectonic activity. Especially in desert areas and hardly accessible regions, high-resolution multispectral satellite images offer a powerful tool for geologic analyses. As the DST is the main subject of this study, focus is put on the surface appearance of the Arava Fault and on related structures recognized in the Arava Valley.

4.1 General Remarks on ASTER images

ASTER is an instrument on Terra, a satellite that was launched in December 1999 as part of NASA's Earth Observing System (EOS). It has a circular, near-polar orbit at an altitude of 705 km. The ASTER instrument consists of three different subsystems. The Visible and Near-Infrared (VNIR) camera records in three bands ($\lambda \approx$ 0.52-0.86 μm) providing a spatial resolution of 15 m. It has an additional backward telescope for stereo. The Shortwave Infrared (SWIR) camera records in 6 bands ($\lambda \approx$ 1.60-2.43 μm) yielding a resolution of 30 m. The thermal Infrared (TIR) has 5 bands ($\lambda \approx$8.13-11.65 μm) with a spatial resolution of 90 m.

Multispectral images have proven to be most useful to discriminate between rocks or minerals, as the reflectance spectra depend on the chemical composition of the soil or the rocks and in particular on the characteristic absorption properties of their constituents (e.g. water, Si–O, Fe–O).

On satellite images faults are generally recognized either by offset lithologic contrasts or by truncations or repetitions of units. Whereas these observations are

---

*The data was provided by the remote sensing department of the GFZ, who also carried out the necessary geometric corrections.

non-ambiguous signs for faulting, other observed **lineaments**[*] might not necessarily be expressions of faults. A lineament usually originates from a geomorphic or tonal contrast, the latter mainly being caused by differences in vegetation, moisture content, and soil or rock composition. Although many lineaments are controlled at least in part by faults, structural dispacement is not a requirement in the definition of a lineament (Sabins, 1996). In fluvial environments, lineaments might also be generated by young stream sediments cutting through older ones.

4.2   ASTER Scenes of the Arava Valley

4.2.1   Method of Analysis

In the following three ASTER scenes will be described, that all span ∼65 km in N–S and ∼35 km in E–W direction. The images represent false-colour composites, where band 7 (2.235-2.285 μm) is displayed in red, band 3 (0.78-0.86 μm) is displayed in green, and band 1 (0.52-0.60 μm) is displayed in blue. This band combination is optimal to discriminate between various rock units, as it showed the highest contrasts in the study region combined with a good resolution. At some places thermal infrared bands with λ between 8 and 14 μm provided additional information. Although in this band of wavelengths the resolution is less, it allows a direct discrimination between rock types, because the most prominent features relate directly to rock-forming minerals rather than minor components such as limonite and clay minerals (Drury, 1993).

In the 7–3–1 images shown (Fig. 4.1–4.3), carbonates usually appear in greyish colours, with Campanian and Eocene chert-rich rocks being cyan. Rocks with a higher Fe–O content are displayed much darker on the false colour composite and show various brown and dark violet shades. Plants and fields are green.

On the interpreted ASTER scenes three types of lineaments are distinguished:

1) Solid lines represent lineaments that are clearly recognized as faults (by displaced geological units, offset alluvial fans or clear 'doglegs' of streams).

2) Dashed lines are used for lineaments that were identified as faults in other, mainly shallow seismic studies (e.g. Frieslander, 2000; Ginat *et al.*, 1998).

---

[*]A lineament is a mappable linear or curvilinear feature of a surface whose parts align in a straight or slightly curving relationship (Sabins, 1996).

3) Dotted lines are lineaments, whose origin could not be clarified because of a lack of other geological or geophysical studies.

The observed structures will be described from the south (∼10 km north of the Gulf of Aqaba) to the north (southern Dead Sea Basin). The interpretation of the satellite data is interlinked with the results of other geological and geophysical studies where possible.

4.2.2   Structural Observations

Character of the Arava Fault

Although in the region of the DESERT NVR seismic profile the location of the Arava Fault seems to be rather well defined (see also section 3.3.3), a distinct fault trace is missing in large parts of the southern Arava Valley (Fig. 4.1a). It is probably covered by young sand dunes and stream sediments. Only at some places, especially on older alluvial surfaces (e.g. between 29.65 and 29.78°N, Fig. 4.1) some fault segments are recognizable. These alluvial fans have been attributed a Pleistocene age by Bender (1974).

Around latitude 29.85°N a stepover of the main fault trace to the left could be inferred from Bouguer gravity data, indicating a basin around 29.8°N (ten Brink *et al.*, 1999, Fig. 4.1b). This basin was referred to as Timna Basin with a modelled depth of 1300 m. The exact location of the AF in this region and ∼35 km towards the north remains unclear.

North of latitude 30.15°N, in the central Arava (Fig. 4.2.2), the AF is well defined by offset alluvial fans and small scarps. One main fault trace runs rather straight from the Jebel El Khureij/Jebel Er Risha area in the south to the Jebel Humrat Fiddan over a distance of 40 km (Fig. 4.2). These 'Jebels' (Arabic for 'hills') are pressure ridges that are related to right stepovers/restraining bends of the AF. Whereas Jebel Er Risha is composed of Miocene gravels (Ginat *et al.*, 1998), Upper Cretaceous rocks crop out at Jebel El Khureij (e.g. Bender, 1968; Sneh *et al.*, 1998). The pressure ridges west of Jebel Humrat Fiddan consist of Lower Cretaceous and Upper Cretaceous sediments (see also subsection 3.3.3). The outcrop of Precambrian granites at Jebel Humrat Fiddan might also be interpreted as part of this pressure ridge. It could, however, also represent a horst structure related to the general uplift of the eastern flank of the Arava Valley. Following considerations support this idea:
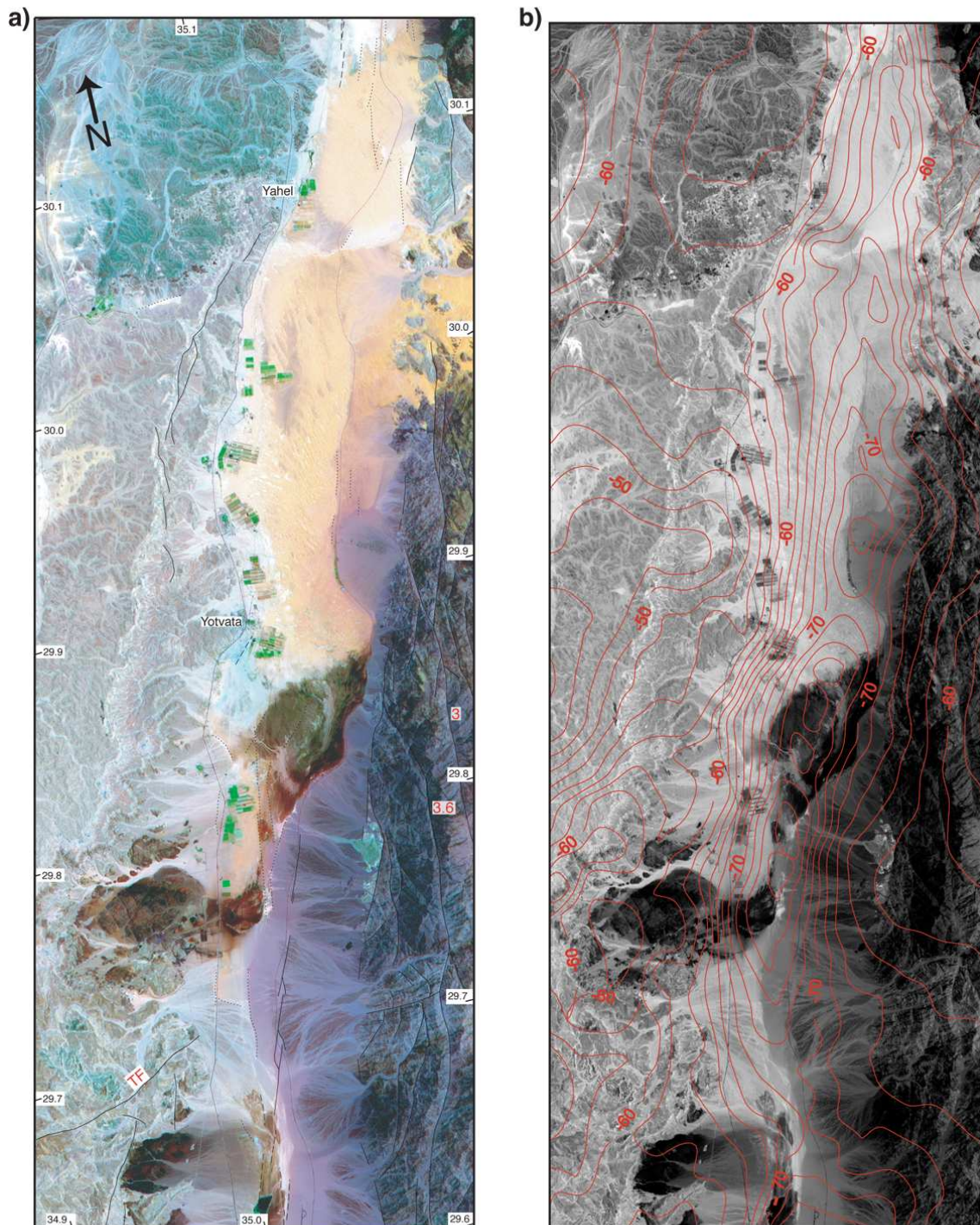
Figure 4.1: a) ASTER scene of the southern Arava Valley taken on June, 6th, 2000. The southern margin is located ∼10 km north of the Gulf of Aqaba. Solid lines represent unambiguous faults; dashed lines are lineaments related to subsurface faults seen in seismic reflection data (Frieslander, 2000; Shtivelman *et al.*, 1998); dotted lines are lineaments of unknown origin. The red numbers represent the amount of sinistral strike-slip motion, that is observed at the faults to their left. TF: Themed Fault. b) Same area as shown in a). Displayed in red are contour lines (values in mGal) of a Bouguer gravity study by ten Brink *et al.* (1999).

- The tomographic model along the NVR profile shows a high-velocity body $\sim$1 km east of the surface trace of the AF at a depth of 1 km (Ryberg *et al.*, 2001; Ritter *et al.*, 2003, Fig. 3.16). This high-velocity body might refer to the same proposed horst structure, only that it was not uplifted above surface.

- Around latitude 30.35°N Precambrian rhyolites crop out east of the AF, flanked by Cretaceous sediments towards the east. As this structure is clearly not related to transpression along a restraining bend of the AF, the Jebel Humrat Fiddan could represent a comparable structure. Generally the area east of the AF is highly faulted and 'structural niches' were described e.g. by Bender (1968) and Ibrahim (1991).

Directly north of the Jebel Humrat Fiddan (Fig. 4.3) the AF is only at places visible on the satellite image by small scarps in the young sediments. Some kilometres northwards it forms the eastern marginal fault of the Arava Valley (Fig. 4.3). Between latitude 30.9 and 31.0°N the AF is hardly expressed, but it can again be delineated further to the north.

Not only the pressure ridges but also other segments of the AF are characterized by a number of subparallel, overlapping fault segments, see e.g. east of the alluvial fan number 3 in Fig. 4.2. Very similar patterns of overlapping, en echelon fault segments have been described from other large strike-slip faults like the San Andreas and the Hayward–Calaveras faults (Aydin and Schultz, 1990).

Displaced Alluvial Fans

Three prominent features in the central Arava are displaced alluvial fans (numbers 1–3 in Fig. 4.2). These surfaces are mainly built up of igneous gravels of the Late Pliocene to Pleistocene Arava Formation (Ginat *et al.*, 1998). As already noted by Ginat *et al.* (1998) the fans are detached from the recent mountain front and have been displaced sinistrally along the AF. These authors showed that the amount of displacement ranges between a minimum of 15 up to a maximum of 30 km from the deposition of the fluvial sediments. Considering the current drainage system and the location of wadis east of the Arava Valley, a displacement of 15 km was favoured. A 15 km movement together with an estimated age of the Arava Formation of 5 to 2 Ma yields a slip rate of 0.3–0.75 cm/a along the AF. These values are in the range of calculated slip rates along the southern DST proposed by other authors (see section 2.1.2).
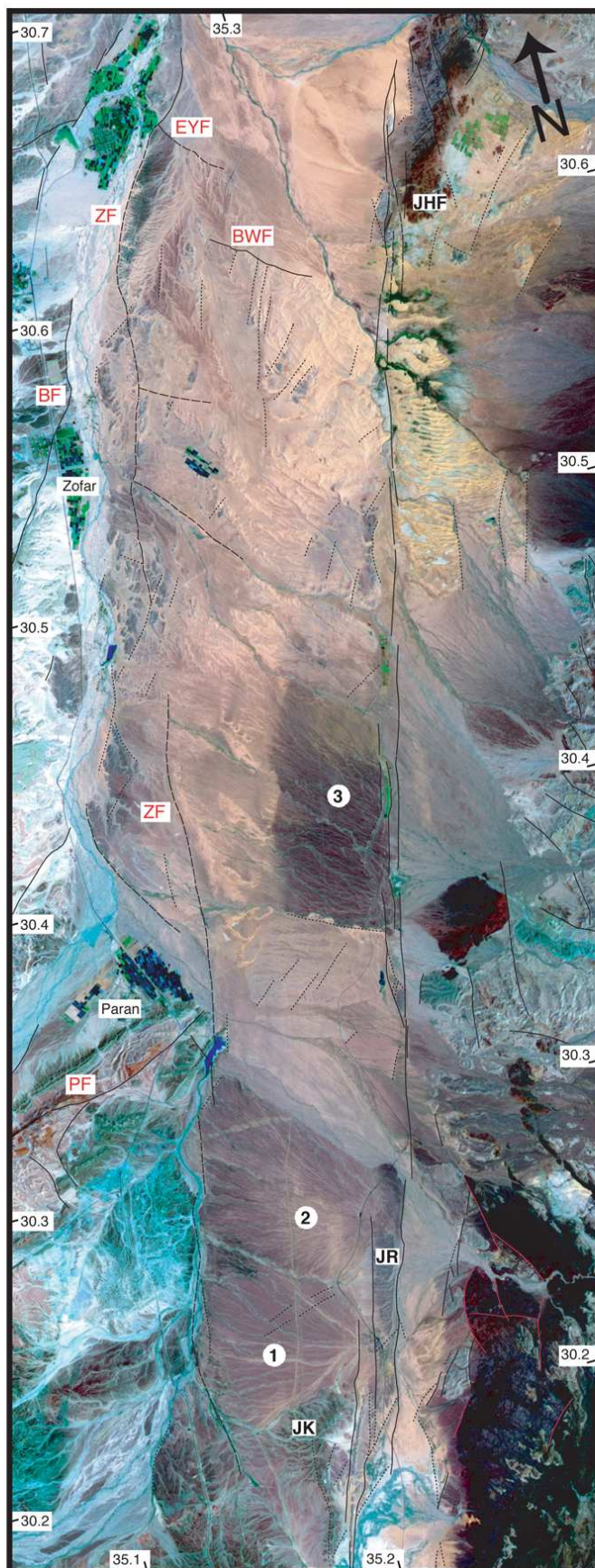
Figure 4.2: ASTER scene of the central Arava Valley taken in April, 6th, 2001. Solid lines represent unambiguous faults; dashed lines are lineaments related to subsurface faults seen in seismic reflection data (Frieslander, 2000); dotted lines are lineaments of unknown origin.

EYF: En Yahav Fault; BWF: Buweirida Fault; ZF: Zofar Fault; BF: Baraq Fault; PF: Paran Fault; JHF: Jebel Humrat Fiddan; JR: Jebel Er Risha; JK: Jebel El Khureij; numbers 1–3 are related to alluvial fans. See text for further explanation.

Faults Subparallel to the Arava Fault

The area flanking the southern Arava Valley towards the east is characterized by several ±N–S trending curvilinear faults (Fig. 4.1a). They cut through Precambrian basement rocks and most of them can be identified as sinistral strike-slip faults by offset dikes or magmatic units. At two of these faults the sinistral offset could be determined to be 3.6 km and 3 km respectively (Fig. 4.1, see also discussion in chapter 5). Clear scarps at some marginal fault segments bordering the Jordanian mountains indicate active vertical motion.

Further to the N the eastern margin of the Arava is dissected into several blocks by various fault systems (e.g. Atallah, 1992; Barjous, 1992, 1995). The complex fault pattern might be related to different stress fields that have acted since Precambrian times (Atallah, 1992; Zaineldeen, 2000) and will not further be discussed. On the satellite images only the most prominent faults are marked. Many of these faults do not show a significant displacement.

Generally the western flank of the Arava Valley does not seem to be as dissected by faults as is the eastern margin. Especially in the central Arava (Fig. 4.2) there are, however, some pronounced fault segments that can be interpreted as western marginal faults of the valley. One of these faults is the Zofar Fault. It is only partly recognizable as clear lineament in the ASTER data, but several E–W trending shallow seismic reflection lines confirmed its existence (Frieslander, 2000; Bartov *et al.*, 1998, see also section 3.3.3).

At the southern end of the DSB, southwest of the Amaziahu Fault (Fig. 4.3), some N–S striking lineaments might be related to a normal fault in the subsurface. This fault was detected on seismic reflection profiles and has a considerable downthrow to the E (Gardosh *et al.*, 1997).[*] N–S trending lineaments in the central Arava Valley south of the Buweirida Fault (Fig. 4.2) do probably not represent currently active faults, because there is no sharp fault trace. They might, however, correspond to the suggested (subsurface) strike-slip fault recognized on seismic reflection profile VWJ-9 (see section 3.3.3, Fig. 3.12). The geometry/trace of these faults cannot be determined on the satellite scenes and would need further shallow seismic investigations.

---

[*]The rather linear tonal contrast west of this fault represents the shoreline of the last high stand lake, that existed in the Dead Sea area between 50 and 15 ka (Neev and Emery, 1967; Garfunkel, 1997). The white to light grey colours on the ASTER scene are attributed to the Lisan Formation, mainly aragonite varves and mudstones, that were deposited during this time.
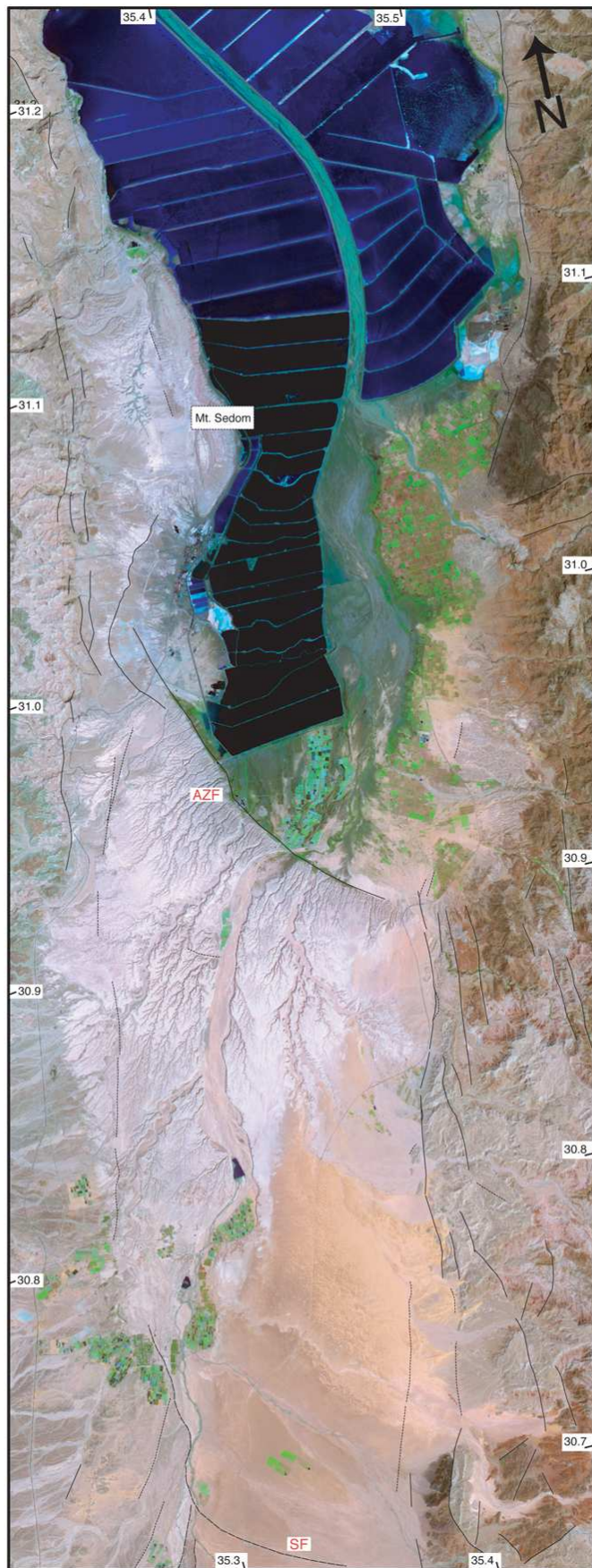
Figure 4.3: ASTER scene of the northern Arava Valley and southern Dead Sea Basin, taken on April, 6th, 2001. Solid lines represent unambiguous faults; dashed lines are lineaments related to subsurface faults seen in seismic reflection data (e.g. Gardosh *et al.*, 1997); dotted lines are lineaments of unknown origin.
AFZ: Amaziahu Fault; SF: Shezaf Fault.

Another eye-catching N–S trending feature is the rather linear tonal contrast associated with the western boundary of alluvial fan 3 (Fig. 4.2). Due to a lack of E–W trending seismic profiles in this region it remains speculative, whether this lineament can be attributed to a subsurface fault zone.

NW–SE Trending Normal Faults

In the central and northern Arava Valley (Figs. 4.2 and 4.3) some ∼NW–SE trending lineaments are conspicuous on the ASTER images. These lineaments were all identified as normal faults dipping to the NE using N–S running seismic reflection profiles in Israel (e.g. Frieslander, 2000) and Jordan (Fig. 4.4). Although a proposed left-lateral displacement along the Zofar Fault could not be proven by geological or geophysical evidence, the southern Dead Sea Basin seems to extend southward to the Buweirida Fault** (Fig. 4.4). The Buweirida Fault forms a clear morphological scarp and thus is probably still active, whereas the Shezaf Fault, a listric normal fault, does not have a morphological fingerprint (Fig. 4.3). The Amaziahu Fault further to the north is certainly the most distinct of these NW–SE trending faults and is expressed by a 50 m high scarp (Garfunkel, 1997). It is thought to be genetically related to salt tectonics of the southern Dead Sea Basin and the development of the Mt. Sedom salt diapir (ten Brink and Ben-Avraham, 1989; Gardosh *et al.*, 1997). It has probably been continuously active since the Early Pleistocene (Gardosh *et al.*, 1997). It flattens at a depth of 6 km (ten Brink and Ben-Avraham, 1989).
N–S stretching of the crust must have started earlier, however. This is inferred from the seismic reflection profile VWJ-6, that shows thickening of Miocene sediments towards the north (Fig. 4.4). A morphological depression in the Dead Sea region already during Miocene times was also suggested by Garfunkel (1997). It is remarkable, that this extension has apparently not been related to significant faulting activity. The location of the Shezaf Fault might be controlled by an older structure in the Pre-Miocene sediments, but the amount of offset along the Shezaf Fault is negligible. It probably soles out in the Upper Cretaceous Ghareb and Taqiyeh formations, equivalent to the Muwaqqar Chalk–Marl unit in Jordan. These Maastrichtian to Paleocene formations build a main detachment horizon in the area (Y.

**Some confusion prevails in the literature concerning the names of the various NW–SE trending faults. Here the nomenclature of Frieslander (2000) and Calvo and Bartov (2001) was adopted. The Shezaf Fault, for example, was named 'Iddan Fault' by Al-Zoubi and ten Brink (2001), and by Gardosh *et al.* (1997), whereas the name 'Iddan Fault' was also used for a subsurface fault some 20 km further to the north by Al-Zoubi and ten Brink (2002).

Bartov, pers. comm., 2003).

A lack of faults that could account for N–S crustal extension – coincident with large-scale subsidence of the Dead Sea region – led Al-Zoubi and ten Brink (2002) to the hypothesis, that lower crustal flow might be the mechanism responsible for lower crustal thinning.

NE–SW Trending Lineaments

Some NE–SW trending lineaments observed on the satellite images cannot directly be linked to surface traces of faults (Fig. 4.3). According to their trend, however, these lineaments might be associated with (subsurface) faults of the Central Negev–Sinai shear zone. Around latitude 30.35°N, for example, such lineaments occur NE of the Paran Fault, that has probably still been active in the recent past (Y. Bartov, pers. comm., 2003). A short NE–SW trending segment at the western margin of the Arava Valley at latitude 30.32°N is displaced 200 m left-laterally by a ∼N–S striking fault and thus seems to be an older feature.

To make a reliable statement on the type and origin of these NE trending lineaments, further evidence from geological field work or geophysical studies is needed.

Figure 4.4: Interpretation of the seismic reflection line VWJ-6 and its location in the northern Arava Valley.

Due to the large amount of traces a 'variable area only' depiction of the data was chosen here. The geological interpretation is based on the stratigraphic information of the Wadi Ghaube well (see A.1) and the correlation with the VWJ-9 and NVR profiles. Like with profile VWJ-9 (section 3.3.3) the seismic data was originally available as unmigrated blueprint only, then scanned, digitized and finally migrated to depth.
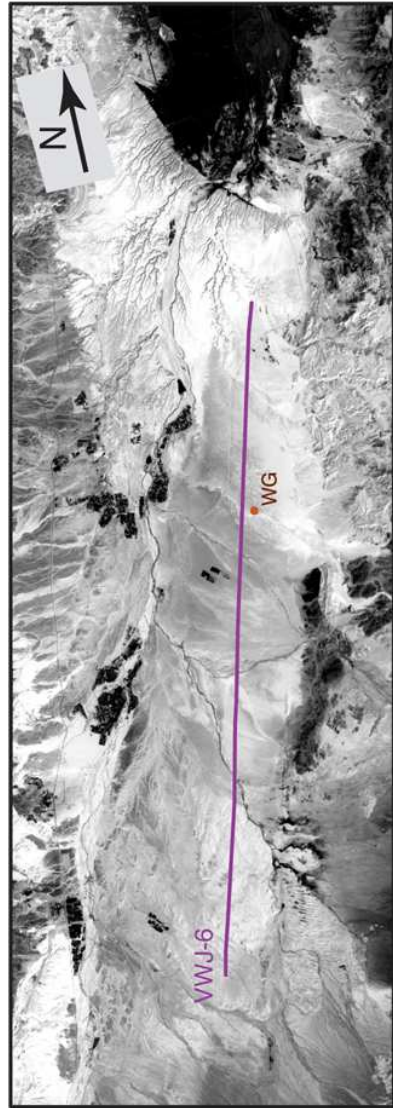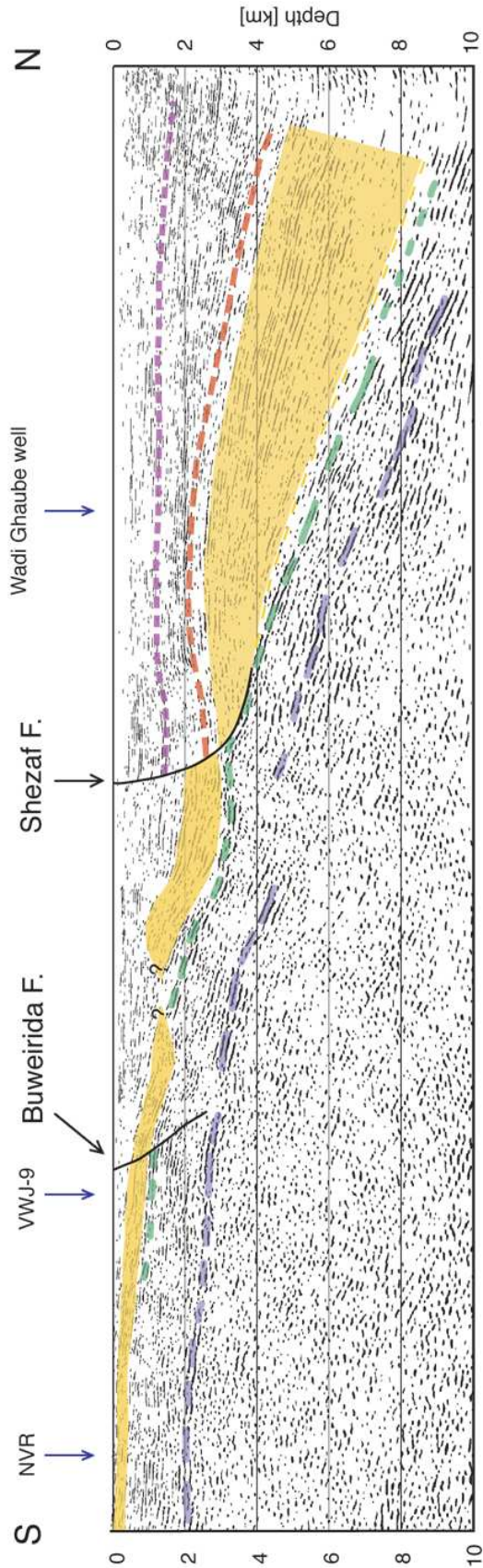
Miocene (Hazeva Formation)

Top of Pleistocene
(Amora F. and Samra-Lisan F.)

Top of Pliocene
(Melekh Sedom Sand)

Top of Turonian (Judea Group)

Top of Precambrian (?)

5 Summary and Discussion

Deep Crustal Structure of the Southern Dead Sea Transform

With the help of the DESERT near-vertical seismic reflection study, important questions concerning the deep structure of a major strike-slip zone could be answered. Despite of a huge amount of other geophysical and geological investigations at the DST this experiment was the first of its kind: no other seismic profile had crossed the DST before — crossing also the national border between Israel and Jordan.

The NVR seismic data showed, that the DST extends through the whole crust into the mantle. This is mainly deduced from a ~15 km wide zone with only diffuse lower crustal reflectivity. In contrast to other large active strike-slip fault zones (e.g. San Andreas Fault, California; Alpine Fault, New Zealand; North Pyranean Fault, Spain) no significant Moho offset was observed at the DST in the Arava Valley. Although a small Moho offset cannot be ruled out on the basis of our seismic data, a coupled upward-downward bending of the Moho is favoured here and is in accordance with other geophysical data (seismic refraction, gravity). Such 'smoother' structures in the topography of the crust/mantle boundary have elsewhere been attributed to older, Paleozoic strike-slip zones (Stern and McBride, 1998, Fig. 5.1). These authors suggest, that sharp vertical steps of the Moho – produced by discrete faulting – could not persist over longer periods of geologic time and would therefore relax into smoother structures. At the same time this does not mean, that active strike-slip faults are necessarily associated with jumps in Moho depth. A missing Moho offset across an active strike-slip zone like the DST could well be the consequence of an originally rather homogeneous Moho structure in the area prior to transform motion. One should keep in mind, however, that one single 2-D profile might not be representative for a larger region. Peculiarities in the crustal structure might exist at a certain location only and might not be a feature related to the fault zone as a whole. Based on gravity data, a Moho offset was proposed to exist, for
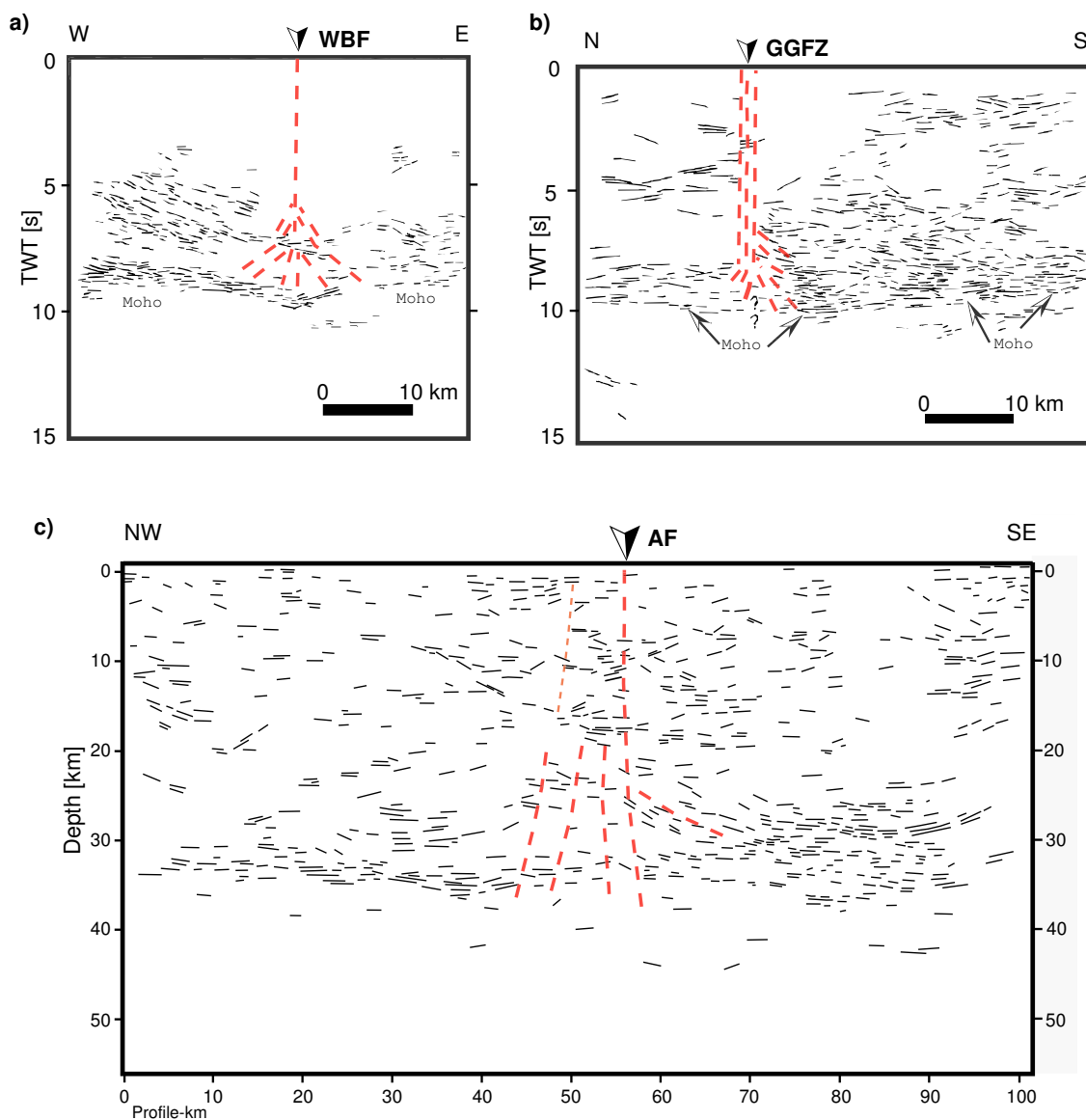
Figure 5.1: Comparison of two interpretive line drawings by Stern and McBride (1998) (a and b) to the NVR profile (c). Dashed red lines indicate the locus of deformation associated with strike-slip, not necessarily faults themselves. a) Interpretive line drawing of a time-migrated seismic reflection profile across the Walls Boundary Fault (WBF), the northern continuation of the Great Glen Fault north of the Shetland Islands, based on a section from McBride (1994); b) Interpretive line drawing of a profile across the Great Glen Fault Zone (GGFZ) north of northern Ireland, based on a frequency-wavenumber migration by Klemperer *et al.* (1991); c) Manual interpretive line drawing of the DESERT NVR profile. The thinner dashed line west of the Arava Fault (AF) indicates the existence of an older, inactive fault segment.

example, below the Dead Sea Basin (ten Brink *et al.*, 1990).

In contrast to the seismic reflection profiles across Paleozoic strike-slip faults that do not show any evidence for a mid crustal detachment (Stern and McBride, 1998), some reflections at ∼18 km depth in the NVR profile might indicate some shear deformation at the base of the upper crust, i.e. localized at a compositional boundary. Considering the result of thermo-mechanical modelling (Sobolev *et al.*, 2004) and shear wave splitting analysis (Rümpker *et al.*, 2003), most of the shear deformation related to lateral transform movement seems to be taken up in the lower crust and upper mantle, however. This is apparently also the case regarding N–S crustal extension associated with the Dead Sea Basin. As seen in the seismic reflection profile VWJ-6 and other seismic data (Al-Zoubi and ten Brink, 2002), only a few faults with minor vertical displacement exist, some of them being connected with young salt tectonics (Al-Zoubi and ten Brink, 2001). A lack of brittle deformation, coincident with large-scale subsidence of the Dead Sea region, led Al-Zoubi and ten Brink (2002) to the hypothesis, that lower crustal flow might be responsible for lower crustal thinning. Aldersons *et al.* (2003) favoured a mainly brittle lower crust due to deep microearthquakes. Nevertheless they could not exclude the existence of lower crustal flow. Generally the DST and the Dead Sea Basin are rather explained by thick-skinned than by thin-skinned tectonics. The deep crustal deformation zone is not centered below the vertical continuation of the Arava Fault but slightly displaced towards the west. This is in accordance with the seismic anisotropy study by Rümpker *et al.* (2003), who modelled a 20 km wide upper mantle deformation zone west of the surface trace of the AF. One reason for this westward 'shift' of the shear zone might be the left stepover of the main fault trace in the region of the DSB. A further explanation could be based on the assumption, that another, now inactive major fault exists a few kilometres west of the AF in the region of the NVR profile (see subsection 3.3.3). This supposition is backed up by the NVR and VWJ-9 seismic profiles and some N–S trending lineaments on satellite images.
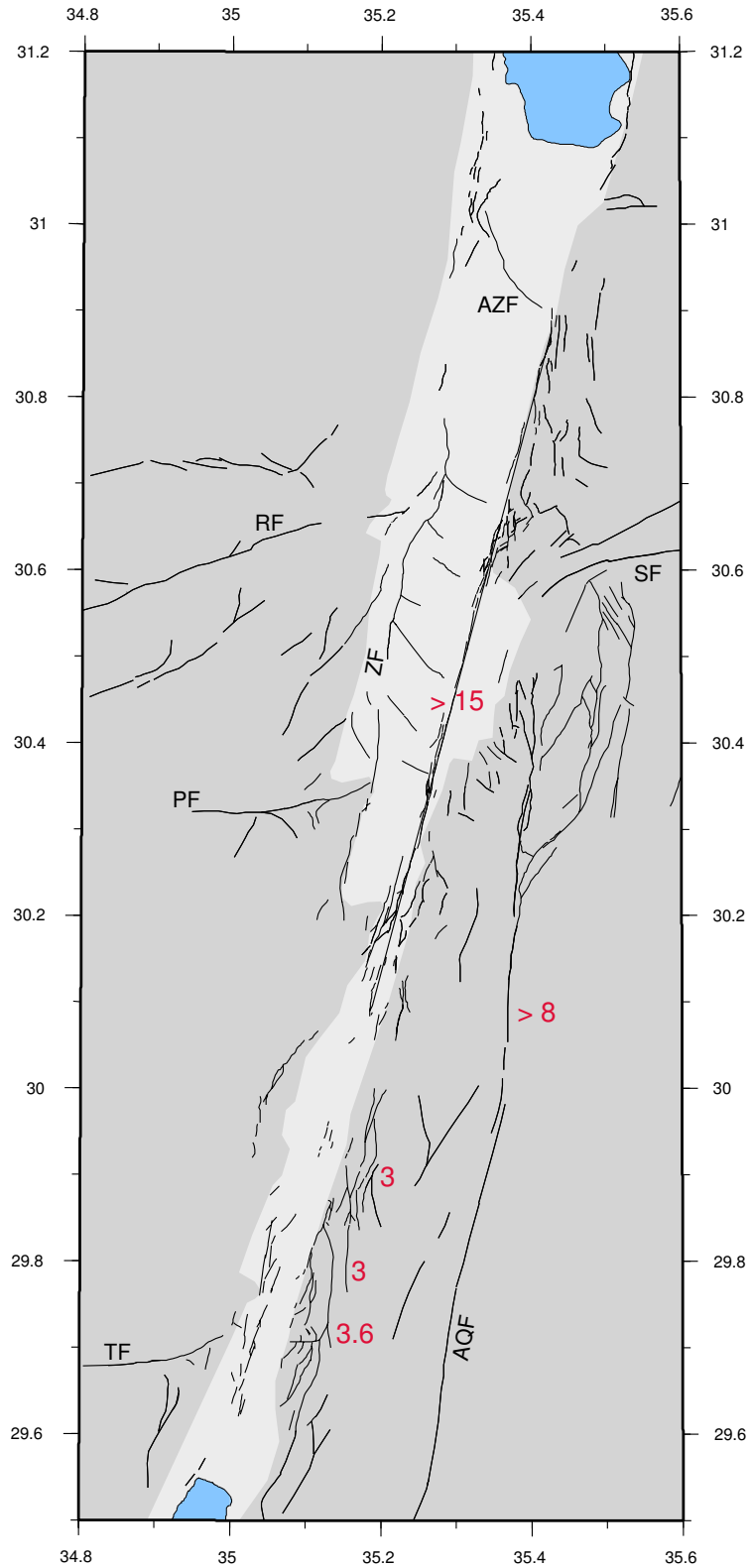
Figure 5.2: Faultmap of the southern Dead Sea Transform, derived from the interpretation of ASTER satellite images. The red numbers indicate the minimum amount of left-lateral strike-slip displacement along the respective faults in km. AQF: Al Quwayra Fault; AZF: Amaziahu Fault; BF: Baraq Fault; PF: Paran Fault; RF: Ramon Fault; SF: Salawan Fault; TF: Themed Fault; ZF: Zofar Fault.

Shallow Structure of the Southern Dead Sea Transform

Based on the interpretation of ASTER satellite images a map with the main faults related to the southern DST is shown in Fig. 5.2. Major E–W trending faults of the Central Negev–Sinai shear belt are also marked.

It is obvious, that there are a number of parallel fault segments that all contribute to take up the total amount of 105 km sinistral displacement, though it has been debated, how the lateral motion has been distributed among the various faults (Haberland *et al.*, 2003, Y. Bartov, pers. comm., 2003). Especially for the faults within the Arava Valley, estimates of horizontal displacement do hardly exist, except for the AF itself. Moreover it could be shown with the seismic reflection data, that additional fault segments are hidden beneath Quaternary sediments. East of the southern Arava, within the Precambrian basement rocks, horizontal displacement can far more easily be determined by offset dikes or contacts between magmatic units. Thus two faults with a sinistral displacement of 3.0 and 3.6 km, respectively, were identified on the multispectral satellite scene. Another fault with 3 km left-lateral displacement was described by Abu Taimeh (1988) around latitude 29.9°N. The most prominent fault in SW Jordan is certainly the Al Quwayra Fault (AQF). This rather straight N–S running fault is more than 100 km long and extends into Saudi Arabia. Surprisingly, only little information is found in the literature about this fault. Abu Taimeh (1988) proposed a left-lateral displacement of 8 km based on offset biotite-muscovite aplite granites around latitude 30.3°N and based on an 8 km long rhomb-shaped graben in this region. In contrast, Barjous (1988) suggested a horizontal slip in the range of 40 km. His assumption was mainly founded on the southernmost outcrops of Precambrian rhyolites, that occur 40 km further to the north east of the AQF. This higher value is also supported by the following stratigraphic observation. Whereas east of the AQF the Lower Cretaceous Kurnub sandstone is underlain by the distinct Disi Formation – bright Ordovician sandstones – west of the Al Quwayra Fault this formation is missing and occurs more than 35 km to the south, implying left-lateral movement along the AQF. The great length of the AQF could also be taken as an argument for a higher displacement. At the same time the argumentation by Abu Taimeh (1988) cannot be disproven and seems to be justified when looking at the geological map by Bender (1974). Further investigations are required to better constrain the various hypotheses.

A similar pattern of subparallel faults cutting through Precambrian rocks as east of the southern Arava Valley appears west of the Gulf of Aqaba. Considering displaced Miocene dikes Eyal *et al.* (1981) suggested, that left-lateral motion along

these faults did not take place before Miocene times. Comparably the sinistral displacement along the faults east of the southern Arava Valley is thought to be related to the motion along the DST. Still these structures are supposed to present older, reactivated structures because of following considerations:

- If younger (especially Mesozoic) sediments are regarded, they do not seem to be cut by such a large amount of faults striking in the same ± N–S direction as are the Precambrian rocks.

- NE–SW, NW–SE, and N–S trending Neoproterozoic dikes, that are widespread in Precambrian basement rocks (e.g. Kessel *et al.*, 1998), indicate a Late Proterozoic stress field that is compatible with ∼N–S trending (normal) faults or 'weakness zones' in the crust. This is in accordance with stress field observation by Zaineldeen (2000).

- On the basis of a magnetic survey, Segev *et al.* (1999) put forward a 'basin and range' like structure in the basement of southern Israel, with the main features being aligned in a NNE–SSW direction.

Age constraint on activity of various DST related faults

Regarding the microseismic activity along the southern DST it seems reasonable to assume, that most of the recent motion along the southern DST is concentrated along the AF, even if it is not everywhere expressed by a clear surface trace. The estimated slip-rate along the AF based on offset alluvial fans lies between 0.3 and 0.75 cm/a during the last 2–5 Ma (Ginat *et al.*, 1998). This is in accordance with slip-rate values for the southern DST as a whole.

It is suggested here, that at the beginning of transform motion deformation occurred in a rather wide belt, with the reactivation of older ∼N–S striking structures. A considerable amount of sinistral motion probably occurred along the Al Quwayra Fault during this phase. Later deformation became concentrated in the region of today's Arava Valley. Till ∼5 Ma ago there might have been another, now extinct fault trace approximately 5 km west of the AF that took up lateral motion. Together with a rearrangement of plates 5 Ma ago (Joffe and Garfunkel, 1987), the main fault trace could have shifted to the position of today's Arava Fault. This would imply that the AF, as it is observed at the surface, is just the most recent active fault of the DST and might have experienced only a small amount of the total 105 km sinistral displacement. This assumption could explain the relatively

narrow fault zone width of $\sim$300 m[*], as determined by Janssen *et al.* (2004), who investigated meso- to microscale faulting east of the AF at latitude 30.8°N. Also a magnetotelluric study by Ritter *et al.* (2003) does not report a broad fault zone conductor that is commonly thought to occur at the position of the fault core of an active fault trace. Rather does the AF act as impermeable barrier for fluid flow (for further details see Ritter *et al.* (2003)). These observations could be explained by an AF, that has only been active recently.

Strength of the AF and Associated Extensional Features

One of the most striking features of the Arava Valley is the transverse (W–E) extension occurring along normal faults. This extension cannot be explained by a NW to NNW trending maximum horizontal stress σ_1 associated with sinistral strike-slip motion along the Arava Fault. Mainly two theories have been put forward to explain such structures.

1. Weak fault hypothesis. This model has been extensively discussed especially regarding the San Andreas Fault (e.g. Zoback *et al.*, 1987; Zoback and Zoback, 1989; Zoback, 2000), but has also been associated with other strike-slip faults like the Great Sumatran Fault and the DST (Garfunkel, 1981; Ben-Avraham and Zoback, 1992; Mount and Suppe, 1992). It explains the rotation of the maximum principal stress σ_1 to a nearly fault-normal (in the case of transpression) or a fault-parallel (in the case of transtension) orientation in the vicinity of the fault by the existence of low shear stresses along the fault plane. Thus a weak fault within a strong adjacent crust may reorient far-field stresses (e.g. Zoback *et al.*, 1987). At the San Andreas Fault high pore pressures within the fault zone were assumed as the reason for extremely low average shear stresses in the order of 10–20 MPa (Zoback *et al.*, 1987).

2. Overlapping en echelon strike-slip fault segments. Overlapping sub-parallel strike-slip faults have been reported from numerous regions around the world. One of the most prominent examples is again the San Andreas Fault Zone in the San Francisco Bay region, where several subparallel faults occur in a $\sim$80 km wide belt (e.g. Aydin and Page, 1984). The Alpine Fault in New Zealand, the Queen Charlotte Fault in Canada, the Great Sumatran Fault in Indonesia, and the

---

[*]Another comparable fault is e.g. the West Fault in Chile, that is 60 to 170 km long, 1 km wide and shows a lateral offest of 35 km (Hoffmann-Rothe, 2002)

Tan-Lu Fault offshore China represent further expamles (e.g. Barnes *et al.*, 2004; Wood *et al.*, 1994; Rohr and Dietrich, 1992; Bellier *et al.*, 1997; Hsiao *et al.*, 2004). Nearly everywhere these large strike-slip faults are associated with vertical movements and a variety of structures that seem to result from fault-normal extension or contraction. Numerical and analog (sandbox) modelling showed, however, that most of these features can be explained by pure strike-slip motion (e.g. ten Brink *et al.*, 1996; Dooley and McClay, 1997). These models show, that fault-perpendicular subsidence and extension, as well as compression, can occur due to fault interaction of en echelon strike-slip faults. Additionally, the fault tip of a single strike-slip fault is associated with coupled uplift and subsidence (ten Brink *et al.*, 1996). Ten Brink *et al.* (1996) further suggest, that the amount of uplift or subsidence depends on the shear stresses acting at the fault. In their models the vertical movements are significant, if the faults are 'weak'. At the same time uplift and subsidence are considerably less, if strong faults with a finite shear strength are modelled. In the case of the DST and the Dead Sea Basin, ten Brink *et al.* (1996) favoured a weak fault model like Ben-Avraham and Zoback (1992). In contrast to the latter authors, they do not see the need for divergent plate motion to explain the extensional features. This is in agreement with thermo-mechanical modelling results by Sobolev *et al.* (2004).

There have not been many direct stress measurements in the vicinity of the AF to substantiate the weak fault theory. Klinger (pers. comm., 2003) determined the stress tensor from fault plane solutions in the Arava Valley with the maximum horizontal stress S_H trending approximately NW–SE. Also the observations by Janssen *et al.* (2004) at the pressure ridge west of Jebel Humrat Fiddan (central Arava) indicate a strong fault with estimated paleodifferential stress magnitudes of about 100 MPa and σ_1 being oriented 45° to the fault plane. Yet it is not clear, whether these values are representative for the whole AF and are not restricted to the restraining bend of the fault trace.

En echelon faults do occur along the southern DST, but the recent activity of the various segments is difficult to assess. Evidence for some recent uplift was found at the AQF close to the NVR profile and also at some faults east of the southern Arava Valley. The microseismic activity seems to concentrate within the Arava Valley, however, and does not give any evidence for strike-slip motion along other, marginal fault segments. With respect to sinistral slip motion these faults might either be completely inactive or might have been locked for some time. An episodic or possibly cyclic nature of faulting (and subsequent healing) has been

proposed for the evolution of fault zones (e.g. Sibson, 1992; Byerlee, 1993). The possibility of clustered seismic activity at the southern DST has been put forward by Marco *et al.* (1996).

Final Remarks

Considering the results of this study it should be clear, that in the investigation of the southern Dead Sea Transform a combination of several geophysical and geological methods has been essential. Neither seismic reflection data nor satellite images alone have the potential to answer important questions concerning the structure and dynamics of a highly complex plate boundary. With an integrated approach, though, both methods have proven to be powerful tools for the structural analysis of a fault zone. Still it cannot be ignored, that with a lack of outcrops of the main fault zone and its various segments, crucial pieces of evidence for the internal structure of the Arava Fault and its mechanical behaviour are missing. Additionally, the role and importance of the Al Quwayra Fault have so far not received adequate attention. With a proposed lateral offset of more than 8 (maybe even 40) km it is thought to have played a major role in the history of the southern DST. Another important question that is still to be answered on a regional scale is the possible relation between lithospheric thinning associated with Neogene magmatism on the Arabian peninsula and the structure and location of the DST.

Studies for future PhD students seem to be assured.

Bibliography

Abou Karaki, N. (1987). *Synthèse et carte sismotectonique des pays de la bordure orientale de la Méditerranée: sismicité du système de failles du Jourdain-Mer Morte.* Ph.D. thesis, University of Strasbourg. France. 12

Abu Taimeh, I. A. E. (1988). Structural and applied remote sensing studies at Gharandal-Petra area, eastern Wadi Araba. Master's thesis, Univ. of Jordan, Department of Geology and Mineralogy. 47, 74

Achmon, M. and Ben-Avraham, Z. (1997). The deep structure of Carmel fault zone, northern Israel. *Tectonics*, **16**, 563–569. 10

Al-Zoubi, A. and Ben-Avraham, Z. (2002). Structure of the earth's crust in Jordan from potential field data. *Tectonophysics*, **346**, 45–59. 17, 38

Al-Zoubi, A. and ten Brink, U. (2002). Lower crustal flow and the role of shear in basin subsidence: An example from the Dead Sea Basin. *Earth Plan. Sci. Lett.*, **199**, 67–79. 14, 67, 68, 72

Al-Zoubi, A. and ten Brink, U. S. (2001). Salt diapirs in the Dead Sea basin and their relationship to Quaternary extensional tectonics. *Marine and Petroleum Geology*, **18**, 779–797. 67, 72

Aldersons, F., Ben-Avraham, Z., Hofstetter, A., Kissling, E., and Al-Yazjeen, T. (2003). Lower crustal strength under the Dead Sea basin from local earthquake data and rheological modeling. *Earth Plan. Sci. Lett.*, **214**, 129–142. 12, 14, 72

Ambraseys, N. N., Melville, C. P., and Adams, R. D. K. (1994). *The Seismicity of Egypt, Arabia and the Red Sea: a Historical Review.* Cambridge University Press, Cambridge. 12

Atallah, M. (1992). Tectonic evolution of northern Wadi Araba, Jordan. *Tectonophysics*, **204**, 17–26. 65

Avni, Y., Bartov, Y., Garfunkel, Z., and Ginat, H. (2001). The Arava Formation—A Pliocene sequence in the Arava Valley and its western margin, southern Israel. *Israel Journal of Earth Sciences*, **50**, 101–120. 52, 53

Aydin, A. and Page, B. M. (1984). Diverse Pliocene–Quaternary tectonics in a transform environment, San Francisco Bay region, California. *GSAB*, **95**, 1303–1317. 76

Aydin, A. and Schultz, R. A. (1990). Effect of mechanical interaction on the development of strike-slip faults with echelon patterns. *J. Struct. Geol.*, **12**(1), 123–129. 63

Badawy, A. and Horváth, F. (1999). Recent stress field of the Sinai subplate region. *Tectonophysics*, **304**, 385–403. 15

Baer, G., Heimann, A., Eshet, Y., Weinberger, R., Musset, A., and Sherwood, G. (1995). The Saharonim basalt: a Late Triassic - Early Jurassic magmatism in southeastern Makhtesh Ramon. *Israel Journal of Earth Sciences*, **44**, 1–10. 7

Baker, J. A., Thirlwall, M. F., and Menzies, M. A. (1996). Sr–Nd–Pb and trace element evidence for crustal contamination of plume–derived flood basalts: Oligocene flood volcanism in western Yemen. *Geochimica et Cosmochimica Acta*, **60**, 2559–2581. 15

Barjous, M. O. (1988). Structural study of the area between Petra and Ash Shawbak. University of Jordan. Unpublished M.Sc. thesis. 74

Barjous, M. O. (1992). The Geology of the Ash Shawbak Area, Map Sheet No. 3151 III. In *1:50.000 Geological Mapping Series*, number 19 in Geological Bulletin. The Hashemite Kingdom of Jordan, Ministry of Energy and Mineral Resources, Natural Resources Authority, Geology Directorate, Geological Mapping Division, Amman. 19, 65

Barjous, M. O. (1995). Petra & Wadi Al Lahyana, 3050 I & 3050 IV, 1:50000. Geological map, Natural Resources Authority, Geology Directorate, Amman, Jordan. 65

Barnes, P. M., Sutherland, R., Davy, B., and Delteil, J. (2004). Rapid creation and destruction of sedimentary basins on mature strike-slip faults: an example from the offshore Alpine Fault, New Zealand. *J. Struct. Geol.*, **23**, 1727–1739. 77

Bartov, Y. (1974). *A structural and paleogeographic study of the central Sinai faults and domes.* Ph.D. thesis, Hebrew University, Jerusalem. in Hebrew. 1, 7, 8, 17

Bartov, Y., Steinitz, G., Eyal, M., and Eyal, Y. (1980). Sinistral movement along the Gulf of Aqaba – its age and relation to the opening of the Red Sea. *Nature*, **285**, 220–222. 1

Bartov, Y., Avni, Y., Calvo, R., and Frieslander, U. (1998). The Zofar Fault – A major intra-rift feature in the Arava rift valley. *Geological Survey of Israel Current Research*, **11**, 27–32. 11, 48, 65

Bellier, O., Sébrier, M., Pramumijoyo, Beaudouin, T., Harjono, H., Bahar, I., and Forni, O. (1997). Paleoseismicity and seismic hazard along the Great Sumatran Fault (Indonesia). *J. Geodynamics*, **24**(1–4), 169–183. 77

Ben-Avraham, Z. (1985). Structural framework of the Gulf of Elat (Aqaba), northern Red Sea. *J. Geophys. Res.*, **90**, 703–726. 10

Ben-Avraham, Z. and Zoback, M. D. (1992). Transform-normal extension and asymmetric basins: an alternative to pull-apart models. *Geology*, **20**(5), 423–426. 76, 77

Ben-Avraham, Z., Almagor, G., and Garfunkel, Z. (1979). Sediments and structure of the Gulf of Elat. *Sedimentary Geology*, **23**, 239–267.   10

Ben-Avraham, Z., Ginzburg, A., Makris, J., and Eppelbaum, L. (2002). Crustal structure of the Levant basin, eastern Mediterranean. *Tectonophysics*, **346**, 23–43.   6, 17

Ben-David, R., Eyal, Y., Zilberman, E., and Bowman, D. (2002). Fluvial systems response to rift margin tectonics: Makhtesh Ramon area, southern Israel. *Geomorphology*, **45**, 147–163.   19

Ben-Menahem, A. (1991). Four thousand years of seismicity along the Dead Sea Rift. *J. Geophys. Res.*, **96**, 20195–20216.   12

Ben-Menahem, A. and Aboodi, E. (1981). Micro- and macroseismicity of the Dead Sea Rift and off-coast Eastern Mediterranean. *Tectonophysics*, **80**, 199–233.   8

Bender, F. (1968). *Geologie von Jordanien*, volume 7 of *Beiträge zur regionalen Geologie der Erde*. Gebrüder Borntraeger, Berlin, Stuttgart.   1, 6, 61, 63

Bender, F. (1974). Geological Map of the Wadi Araba, Jordan (Scale 1:100000, 3 Sheets). Geol. Surv. of the Fed. Rep. of Germany, Hannover.   52, 61, 74

Bender, F., Futian, A., Grieger, J., Haddadin, M., Heimbach, W., Ibrahim, H., Jeresat, K., Khdeir, K., Lenz, R., Ruef, M., Sunna, B., and Wiesemann, G. (1968). Geological Map of Jordan, scale 1:250000. — 5 sheets. Geol. Surv. of the Fed. Rep. of Germany, Hannover.   18

Blanckenhorn, M. (1893). Die Strukturlinien Syriens und des Roten Meeres. *Richthoven Festschr., Berlin*, pages 115–180.   1

Blanckenhorn, M. (1896). Entstehung und Geschichte des Toten Meeres. Ein Beitrag zur Geologie Palaestinas. *Z. Dtsch. Palaest. Ver.*, **19**, 1–59.   1

Brocher, T. M., McCarthy, J., Hart, P. E., Holbrook, W. S., Furlong, K. P., McEvilly, T. V., Hole, J. A., and Klemperer, S. L. (1994). Seismic evidence for a lower-crustal detachment beneath San Francisco Bay, California. *Science*, **265**, 1436–1439.   46

Butler, R. W. H., Spencer, S., and Griffith, H. M. (1997). Transcurrent fault activity on the Dead Sea Transform in Lebanon and its implications for plate tectonics and seismic hazard. *Journal Geol. Soc. London*, **154**(5), 757–760.   10

Byerlee, J. (1993). Model for episodic flow of high-pressure water in fault zones before earthquakes. *Geology*, **21**, 303–306.   78

Calvo, R. and Bartov, Y. (2001). Hazeva Group, southern Israel: New observations, and their implications for its stratigraphy, paleogeography, and tectono–sedimentary regime. *Israel Journal of Earth Sciences*, **50**, 71–99.   52, 67

Camp, V. E. and Roobol, M. J. (1992). Upwelling asthenosphere beneath western Arabia and its regional implications. *J. Geophys. Res.*, **97**, 15,255–15,271.   15, 16

Chester, F. M. and Logan, J. M. (1986). Implication for mechanical properties of brittle faults from observations of Punchbowl fault zone, California. *Pure and Applied Geophysics*, **12**, 79–106. 3, 54

Chester, F. M., Evans, J. P., and Biegel, R. L. (1993). Internal structure and weakening mechanisms of the San Andreas Fault. *J. Geophys. Res.*, **98**, 771–786. 3, 54

Clark, M. D. (1985). Late Proterozoic crustal evolution of the Midyan region, northwestern Saudi Arabia. *Geology*, **13**, 611–615. 6

DESERT Group (2000). Multinational geoscientific research kicks off in the Middle East. *EOS Trans. Am. Geophys. Union*, **81**(50), 609, 616–617. 2

DESERT Group (2004). The crustal structure of the Dead Sea Transform. *Geophys. J. Int.*, **156**, 655–681. 31, 38, 41, 42

Dewey, J. F., Pitman, C. C. I., Ryan, W. B. F., and Bonnin, J. (1973). Plate tectonics and the evolution of the Alpine system. *Geol. Soc. Amer. Bull.*, **84**, 3137–3180. 6

D'Onfro, P. and Glagola, P. (1983). Wrench fault, southeast Asia. In A. W. Bally, editor, *Seismic Expression of Structural Styles (vol.3)*, American Association of Petroleum Geologists Studies in Geology, Series 15, pages 4.2–1 to 4.2–8. 52

Dooley, T. and McClay, K. (1997). Analog Modeling of Pull-Apart Basins. *AAPG Bulletin*, **81**(11), 1804–1826. 77

Drury, S. A. (1993). *Image Interpretation in Geology*. Chapman & Hall, London, Glasgow, New York, Tokyo, Melbourne, Madras, second edition. 60

Dubertret, L. (1970). Review of structural geology of the Red Sea and surrounding area. *Philos. Trans. R. Soc. London, A*, **267**, 107–130. 1

Eisbacher, G. H. (1996). *Einführung in die Tektonik*. Ferdinand Enke Verlag, Stuttgart, 2nd edition. 51

El-Isa, Z. H., Mechie, J., Prodehl, C., Makris, J., and Rihm, R. (1987). A crustal structure study of Jordan derived from seismic refraction data. *Tectonophysics*, **138**, 235–253. 17, 38

El-Kelani, R., Götze, H.-J., Rybakov, M., Hassouneh, M., and Schmidt, S. (2003). Crustal structure along the DESERT 2000 Transect inferred from 3–D gravity modelling. In *EOS Trans. Am. Geophys. Union*, volume 84 (46). Fall Meeting Supplement, abstract S21F–0399. 41, 42

Eyal, M., Eyal, Y., Bartov, Y., and Steinitz, G. (1981). The tectonic development of the western margin of the Gulf of Elat (Aqaba) rift. *Tectonophysics*, **80**, 39–66. 74

Eyal, Y. (1996). Tectonic analysis of the Dead Sea Rift Region since the Late Cretaceous based on mesostructures. *Tectonics*, **15**(1), 157–170. 15

Eyal, Y. and Reches, Z. (1983). Stress field fluctuations along the Dead Sea rift since the middle Miocene. *Tectonics*, **2**(2), 167–185. 15

Faulkner, D. R., Lewis, A. C., and Rutter, E. H. (2003). On the internal structure and mechanics of large strike-slip fault zones: field observations of the Carboneras fault in southeastern Spain. *Tectonophysics*, **367**, 235–251. 3, 54

Fleischer, L. and Varshavsky, A. (2002). A Lithostratigraphic Data Base of Oil and Gas Wells Drilled in Israel. Report no. OG/9/02, Ministry of National Infrastructures, Oil & Gas Unit, Jerusalem, Israel. 19

Flexer, A. (2001). The pre-Neogene geology of the Near East. In A.Horowitz, editor, *The Jordan Rift Valley*, pages 123–163. A. A. Balkema Publishers, Lisse, Netherlands. 6, 7

Freund, R. (1961). Distribution of lower Turonian ammonites in Israel and the neighbouring countries. *Bull. Res. Counc. Isr.*, **G10**, 79–100. 1

Freund, R. (1965). A model of the structural development of Israel and adjacent areas since upper Cretaceous times. *Geol. Mag.*, **102**, 189–205. 1, 8, 10

Freund, R., Zak, I., and Garfunkel, Z. (1968). Age and rate of movement along the Dead Sea Rift. *Nature*, **220**, 253–255. 1

Freund, R., Garfunkel, Z., Zak, I., Goldberg, M., Weissbrod, T., and Derin, B. (1970). The shear along the Dead Sea rift. *Philosophical Transactions of the Royal Society of London*, **267**, 107–130. 1, 8, 10

Frieslander, U. (2000). *The structure of the Dead Sea Transform emphasizing the Arava, using new geophysical data.* Ph.D. thesis, Hebrew University, Jerusalem. in Hebrew. 18, 48, 60, 62, 64, 65, 67

Furlong, K. P., Hugo, W. D., and Zandt, G. (1989). Geometry and evolution of the San Andreas fault zone in northern California. *J. Geophys. Res.*, **94**, 3100–3110. 46

Gardosh, M., Kashai, E., Salhov, S., Shulman, H., and Tannenbaum, E. (1997). Hydrocarbon exploration in the southern Dead Sea area. In T. M. Niemi, Z. Ben-Avraham, and J. R. Gat, editors, *The Dead Sea – The Lake and its Setting*, volume 36 of *Oxford Monographs on Geology and Geophysics*, pages 57–72. Oxford University Press, Oxford. 65, 66, 67, 95

Garfunkel, Z. (1981). Internal structure of the Dead Sea leaky transform (rift) in relation to plate kinematics. *Tectonophysics*, **80**, 81–108. 1, 8, 9, 10, 11, 16, 76

Garfunkel, Z. (1989). Tectonic setting of Phanerozoic magmatism in Israel. *Israel Journal of Earth Sciences*, **38**, 51–74. 6, 15

Garfunkel, Z. (1992). Darfur-Levant array of volcanics – A 140-Ma-long record of a hot spot beneath the African-Arabian continent, and its bearing on Africa's absolute motion. *Israel Journal of Earth Sciences*, **40**, 135–150. 7

Garfunkel, Z. (1997). The history and formation of the Dead Sea basin. In T. M. Niemi, Z. Ben-Avraham, and J. R. Gat, editors, *The Dead Sea – The Lake and its Setting*, volume 36 of *Oxford Monographs on Geology and Geophysics*, pages 36–56. Oxford University Press, Oxford. 7, 10, 11, 65, 67

Garfunkel, Z. (2000). History and paleogeography during the Pan-African orogen to stable platform transition: Reappraisal of the evidence from the Elat area and the northern Arabian-Nubian shield. *Israel Journal of Earth Sciences*, **48**, 135–157. 5, 6

Garfunkel, Z. and Ben-Avraham, Z. (2001). Basins along the Dead Sea Transform. In P. A. Ziegler, W. Cavazza, A. H. F. Robertson, and S. Crasquin-Soleau, editors, *Peri-Tethys Memoir 6: Peri-Tethyan Rift/Wrench Basins and Passive Margins*, volume 186 of *Mém. Mus. natn. Hist. nat.*, pages 607–627, Paris, ISBN: 2–85653–528–3. 10

Garfunkel, Z. and Derin, B. (1984). Permian-early Mesozoic tectonism and continental margin formation in Israel and its implications for the history of the Eastern Mediterranean. In J. E. Dixon and A. H. F. Robertson, editors, *The Geologic Evolution of the Eastern Mediterranean*, volume 17 of *Geol. Soc. Spec. Publ.*, pages 187–201. 6

Garfunkel, Z., Zak, I., and Freund, R. (1981). Active faulting in the Dead Sea Rift. *Tectonophysics*, **80**, 1–26. 10, 11, 15

Ginat, H., Enzel, Y., and Avni, Y. (1998). Translocated Plio-Pleistocene drainage systems along the Arava fault of the Dead Sea transform. *Tectonophysics*, **284**, 151–160. 8, 60, 61, 63, 75

Ginzburg, A. and Ben-Avraham, Z. (1987). The deep structure of the Central and Southern Levant continental margin. *Ann. Tecton.*, **1**, 105–115. 10

Ginzburg, A., Makris, J., Fuchs, K., Prodehl, C., Kaminski, W., and Amitai, U. (1979). A seismic study of the crust and upper mantle of the Jordan – Dead Sea Rift and their transition toward the Mediterranean Sea. *J. Geophys. Res.*, **84**, 1569–1582. 6, 17, 38

Guiraud, R. and Bosworth, W. (1999). Phanerozoic geodynamic evolution of northeastern Africa and the northwestern Arabian platform. *Tectonophysics*, **315**, 73–108. 6

Haberland, C., Agnon, A., El-Kelani, R., Maercklin, N., Qabbani, I., Rümpker, G., Ryberg, T., Scherbaum, F., and Weber, M. (2003). Modeling of seismic guided waves at the Dead Sea Transform. *J. Geophys. Res.*, **108**(B7), doi:10.1029/2002JB002309. 74

Harding, T. P. (1983). Divergent wrench fault and negative flower structure, Andaman Sea. In A. W. Bally, editor, *Seismic Expression of Structural Styles (vol.3)*, American Association of Petroleum Geologists Studies in Geology, Series 15, pages 4.2–1 to 4.2–8. 52

Harding, T. P. (1985). Seismic characteristics and identification of negative flower structures, positive flower structures and positive structural inversion. *American Association of Petroleum Geologists Bulletin*, **69**, 582–600. 52

Harding, T. P. and Lowell, J. D. (1979). Structural styles, their plate–tectonic habitats and hydrocarbon traps in petroleum provinces. *American Association of Petroleum Geologists Bulletin*, **63**, 1016–1058. 52

Harding, T. P., Vierbuchen, R. C., and Christie-Blick, N. (1985). Structural styles, plate-tectonic settings and hydrocarbon traps of divergent (transtensional) wrench faults. *The Society of Economic Paleontologists and Mineralogists*, **37**, 51–77. 11

Hatcher, R. D., Zeiz, I., Reagan, R. D., and Abu-Ajameh, M. (1981). Sinistral strike-slip motion of the Dead Sea rift: confirmation from new magnetic data. *Geology*, **9**, 458–462. 8

Hempton, M. (1985). Structure and deformation of the Bitlis suture near Lake Hazar, southeastern Turkey. *Geol. Soc. Amer. Bull.*, **96**, 233–243. 7

Henjes-Kunst, F., Altherr, R., and Baumann, A. (1990). Evolution and composition of the lithospheric mantle underneath the western Arabian peninsula: constraints from Sr-Nd isotope systematics of mantle xenoliths. *Contrib. Mineral. Petrol.*, **105**, 460–472. 5

Henstock, T. J., Levander, A., and Hole, J. A. (1997). Deformation in the Lower Crust of the San Andreas Fault System in Northern California. *Science*, **278**, 650–653. 45

Hoffmann-Rothe, A. (2002). *Combined structural and magnetotelluric investigation across the West Fault Zone in northern Chile.* Ph.D. thesis, Mathematisch-Naturwissenschaftliche Fakultät, Universität Potsdam. http://pub.ub.uni-potsdam.de/2002/0025/ahoro.pdf. 76

Hofstetter, A. and Bock, G. (2003). Shear-wave velocity structure of the Sinai subplate from receiver function analysis. submitted to *Geophysical Journal International*. 16

Hofstetter, A., Eck, T. V., and Shapira, A. (1996). Seismic activity along fault branches of the Dead Sea – Jordan transform system: The Carmel-Tirtza fault system. *Tectonophysics*, **267**, 317–330. 10

Hofstetter, A., Dorbath, C., Rybakov, M., and Goldshmidt, V. (2000). Crustal and upper mantle structure across the Dead Sea rift and Israel from teleseismic P-wave tomography and gravity data. *Tectonophysics*, **327**, 37–59. 38

Holbrook, W. S., Brocher, T. M., Brink, U. S. T., and Hole, J. A. (1996). Crustal structure of a transform plate boundary: San Francisco Bay and the central California continental margin. *J. Geophys. Res.*, **101**(B10), 22311–22334. 46

Holliger, K. and Levander, A. (1994). Lower crustal reflectivity modeled by rheological controls on mafic intrusions. *Geology*, **22**, 367–370. 45

Horowitz, A. (2001). Review of the northern Arava late Cenocoic stratigraphy. *Israel Journal of Earth Sciences*, **50**, 137–158. 52

Hsiao, L.-Y., Graham, S. A., and Tilander, N. (2004). Seismic reflection imaging of a major strike-slip fault zone in a rift system: Paleogene structure and evolution of the Tan-Lu fault system, Liadong Bay, Bohai, offshore China. *AAPG Bulletin*, **88**(1), 71–97. 77

Husseini, M. I. (1989). Tectonic and Deposition Model of Late Precambrian-Cambrian Arabian and Adjoining Plates. *The Am. Assoc. of Petrol. Geol. Bulletin*, **73**(9), 1117–1131. 5, 6, 38

Ibrahim, K. M. and McCourt, W. J. (1995). Neoproterozoic granitic magmatism and tectonic evolution of the northern Arabian Shield: evidence from southwest Jordan. *Journal of African Earth Sciences*, **20**(2), 103–118. 5

Ibrahim, K. M. K. (1991). The Geology of the Wadi Rahma, Map Sheet No. 3049 IV. In *1:50.000 Geological Mapping Series*, number 15 in Geological Bulletin. The Hashemite Kingdom of Jordan, Minestry of Energy and Mineral Resources, Natural Resources Authority, Geology Directorate, Geological Mapping Division, Amman. 63

Janssen, C., , Romer, R. L., Hoffmann-Rothe, A., Kesten, D., Al-Zubi, H., and the DESERT Research Group (2004). The Dead Sea Transform: Evidences for a strong fault? in press. 76, 77

Jarrar, G. H. (2002). Duheila Hornblenditic Suite, Wadi Araba, SW Jordan: Geochemistry and Petrogenesis. *Dirasat, Pure Sciences*, **29**(1), 89–104. 38

Joffe, S. and Garfunkel, Z. (1987). The plate kinematics of the circum Red Sea — A reevaluation. *Tectonophysics*, **141**, 5–22. ii, iv, 1, 2, 8, 52, 75

Kessel, R., Stein, M., and Navon, O. (1998). Petrogenesis of late Neoproterozoic dikes in the northern Arabian-Nubian Shield. Implications for the origin of A-type granites. *Precambrian Research*, **92**, 195–213. 5, 75

Khair, K. (2001). Geomorphology and seismicity of the Roum fault as one of the active branches of the Dead Sea fault system in Lebanon. *Journal of Geophysical Research*, **106**(B3), 4233–4245. 8, 10

Klemperer, S. L., Ryan, P. D., and Snyder, D. B. (1991). A deep seismic reflection transect across the Irish Caledonides. *J. Geol. Soc. London*, **148**, 149–164. 71

Klinger, Y. (1999). *Sismotectonique de la faille du Levant.* Ph.D. thesis, University of Strasbourg, France. 13, 14

Klinger, Y., Rivera, L., Haessler, H., and Maurin, J. C. (1999). Active faulting in the Gulf of Aqaba: New knowledge from the Mw 7.3 earthquake of 22 November 1995. *Bull. Seism. Soc. Am.*, **89**, 1025–1036. 8, 12

Klinger, Y., Avouac, J. P., Dorbath, L., Karaki, N. A., and Tisnerat, N. (2000a). Seismic behaviour of the Dead Sea fault along the Araba valley, Jordan. *Geophys. J. Int.*, **142**(3), 769–782. 11, 12

Klinger, Y., Avouac, J. P., Karaki, N. A., Dorbath, L., Bourles, D., and Reyss, J. L. (2000b). Slip rate on the Dead Sea transform fault in northern Araba valley, (Jordan). *Geophys. J. Int.*, **142**(3), 755–768. 8

Kröner, A. (1984). Late Precambrian Plate tectonics and orogeny: a need to redefine the term Pan-African. In J. Klerkx and J. Michot, editors, *African Geology*, pages 23–28. Musées R. l'Afrique Centrale, Tervuren. 5

Kusznir, N. J. and Ziegler, P. A. (1992). The mechanics of continental extension and sedimentary basin formation: A simple-shear/pure-shear flexural cantilever model. *Tectonophysics*, **215**, 117–131. 46, 47

Kusznir, N. J., Marsden, G., and Egan, S. S. (1991). A flexural-cantilever simple-shear model of continental lithosphere extension: applications to the Jeanne d'Arc Basin, Grand Banks and Viking Graben, North Sea. In A. M. Roberts, G. Yielding, and B. Freeman, editors, *The Geometry of Normal Faults*, volume 56 of *Geological Society Special Publication*, pages 41–60. 46, 47

Larsen, B. D., Ben-Avraham, Z., and Shulman, H. (2002). Fault and salt tectonics in the southern Dead Sea basin. *Tectonophysics*, **346**, 71–90. 95

Le Pichon, X. and Francheteau, J. (1978). A plate tectonic analysis of the Red Sea–Gulf of Aden area. *Tectonophysics*, **46**, 369–406. 8

Maercklin, N., Haberland, C., Ryberg, T., Weber, M., Qabbani, I., El-Kelani, R., Scherbaum, F., and the DESERT Working Group (2002). Oberflächennahe 3-D Geschwindigkeitsstruktur im Wadi Arava, Jordanien. In *62. Jahrestagung, Deutsche Geophysikalische Gesellschaft*. Poster GDP11. 56

Maercklin, N., Haberland, C., Ryberg, T., Weber, M., Bartov, Y., and DESERT Group (2004). Seismic refraction profiles between Cyprus and Israel and their interpretation. *Geophys. J. Int.*, **158**, 179–186. 53

Makris, J., Ben-Avraham, Z., Behle, A., Ginzburg, A., Giese, P., Steinmetz, L., Whitmarsh, R. B., and Eleftheriou, S. (1983). Seismic refraction profiles between Cyprus and Israel and their interpretation. *Geophysical Journal of the Royal Astronomical Society*, **75**, 575–591. 6, 17

Marco, S., Stein, M., and Agnon, A. (1996). Long-term earthquake clustering: A 50,000-year paleoseismic record in the Dead Sea Graben. *J. Geophys. Res.*, **101**, 6179–6191. 12, 78

Mart, Y. (1991). The Dead Sea Rift: from continental rift to incipient ocean. *Tectonophysics*, **197**, 155–179. 1

McBride, J. H. (1994). Structure of a continental strike-slip fault from deep seismic reflection: Walls Boundary fault, northern British Caledonides. *J. Geophys. Res.*, **99**, 23985–24005. 46, 47, 71

McCourt, W. J., Rashdan, M., Ibrahim, K., Rabba, I., and Abdelhamid, G. (1990). A new geological framework for the late Proterozoic basement of Jordan. *Proc. 3rd Jor. Geol. Conf.*, pages 283–314. 5

Meissner, R. (1989). Rupture, creep, lamellae and crocodiles: Happenings in the continental crust. *Terra Nova*, **1**, 17–28. 42

Meissner, R. (1996). Faults and folds, fact and fiction. *Tectonophysics*, **264**, 279–293. 45

Mohsen, A. (2004). *A receiver function study of the crust and upper mantle across the Dead Sea Transform*. Ph.D. thesis, Free University of Berlin, Germany. 44

Mohsen, A., Hofstetter, R., Bock, G., Kind, R., Weber, M., Wylegalla, K., and DESERT Group (2004). A receiver function study across the Dead Sea Transform. submitted to *Geophysical Journal International*.   43

Mooney, W. D. and Brocher, T. M. (1987). Coincident seismic reflection/refraction studies of the continental lithosphere: A global review. *Reviews of Geophysics*, **25**, 723–724. 34, 35, 36, 38

Mooney, W. D. and Meissner, R. (1992). Multi-genetic origin of crustal reflectivity: a review of seismic reflection profiling of the continental lower crust and Moho. In D. M. Fountain, R. Arculus, and R. W. Kay, editors, *Continental Lower Crust*, pages 45–79. Elsevier, Amsterdam.   34

Mount, V. S. and Suppe, J. (1992). Present-Day Stress Orientations Adjacent to Active Strike-Slip Faults: California and Sumatra. *J. Geophys. Res.*, **97**(B8), 11,995–12,013. 76

Neev, D. and Emery, K. O. (1967). The Dead Sea: Depositional processes and environments of evaporites. *Geological Survey of Israel Bulletin*, **41**.   65

Pe'eri, S., Wdowinski, S., Shtivelman, A., Bechor, N., Bock, Y., Nikolaidis, R., and van Domselar, M. (2002). Current plate motion across the Dead Sea Fault from three years of continous GPS monitoring. *Geophys. Res. Lett.*, **29**(14), doi:10.1029/2001GL013879. 8

Picard, L. (1943). Structure and evolution of Palestine. *Bull. Geol. Dep. Hebrew Univ.*, **4**, 1–134.   1

Picard, L. (1987). The Elat (Aqaba)-Dead Sea-Jordan sub-graben system. *Tectonophysics*, **141**, 23–32.   1

Quennell, A. M. (1958). The structural and geomorphic evolution of the Dead Sea rift. *Quarterly Journal of the Geological Society of London*, **114**, 1–24.   1

Quennell, A. M. (1959). Tectonics of the Dead Sea rift. In *20th International Geological Congress, Association of African Geological Surveys*, pages 385–405.   1, 8, 10

Quennell, A. M. (1984). Western Arabia rift system. In J. E. Dixon and A. H. F. Robertson, editors, *Symp. East Mediterranean*, pages 775–789, Oxford. Blackwell.   10

Rabb'a, I. (1991). Al Qurayqira, 3051 II, 1:50000. Geological map, Natural Resources Authority, Geology Directorate, Amman, Jordan.   52

Reinecker, J., Heidbach, O., and Mueller, B. (2003). The 2003 release of the World Stress Map. (available online at www.world-stress-map.org).   15

Reynolds, J. M. (1997). *An Introduction to Applied and Environmental Geophysics*. John Wiley & Sons, Chichester, UK. ISBN 0-471-96802-1.   20, 21

Ritter, O., Ryberg, T., Weckmann, U., Hoffmann-Rothe, A., Abueladas, A., Garfunkel, Z., and DESERT Group (2003). Geophysical images of the Dead Sea Transform in Jordan reveal an impermeable barrier for fluid flow. *Geophys. Res. Lett.*, **30**(14), doi:10.1029/2003GL017541. 56, 63, 76

Rohr, K. M. and Dietrich, J. R. (1992). Strike-slip tectonics and development of the Tertiary Queen Charlotte Basin, offshore western Canada: evidence from seismic reflection data. *Basin Research*, **4**, 1–19. 77

Rotstein, Y., Yuval, Z., and Trachtman, P. (1987). Deep seismic reflection studies in Israel - an update. *Geophysical Journal of the Royal Astronomical Society*, **89**, 389–394. 41

Rotstein, Y., Bartov, Y., and Frieslander, U. (1992). Evidence for local shifting of the main fault and changes in the structural setting, Kinarot basin, Dead Sea Transform. *Geology*, **20**, 251–254. 52

Rümpker, G., Ryberg, T., Bock, G., and DESERT Seismology Group (2003). Boundary-layer mantle flow under the Dead Sea transform fault inferred from seismic anisotropy. *Nature*, **425**, 497–501. 47, 72

Ryberg, T., Garfunkel, Z., Qabbani, I., El-Kelani, R., and the DESERT Team (2001). Shallow, high-resolution velocity structure across the Dead Sea transform fault, Dead Sea rift valley, from Vibroseis data - project DESERT 2000. In *AGU Fall Meeting, San Francisco, California*. Poster S41A–0586. 56, 58, 63

Sabins, F. F. (1996). *Remote Sensing: principles and interpretation*. W. H. Freeman and Company, New York, third edition. 60

Salamon, A. (1993). *Seismotectonic analysis of earthquakes in Israel and adjacent areas*. Ph.D. thesis, Hebrew University, Jerusalem. in Hebrew with English abstract. 8

Schulz, S. E. and Evans, J. P. (1998). Spatial variability in microscopic deformation and composition of the Punchbowl fault, southern California: implications for mechanisms, fluid–rock interactions, and fault morphology. *Tectonophysics*, **295**, 223–244. 3, 54

Segev, A., Itamar, V. G. A., and Rybakov, M. (1996). Effects of Mesozoic magmatism on composition, structure and metallic mineralization in the Ramon area (southern Israel): Magnetometric and gravimetric evidence. *Israel Journal of Earth Sciences*, **45**, 89–112. 7

Segev, A., Goldshmidt, V., and Rybakov, M. (1999). Late Precambrian-Cambrian tectonic setting of the crystalline basement in the northern Arabian-Nubian Shield as derived from gravity and magnetic data: Basin-and-range characteristics. *Israel Journal of Earth Sciences*, **48**, 159–178. 6, 75

Shaw, J. E., Baker, J. A., Menzies, M. A., Thirlwall, M. F., and Ibrahim, K. M. (2003). Petrogenesis of the Largest Intraplate Volcanic Field on the Arabian Plate (Jordan): a Mixed Lithosphere-Asthenosphere Source Activated by Lithospheric Extension. *Journal of Petrology*, **44**, 1657–1679. 16

Sheriff, R. E. and Geldart, L. P. (1986). *History, theory, and data acquisition*, volume 1 of *Exploration seismology*. Cambridge University Press, Cambridge.   21

Shtivelman, V., Frieslander, U., Zilberman, E., and Amit, R. (1998). Mapping shallow faults at the Evrona playa site using high-resolution reflection method. *Geophysics*, **63**(4), 1257–1264.   52, 62

Sibson, R. H. (1992). Implications of fault-valve behaviour for rupture nucleation and recurrence. *Tectonophysics*, **192**, 283–293.   78

Sneh, A., Bartov, Y., Weissbrod, T., and Rosensaft, M. (1998). Geological map of Israel 1:200000, sheets 3 and 4. Geological Survey of Israel, Jerusalem.   18, 52, 61

Sobolev, S. V. and Babeyko, A. Y. (1994). Modelling of mineralogical composition, density and elastic wave velocities in unhydrous rocks. *Surveys in Geophysics*, **15**, 515–544.   42, 43

Sobolev, S. V., Babeyko, A. Y., Garfunkel, Z., and DESERT Group (2004). Thermo-mechanical model of the Dead Sea Transform. submitted to *EPSL*.   10, 11, 16, 42, 47, 72, 77

Stampfli, G. M. and Borel, G. D. (2002). A plate tectonic model for the Paleozoic and Mesozoic constrained by dynamic plate boundaries and restored synthetic oceanic isochrons. *Earth Plan. Sci. Lett.*, **196**, 17–33.   6

Stein, M., Garfunkel, Z., and Jagoutz, E. (1993). Chronothermometry of peridotitic and pyroxenitic xenoliths: Implications for the thermal evolution of the Arabian lithosphere. *Geochimica et Cosmochimica Acta*, **57**(6), 1325–1337.   16

Steinitz, G. (1980). Rb-Sr age determinations on basement rocks from Helez Deep 1a well. Report MM/1/80, Geological Survey of Israel.   6

Steinitz, G., Bartov, Y., and Hunziker, J. C. (1978). K–Ar age determintaions of some Miocene-Pliocene basalts in Israel: their significance to the tectonics of the Rift Valley. *Geological Magazine*, **115**(5), 329–340.   1

Steinitz, G., Bartov, Y., and Eyal, M. (1992). K-Ar dating and Ar-Ar dating of Permo-Triassic magmatism in Sinai and Israel – initial results. Abstracts, p. 147, Israel Geological Society Annual Meeting.   6

Stern, R. J. (1994). Arc assembly and continental collision in the Neoproterozoic East African orogen: Implications for the Consolidation of Gondwanaland. *Annual Reviews of Earth and Planetary Sciences*, **22**, 319–351.   5, 38

Stern, R. J., Gottfried, D., and Hedge, C. E. (1984). Late Precambrian rifting and crustal evolution in the northeastern Desert of Egypt. *Geology*, **12**, 168–172.   6

Stern, T. A. and McBride, J. H. (1998). Seismic exploration of continental strike-slip zones. *Tectonophysics*, **286**, 63–78.   46, 70, 71, 72

Stoeser, D. B. and Camp, V. E. (1985). Pan-African microplate accretion of the Arabian Shield. *Geological Society of America Bulletin*, **96**, 817–826. 5

Stolt, R. H. and Benson, A. K. (1986). *Seismic migration — theory and practice*. Geophysical Press, London–Amsterdam. 22, 31

ten Brink, U. (2002). Corrigendum to 'Lower crustal flow and the role of shear in basin subsidence: An example from the Dead Sea Basin', EPSL 199. *Earth Plan. Sci. Lett.*, **201**, 447–448. 14

ten Brink, U. S. and Ben-Avraham, Z. (1989). The anatomy of a pull-apart basin: seismic reflection observations of the Dead Sea basin. *Tectonics*, **8**, 333–350. 67

ten Brink, U. S., Schoenberg, N., Kovach, R. L., and Ben-Avraham, Z. (1990). Uplift and a possible Moho offset across the Dead Sea transform. *Tectonophysics*, **180**, 71–85. 45, 72

ten Brink, U. S., Katzman, R., and Lin, J. (1996). Three-dimensional models of deformation near strike-slip faults. *J. Geophys. Res.*, **101**(B7), 16205–16220. 47, 77

ten Brink, U. S., Rybakov, M., Al-Zoubi, A. S., Hassouneh, M., Frieslander, U., Batayneh, A. T., Goldschmidt, V., Daoud, M. N., Rotstein, Y., and Hall, J. K. (1999). Anatomy of the Dead Sea transform: does it reflect continuous changes in plate motion? *Geology*, **27**, 887–890. 61, 62

van Eck, T. and Hofstetter, A. (1990). Fault geometry and spatial clustering of microeartquakes along the Dead Sea – Jordan rift fault zone. *Tectonophysics*, **180**, 15–27. 14

Walley, C. D. (1988). A braided strike-slip model for the northern continuation of the Dead Sea Fault and its implication for Levantine tectonics. *Tectonophysics*, **145**, 63–72. 10

Walley, C. D. (1998). Some outstanding issues in the geology of Lebanon and their importance in the tectonic evolution of the Levantine region. In A. H. F. Robertson and M. Comas, editors, *Collision-Related Tectonic Processes in the Mediterranean Region*, volume 298 (1–3) of *Tectonophysics*, pages 37–62. 7, 10

Walley, C. D. (2001). The Lebanon passive margin and the evolution of the Levantine Neo-Tethys. In P. A. Ziegler, W. Cavazza, A. H. F. Robertson, and S. Crasquin-Soleau, editors, *Peri-Tethys Memoir 6: Peri-Tethyan Rift/Wrench Basins and Passive Margins*, volume 186 of *Mm. Mus. natn. Hist. nat.*, pages 407–439, Paris, ISBN: 2–85653–528–3. 10

Warner, M. R. (1990). Basalts, water or shear zones in the lower continental crust? *Tectonophysics*, **173**, 163–174. 44

Weissbrod, T. and Sneh, A. (2002). Sedimentology and paleogeography of the Late Precambrian – Early Cambrian arkosic and conglomeratic facies in the northern margins of the Arabo-Nubian Shield. *Geological Survey of Israel Bulletin*, **87**. 17

Wood, R. A., Pettinga, J. R., Bannister, S., Lamarche, G., and McMorran, T. J. (1994). Structure of the Hammer strike-slip basin, Hope fault, New Zealand. *Geol. Soc. Am. Bull.*, **106**, 1459–1473.   77

Yilmaz, Ö. (1987). *Seismic Data Processing*, volume 2 of *Investigations in Geophysics*. Society of Exploration Geophysicists, Tulsa.   21, 22, 29, 31, 43

Yuval, Z. and Rotstein, Y. (1987). Deep Crustal Reflection Survey in Central Israel. *Journal of Geodynamics*, **8**, 17–31.   41

Zaineldeen, U. (2000). *Tectonic evolution in the Wadi Araba segment of the Dead Sea Rift, Southwestern Jordan.* Ph.D. thesis, University of Gent.   15, 65, 75

Zilberman, E., Amit, R., Porat, N., and Avner, U. (1998). Relocation of the epicenter of the 1068 earthquake in the Avrona playa, southern Dead Sea Rift, using paleoseismic and archeoseismic evidence. abstract, 26th General Assembly of the European Seismological Commission, Tel-Aviv, Israel.   12

Zoback, M. D. (2000). Strength of the San Andreas. *Nature*, **405**, 31–32.   76

Zoback, M. D., Zoback, M. L., Mount, V. S., Suppe, J., Eaton, J. P., Healy, J. H., Oppenheimer, D., Reasenberg, P., Jones, L., Raleigh, C. B., Wong, I. G., C., O. S., and Wentworth (1987). New evidence on the state of stress of the San Andreas Fault System. *Science*, **238**, 1105–1111.   76

Zoback, M. L. (1992). First and second order patterns of stress in the lithosphere: The World Stress Map Project. *J. Geophys. Res.*, **97**(B8), 11,703–11,728.   15

Zoback, M. L. and Zoback, M. D. (1989). Tectonic stress field of the Continental United States. In L. C. Pakiser and W. D. Mooney, editors, *Geophysical Framework of the Continental United States*, volume 172 of *Geol. Soc. Am. Mem.*, pages 523–539.   76
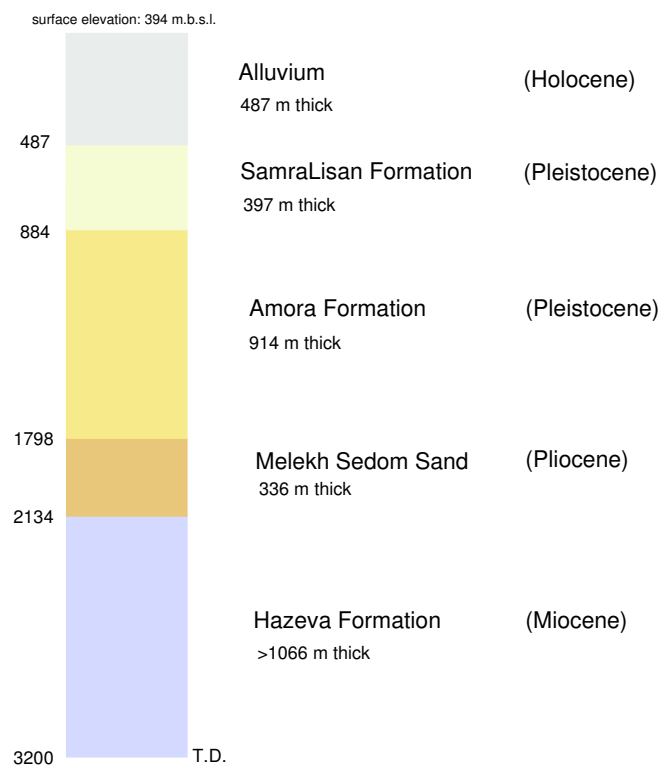
List of Figures

Appendix

A1. Wadi Ghaube Well

surface elevation: 394 m.b.s.l.

Depth	Formation	Age
	Alluvium 487 m thick	(Holocene)
487	SamraLisan Formation 397 m thick	(Pleistocene)
884	Amora Formation 914 m thick	(Pleistocene)
1798	Melekh Sedom Sand 336 m thick	(Pliocene)
2134	Hazeva Formation >1066 m thick	(Miocene)
3200	T.D.	

This well is located at 35.361°W and 30.747°N in the Arava Valley and was drilled by Amoco in 1988. The log data and drill report of this well were made available by the Natural Resources Authority, Amman, Jordan.

The interpretation is mainly based on the lithological description of the drilled units and the correlation of the gamma ray log with information from Israeli deep wells in the southern Dead Sea area (e.g. Gardosh *et al.*, 1997; Larsen *et al.*, 2002). Especially the gamma ray log revealed to be valuable, as it helped to distinguish the more shaly units (the Amora Formation and the upper part of the Hazeva Formation) from the usually sandy sediments.

95

Acknowledgements

One question a PhD student may ask oneself is: Is it worth spending 4 years of one's life – who noone knows how long it will be – writing some scientific stuff that hardly helps anyone living on this world??? With no answer for this question I have to acknowledge that there are many things I would not have experienced and learned without these four years. DESERT was a special project – special because it brought together Palestinians, Jordanians, Israelis, and Germans; special, because geologists and geophysicists worked productively together; special, because it probably would have been possible neither before nor after the year 2000.

Several weeks in the field and in the desert – employing seismometers and geophones, digging holes and walking around with my hammer – would have been not even half as enjoyable and instructive in many various respects, if there had not been Sandra Bourguignon, Radwan El-Kelani, Christian Haberland, Gabby Heim, Karl Otto, Issam Qabbani, Ibrahim Rabb'a, Trond Ryberg, Ali Schulze, Yosef Shahin, Ghassan Sweidan, Nayef Tahboub, Darwish Yasser and of course the bedouins, Marzouk and his friends.

Back at the GFZ, not having any experience in seismic processing, I don't know how I would have survived with 100 GBytes of seismic data without Manfred Stiller, who was a very patient teacher and always took his time to explain and help me with any problem that occurred.

Discussions about various geological and geophysical problems or aspects have always been possible and fruitful with colleagues and members of the DESERT Group, so I wish to thank Amotz Agnon, Yossi Bartov, Zvi Ben-Avraham, Uri Frieslander, Andrea and Hans-Jürgen Förster, Zvi Garfunkel, Hajo Götze, Arne Hoffmann-Rothe, Christoph Janssen, Lotte Krawczyk, Ayman Mohsen, Georg Rümpker, Sabine Schmidt, Stephan Sobolev, Uri ten Brink, and especially Jim Mechie who helped with good comments, suggestions and read through parts of my manuscript.

Michael Weber, without who the DESERT project would not have been 'born', always had an open ear and open door – thank you for that, Micha!

The remote sensing group from the GFZ assisted me a lot with getting and preparing the ASTER images and giving good hints for the interpretation – thanks a lot to Charly Kaufmann, Sylvia Magnussen, Martin Schodlok, Karl Segl and Uli Wetzel.

Scanning, digitizing, typing references, preparing some figures... I'm very grateful that Manuela Dziggel, Björn Lewerenz, Carola Ocholt, and Ariane Siebert were always willing to give their support. Moreover I'm very glad that Christof Lendl was (literally) 'next to me' for espresso breaks and emergency calls whenever computer problems would occur. And I was happy to share a room with Andrei Babeyko and Ivan Koulakov – unfortunately I did not learn any Russian, but we had a very good, fresh-air-atmosphere in E320!

Thomas Granzer spent several hours (days?) reading through many pages of 'weird geology' from an astrophysical point of view, corrected not only typing mistakes, and supported me not only with printing out four copies of my thesis at the very last minute. I more than appreciate all this, Thomas!

"Geteiltes Leid ist halbes Leid"! Nils Maercklin shared 4 years of PhD time with me and was always very helpful and better informed about LaTeX and bureaucracy stuff – things he selflessly passed on! How many pints did we have together at the 'Doktoranden-stammtisch' (or 'social meeting') during these years, talking about (PhD) life, different cultures, experiences, and Pumuckl – together with Arne, Bertram, Christiane, Christof, Georg, Jana, Jeromy, Martin, Paolo, Stefan, Christof, Sabine, Stephan, Thomas, Tobias, Ute, Zuzi...?!

A special person I want to mention is Khalil Abu-Ayyash – with his great charisma and generosity he not only constituted the central figure of DESERT but he also became a wonderful friend!

In the end I want to say thank you to all of you – you, who I have mentioned personally some lines before and you, who I have not mentioned but who have always 'just been there' – each of you with your own and special way to make my life worth living (which is more important than any academic title)!

Curriculum Vitae

Name:	Dagmar Kesten
Born:	13/12/1973, Frankfurt/Main (Germany)
Citizenship:	German

Education

1980 – 1986	Primary School in Dietzenbach near Frankfurt
1986 – 1993	Grammar School (Gymnasium) in Lörrach, Degree: Abitur
1993 – 1994	Aupair in England, Cambridge Certificate of Proficiency
	Italian Language Courses at the 'Universita per Stranieri'
	in Siena, Italy

University

1994 – 2000	University of Karlsruhe (TU), Germany
	Degree: Diploma in Geology
1996 – 1997	Oxford Brookes University, U.K.
	Studies in Geology within the 'Erasmus Programme'

Career

2000 – 2004	Scientist at the GeoForschungsZentrum (GFZ) Potsdam,
	Section 2.2 *Deep Geophysical Sounding* (Prof. Dr. M. Weber)
	(PhD student at the University of Potsdam)
Since 06/2004	Scientist at the 'Landesamt für Geologie, Rohstoffe
	und Bergbau Baden-Württemberg', Germany